Multifunctional polydopamine-based nanoparticles: synthesis, physico-chemical properties and applications for bimodal photothermal/photodynamic therapy of cancer

Islam Zmerli, Jean-Philippe Michel, Ali Makky

Multifunctional polydopamine-based nanoparticles: Synthesis, physico-chemical properties and applications for bimodal photothermal/photodynamic therapy of cancer

Islam Zmerli* [a], Jean-Philippe Michel [a], Ali Makky* [a]

[a] Université Paris-Saclay, CNRS, Institut Galien Paris Sud, 92296, Châtenay-Malabry, France

* Corresponding authors: zmerli.islem@gmail.com, ali.makky@universite-paris-saclay.fr

Abstract

Polydopamine (PDA) is a mussel-inspired and a melanin-mimicking material that has attracted considerable attention during the recent years. This "polymer" displays diverse promising properties, like its simple preparation procedures, easy functionalization, free radicals scavenging activity, outstanding photothermal and photoacoustic performance, and its great biocompatibility and biodegradability. A remarkable feature of PDA is its ability to form colloidal nano-sized particles or nanoscaled coatings, allowing the preparation of various nanoparticulate structures. The first studies regarding PDA explored mainly the polymerization mechanisms of this material and the development of controlled preparation protocols. Later works focused on the investigation of these nanomaterials for the design and development of multifunctional platforms and their implementation in multiple biomedical fields, particularly in cancer treatment and bio-imaging. The purpose of this review is to (i) give a detailed overview about the synthesis methods of PDA and the formation mechanisms proposed so far in the literature, (ii) outline the remarkable physico-chemical and functional properties of PDA nanomaterials, and (iii) summarize the application of PDA-derived nanosystems in cancer theranostics and particularly in drug delivery and light-mediated cancer therapy with a special emphasis on the different strategies that can be used for the design of smart nanosystems with bimodal photothermal/photodynamic properties. Finally, a comparison of physicochemical properties and biomedical applications between PDA and other cathecolamine derivatives is made.

1. Introduction

The development of bio-inspired and bio-mimicking materials has become a predominant strategy for the design of novel nanomaterials with interesting potential functions and promising biomedical applications such as for the treatment of cancer [1-2] and bacterial

infections [3]. To this end, melanin pigments have gained growing interest among the bioinspired materials for the design of multifunctional nanomaterials for many biomedical applications. In fact, melanin pigments are ubiquitous natural biopolymers of dark color that can be found in many types of living organisms ranging from bacteria [4] and fungi [5] to plants [6] and mammals [7]. The key enzyme of melanogenesis in many microorganisms and animals is the tyrosinase [8]. While these pigments contribute to the pathogenesis of some microorganisms and to the seeds color in plants, they play different physiological roles in mammals. In these latter species, melanin pigments can be found in various parts of living organisms such as skin, eye, hair and brain medulla, and can be divided into different groups depending on their origin and location, including eumelanin, pheomelanin, neuromelanin, allomelanin, etc. [9-10]. Due to their intrinsic properties, natural melanin pigments and their vesicles have been extracted from natural sources such as cuttlefish ink [11], hair [12] and skin [13], however due to the complicated extraction and purification procedures, synthetic methods of melanin derivatives were required.

On another hand, the astonishing strong adhesion of marine mussels, *Mytilus edulis*, to diverse wet surfaces has been a great inspiration for the design of new biomaterials for surface coating [14-17]. This mussel unique robust adhesion was long investigated and was ascribed to the *Mytilus edulis* foot proteins (Mefps), particularly Mefp-5, which is found preferentially near the adhesive plaque/substrate interface and is able to glue surfaces with a high strength and stability [18]. These Mefps were found to be rich in 3,4-dihydroxyphenylalanine (DOPA) and lysine residues [19-21]. Inspired by these proteins' chemistry, Messersmith's group reported that, under mild alkaline conditions, dopamine hydrochloride can spontaneously undergo an oxidative self-polymerization process to afford a strong black-colored coating material, called "polydopamine" (PDA), able to adhere to the surface of all tested inorganic and organic substrates [18] (Figure 1A). Indeed, dopamine is a DOPA derivative catecholamine bearing both catechol and amine functions and represents hence a powerful building block for the elaboration of Mefps mimics.

The dopamine auto-oxidation was investigated long before by Swan et al. in 1970 for the synthesis of a "dopamine-melanin" material in studies related to the chemistry of melanins [22]. However, since the pioneering report by Lee et al., polydopamine has mainly emerged as an attractive organic coating material, superior to the common surface modification strategies like layer-by-layer assembly or self-assembled monolayers [23-24]. Interestingly, owing to the abundant nucleophilic and electrophilic reactive sites [25], polydopamine coatings were proven able to undergo secondary reactions, offering thus an interesting

platform for the immobilization of a large repertoire of molecules on the polydopamine-modified substrates [18]. Hence, polydopamine served as a versatile surface coating and functionalization material in diverse material science fields and allowed the development of diverse polydopamine-coated nanostructures including multifunctional core@shell nanocomposites and hollow nanocapsules or nanotubes [23, 26-28].

Besides, as it shares the same precursor molecules, synthesis mechanisms and similar structural and physicochemical properties with natural eumelanin pigment, polydopamine is also regarded as a synthetic analogue of naturally occurring melanin (Figure 1B). Actually, the oxidative process yielding polydopamine coatings leads simultaneously to the formation of aggregates in the bulk solution. Efforts have been devoted to the valorization of such aggregates and the control of polydopamine growth processes in order to obtain stable nano-colloids, that can be used as melanin-like nanoparticles.

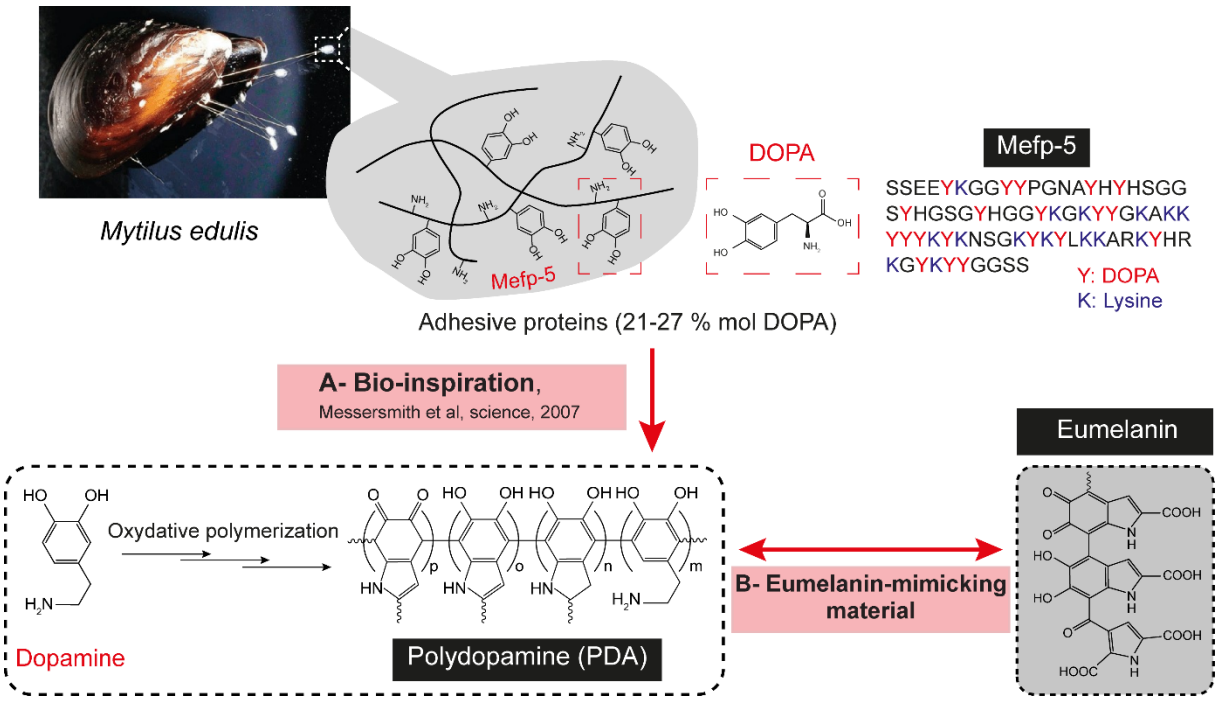

Figure 1. Polydopamine, a nature-inspired polymer, (A) The molecular composition of *Mytilus edulis* foot proteins rich in DOPA and lysine amino acids inspired the preparation of a strongly adhesive coating material, polydopamine, obtained from dopamine oxidation, (B) The oxidative polymerization of dopamine leads to a eumelanin-mimicking structure.

Eumelanin, a brown-black melanin derived from Tyrosine oxidation into L-DOPA displays a number of intriguing physico-chemical properties at the origin of their important roles in diverse biochemical processes and biological activities. For instance, owing to its broad absorption spectra covering the entire UV-visible-NIR regions, its radical scavenging effect,

redox active metal ions chelation and anti-oxidant ability, its fast non-radiative relaxation process and so forth, eumelanin exhibits important photo-protective and anti-oxidation functions and contributes to the homeostasis of several biochemical systems [9]. Importantly, eumelanin is biologically degradable into non-toxic metabolites. These inherent properties are closely related to their chemical composition and molecular buildup. Similarly, owing to its outstanding physico-chemical properties, polydopamine eumelanin-like nanoparticles emerged as powerful biocompatible and biodegradable nanoplatforms with interesting properties such as anti-oxidant effects, photothermal conversion ability and photoacoustic properties [26, 29-31].

Altogether, due to the advantageous concomitant features derived from both mussel- and melanin-mimicking properties, polydopamine has attracted extensive attention for the design of novel smart nanoplatforms with a plethora of possible applications including in energy and environmental materials sciences but particularly in the biomedical field where it emerged as a material of choice for the elaboration of a diverse multifunctional nanosystems of great potential in fields like cancer therapy (Figure 2), infections treatment, biosensing and bioimaging, tissue engineering, etc.

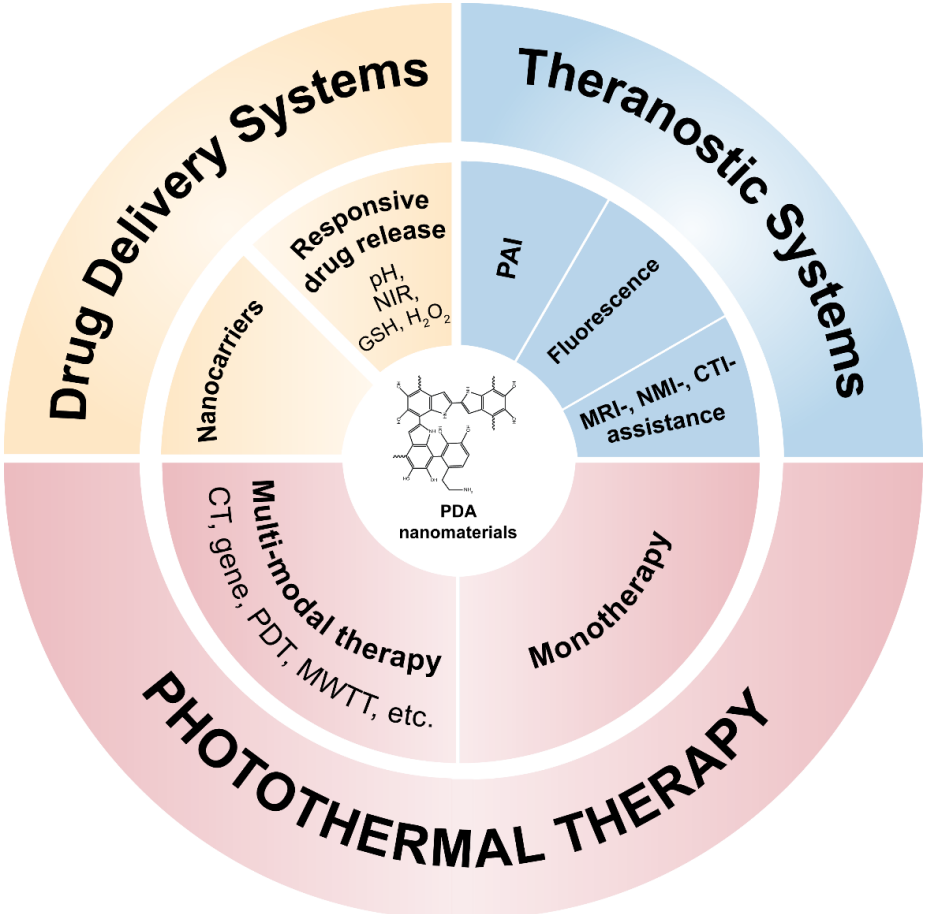

Figure 2. Applications of polydopamine nanomaterials in cancer therapeutic / theranostic fields.

CT: Chemotherapy, PDT: Photodynamic therapy, MWTT: Microwave thermal therapy, PAI: Photoacoustic imaging, Fluorescence: Fluorescence imaging, MRI: Magnetic resonance imaging, NMI: Nuclear medical imaging, CTI: Computed tomography

Excellent reviews have been published in the recent years regarding polydopamine-based nanomaterials with a great focus on the achievements in PDA-derived platforms development and their applications in different domains [26, 29-36]. However, recent comprehensive reviews about the physico-chemical prospects governing the formation, behavior and functions of polydopamine nanomaterials are still lacking. Therefore, in this review, we will outline the significant known features and bridge them with the recent advancement in the understanding of the structure-properties-processing relationships. Throughout this review, the discussion will only concern PDA-based particulate nanosystems, *i.e.*, PDA nanospheres, PDA nanocapsules, and PDA-coated nanosystems. First, we will describe the preparation methods reported for the fabrication of polydopamine products and the major key factors allowing to elaborate polydopamine colloidal structures and shells of controlled properties. Next, we will overview the most relevant structural models proposed, to date, for polydopamine and the underlying formation mechanisms. Thereafter, we will discuss the fundamental physico-chemical properties of polydopamine nanomaterials and elucidate their direct implementation in cancer treatment and/or diagnosis, in particular the drug delivery of anticancerous molecules and the photo-based cancer therapies mainly photothermal therapy (PTT) and photodynamic therapy (PDT). Analogies between polydopamine and eumelanin will be made in the different sections of this paper to give a general understanding of polydopamine properties.

2. Preparation strategies of polydopamine-based materials

The preparation methods of polydopamine nanomaterials have largely evolved from the first protocol described by Messersmith's group in 2007 [18]. Generally, in presence of a substrate, with dimensions down to the nanoscale, a thin polydopamine layer can be deposited overtime on the substrate's surface, *via* the oxidation of dopamine precursor. Simultaneously, insoluble polydopamine aggregates are formed in the medium and continue to grow into particles. Many progresses have been achieved in the comprehension of the mechanisms governing polydopamine growth and its aggregation processes. In addition, several efforts have been devoted in the aim of expanding the synthetic toolbox of polydopamine materials and adjusting the set of experimental parameters for the formation of polydopamine shells or

particles with strictly controlled morphological and physico-chemical properties. In this section, we will describe the most reported strategies applied to control polydopamine synthesis, particularly PDA nanocolloids and PDA-coated nanosystems. They are commonly categorized into three major approaches, namely the solution oxidation (Figure 3A), the enzymatic oxidation (Figure 3B) and the electropolymerization (Figure 3C) of dopamine monomers. We will discuss the different key parameters shown to have a great impact on the dopamine oxidation kinetics and consequently on the prepared polydopamine nanomaterials.

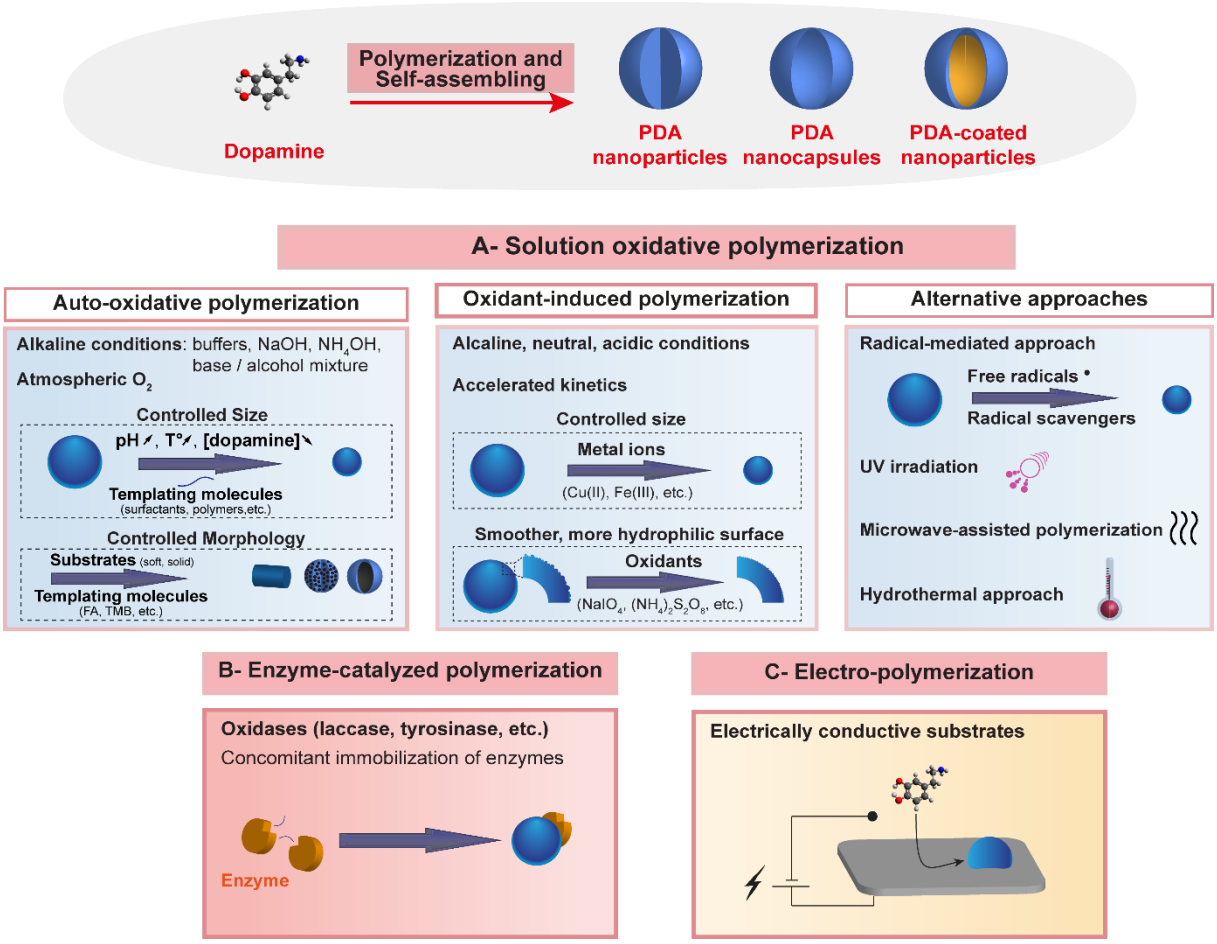

Figure 3. Illustration of the preparation methods used for polydopamine synthesis: (A) Solution oxidation of dopamine and typical parameters and additives controlling dopamine oxidation and polymerization rates, and the structural characteristics of nanoparticles size and coatings deposition, (B) Enzyme-catalyzed oxidation of dopamine following a melanin biosynthesis-mimicking approach, (C) Anodic oxidation of dopamine. FA: Folic acid, TMB:1,3,5-trimethylbenzene

2.1. Solution dopamine oxidative polymerization

2.1.1. Auto-oxidative polymerization in alkaline conditions

To date, the solution auto-oxidative self-polymerization of dopamine hydrochloride in mild alkaline solution (pH > 7.5) under ambient atmosphere remains the simplest and most

common strategy used for the preparation of polydopamine products, due to its versatility, cost-effectiveness and reproducibility. Polydopamine synthesis occurs rapidly and is accompanied with a color change of the solution from colorless to pale brown turning progressively to dark brown or black.

At first, this method has been described for the preparation of PDA coatings and was achieved in an aqueous Tris buffer solution (pH 8.5) [18]. Soon later, this protocol was further adapted to produce polydopamine coatings of controlled thicknesses and morphologies and more interestingly to valorize the polydopamine aggregates formed in the bulk solution. It was proposed that the oxidation of dopamine monomer leads to the formation of a dopamine-quinone moiety, which undergoes cyclization and further oxidation and rearrangement processes, yielding eventually polydopamine products. Kinetics studies have generally agreed that the first oxidation step of the deprotonated dopamine was the rate-determining step in polydopamine formation. The following intramolecular cyclization process was relatively rapid. Consequently, several strategies have emerged based on controlling the oxidation reaction kinetics mainly through tailoring the following experimental conditions: the solution pH, the used buffer/solvent, dopamine concentration and the temperature (Figure 3A).

2.1.1.1. Choice of solvent and pH value

The pH value of the reaction solution is a vital factor allowing control the kinetics of dopamine auto-oxidative self-polymerization. Based on the generally adopted mechanism of polydopamine synthesis (Scheme 1A), a basic pH appears crucial for the consumption of the hydrogen protons produced as polydopamine formation progresses. This allows the shift of the redox equilibrium towards polydopamine production [26] and an increase in the initial solution pH leads to the acceleration of dopamine oxidation rates [37-38]. Hence, by increasing the initial pH, an increase in the thickness of the PDA deposited layer could be achieved in the case of polydopamine coatings [39], while when producing polydopamine nanoparticles, a decrease in the particles size could be obtained [40]. The choice of the reactant solvent is another critical factor of a great impact on the outcomes of dopamine oxidative polymerization.

Alkaline buffers:

To date, the use of Tris buffer (at pH 8.5) as a basic polymerization initiator remains the most common method used for the preparation of polydopamine coatings [41]. It is worth noting that the structural investigation of the as-prepared coatings revealed that Tris could be incorporated in polydopamine scaffold *via* covalent coupling between its primary amine and

the dopamine-quinone intermediate, which risks impacting the materials properties [42-43]. However, Tris incorporation in PDA matrix was found to be prevalent only at the highest Tris/dopamine molar ratios [42]. To avoid such interference, other amine-free alkaline buffers were reported for the preparation of PDA coatings, in particular phosphate and bicarbonate buffers [42-44].

NaOH solution:

To fabricate colloidal PDA nanospheres, further acceleration of the dopamine oxidation kinetics is needed. The synthesis of nano-sized particles was reported for the first time in 2011 by Ju et al. [37]. In their protocol, sodium hydroxide (NaOH) aqueous solution was used in replacement to the above-mentioned basic buffers, which affected considerably the kinetics of deprotonated dopamine's oxidation and allowed the production of nanoparticles with a size less than 100 nm. This protocol was later adopted by several groups for the synthesis of melanin-mimetic nanospheres [45-46]. Later, Cho et al. investigated more in depth the hydroxide-ion mediated synthesis of stable polydopamine nanoparticles [38]. Considering their critical role in hydrogen abstraction during dopamine oxidation, it was found that the concentration of hydroxide ions influences directly the initial dopamine oxidation rate which determines the number of nuclei for nanospheres growth and enables the control of nanospheres diameter. Precisely, an increase of hydroxide ions concentration induced a linear acceleration of the oxidation rate and an early saturation of the solution with oxidized dopamine, leading therefore to the formation of more nucleation sites and consequently the production of smaller nanospheres [38]. Moreover, in the used hydroxide concentrations range, nanoparticles surface charge was highly negative (-44 mV) which prohibited particles aggregation and maintained their colloidal stability.

Although sodium hydroxide-mediated protocol was revealed efficient for the preparation of nano-sized PDA spheres with a reproducible fine control over their size and a good colloidal stability in water and biological media, large polydopamine aggregates were simultaneously produced in the reaction media, which necessitated an additional time-consuming purification step in order to be removed from the final preparation (by low-speed centrifugation, supplementary filtration, etc.) [37, 45]. Relatively high temperatures were also needed to reach the desired nanometric size (around 50 °C).

Water/organic solvents mixture or organic solvents:

Further efforts have been devoted to establish alternative preparation pathways offering a better control of the nanospheres size distribution. In this context, Lu's group reported for the first time a new protocol allowing the direct synthesis of monodisperse PDA nanospheres

with a highly controlled size and morphology, using a water-ethanol mixed solvent (with 29 % (v/v) ethanol) in presence of ammonium hydroxide (NH_4OH) as the basic catalyst [47-48]. The size of the as-prepared nanospheres could be tightly tuned in the range of several tens to hundreds of nanometers by varying the ammonia to dopamine molar ratio; higher ratios resulted in smaller nanoparticles. In a parallel study, Yan et al. highlighted the important role of water-alcohol mixed systems in the preparation of monodisperse spherical polydopamine nanoparticles; dopamine oxidation was conducted here in presence of Tris buffer at pH 8.5 and ethanol mixture [49]. Interestingly, it was revealed that pure ethanol could impede dopamine polymerization [49-50], which suggested that its introduction in the reactant medium as a co-solvent may offer a control over the polymerization rate and consequently over polydopamine particles growth process. To better explain all these findings, Jiang et al. studied the formation of PDA particles achieved in ammonium hydroxide in presence of various alcohol-water mixtures and calculated the Hansen solubility parameter corresponding to each solvent system [50]. Their results demonstrated that the monodisperse PDA nanospheres could only be obtained at an appropriate volume fraction of ethanol ranging from 25% to 40%, which corresponded to the solvent mixture solubilizing at best the dopamine monomer. The highest conversion of dopamine was also obtained in this range of ethanol / water volume ratios. This alcohol-water system was not only limited to ethanol, but other alcohols such as methanol (at 10% or 20%) or 2-propanol (at 40%) were also proven to be efficient in the preparation of spherical monodisperse nanoparticles. Isopropyl alcohol and ethylene glycol were also reported in other studies for PDA nanoparticles preparation and showed similar results [49].

It should be noted that dopamine polymerization could be also achieved in pure organic basic solvents like piperidine, which allowed to expand polydopamine applications to hydrolysable substrates coating but also to simultaneous immobilization of water-insoluble molecules [51].

2.1.1.2. Dopamine concentration

Dopamine concentration is another key parameter which considerably affects polydopamine particles morphology and films deposition kinetics and characteristics [39, 42]. Increasing the initial dopamine concentration (from 0.1 to 5 $g.l^{-1}$) resulted in a linear increase of the coating thickness [39, 52], but also in increasing the coatings surface roughness [43]. The dopamine concentration first reported by Lee et al. and commonly used for general surface functionalization purposes is of 2 $g.l^{-1}$, however, lower concentrations (< 0.5 $g.l^{-1}$) were preconized when polydopamine is used for the functionalization of nanostructures [52]. In

fact, the decrease of dopamine concentration to such low values allowed to effectively reduce the formation of polydopamine particles and thus their aggregation limiting the inevitable increase of PDA shells roughness [53]. Furthermore, it should be taken into account that dopamine concentration can also impact the molecular composition of the polydopamine products, in particular the relative proportions of cyclized and uncyclized units. In fact, at very low concentrations of this catecholamine (0.1 $g.l^{-1}$), a larger ratio of cyclized indole units is obtained [42]. Dopamine concentration should also be properly adjusted for the preparation of monodisperse polydopamine nanoparticles, since unstable small nanospheres were obtained at low dopamine concentrations, while high values led to large nanospheres with an irregular shape [38]. Hence, tailoring dopamine concentration in the range yielding monodisperse nanoparticles allows the control of nanoparticles size and yield [37-38, 54].

2.1.1.3. Temperature

The experimental temperature is another important factor that has to be carefully adjusted in order to control dopamine oxidation rates. Indeed, increasing the reaction temperature resulted in accelerated polydopamine deposition rates, leading to thicker and more hydrophilic polydopamine coatings in comparison to those formed at lower temperatures [55]. On the other hand, in the case of polydopamine nanoparticles production, increasing the temperature gave rise to smaller nanospheres with higher yields [37, 54], which could be explained by enhanced dopamine oxidation kinetics. Cho et al. suggested that the temperature can impact the size of polydopamine nanospheres *via* different modalities [38]. At high values, the hydroxide ions concentration would increase as a result of pK_{water} decrease, which leads to more nucleation sites and eventually smaller nanoparticles.

2.1.1.4. Templates

To date, the traditional template-free synthesis strategy based on the simple dopamine polymerization in alkaline aqueous or water-ethanol solutions remains largely adopted for the preparation of the PDA-based nanoplatforms. However, several templates-guided approaches have been also developed, permitting to further monitor dopamine polymerization and to shape polydopamine-based nanostructures into colloidal polydopamine nanoparticles, hollow nanocapsules or tubes, mesoporous nanoparticles, etc.

For instance, a reverse microemulsion-based method was employed to prepare relatively small monodisperse polydopamine nanospheres with a tunable size ranging from 25 to 43 nm [56]. In this method, ammonium hydroxide was used as the aqueous phase and was added to a

mixture of cyclohexane, used as the oil phase, and Igepal CO-520, used as the surfactant. After sonication and stirring, ammonia aqueous nanosized droplets are formed in the oil cyclohexane phase and act as a confined nanoreactor for the synthesis of polydopamine nanospheres, with a tunable size obtained by tailoring the amount of ammonium hydroxide and the reaction temperature.

Besides, polydopamine nanoparticles synthesis could also be controlled through the addition of templating molecules such as surfactants [57], polyelectrolytes [58] and other polymers [59]. Cationic and anionic surfactants (like hexadecyltrimethylammonium bromide (HTAB) and sodium dodecylsulfate (SDS), respectively) [57] allowed the preparation of small nanoparticles with a tunable size that could be considerably decreased by increasing of surfactant's concentration. For the highest concentrations of surfactants, exceeding their critical micellar concentrations, nanoparticles could reach a range of sizes only slightly higher than those of surfactants micelles [25]. It was proposed that surfactants interact with dopamine and act as templates for confined polydopamine growth. The structure of the as-prepared polydopamine was similar to the conventionally produced polydopamine. Similar to surfactants, a vast repertoire of polyelectrolytes were found effective in controlling the size of PDA nanospheres in a concentration-dependent manner [58]. It was proposed that the mechanisms by which polyelectrolytes act may differ depending on their chemical nature. As an example, it was suggested that polycations bearing primary amin functions, like poly(allylamine hydrochloride), would interact covalently with the quinone groups of oxidized dopamine units and small polydopamine aggregates and act as "capping agents" limiting preferentially polydopamine formation near the polyelectrolyte and yielding, for sufficiently high polyelectrolyte concentrations, nanoparticles slightly larger than the polyelectrolyte diameter.

Several other templating molecules were reported in the literature for the controlled preparation of polydopamine-based nanomaterials, including certain proteins like human serum albumin [60] which allowed the increase of dopamine oxidation rates and yielded small stable biocompatible polydopamine nanoparticles. Interestingly, by screening the proteins of skin melanocytes found usually surrounding eumelanin, a specific amino acids diad in proteins, L-lysine (K) – L-glutamic acid (E), was found particularly efficient in the oxidation control process [61-62]. This KE diad would likely play a templating effect in polydopamine nanoparticles assembly *via* establishing synergistic interactions with dopamine (hydrogen bonding and π-cation interactions) leading to an increased residence time of dopamine on this dipeptide as investigated by molecular dynamics simulations [62].

Template-guided dopamine polymerization pathways could also induce significant morphological changes of polydopamine assemblies. The most cited studies to this regard described the drastic impact of folic acid (FA) on the obtained PDA nanostructure [63-64]. In fact, when this molecule was added to dopamine solution, new aggregated nanobelts- and nanofibers-type structures were generated in the alkaline solution, preferentially at 60 °C. The authors proposed that the presence of FA favored the formation of porphyrin-like indolic tetramers and enhanced their ordered stacking through π-π stacking interactions, which would lead preferentially to an aggregation into the graphite-like ordered nanostructures. Mesoporous polydopamine nanostructures could also be designed using triblock copolymer Pluronic F127 / 1,3,5-trimethylbenzene (TMB) emulsion composites as organic templates in Tris buffer solution [65-66]. It was proposed that the formation of the mesoporous structure was favored by the π-π stacking interactions between polydopamine aggregates and the π-electron-rich TMB. Primary polydopamine particles formed in the solution would diffuse into the organic TMB phase and subsequent packing of PDA particles would occur leading to the mesoporous nanostructure with particles and pores sizes tunable *via* varying TMB / F127 weight ratios. The preparation of polydopamine-based Janus composites as multifunctional nanoplatforms was also described in several reports, using diverse innovative strategies [67-70]. In addition, hollow polydopamine (nano)capsules or (nano)tubes could also be obtained through polymerization of dopamine on soft templates (liquid-liquid interface) like emulsion droplets [71-74] and tetrahydrofuran-Tris buffer mixture [75] or on solid particulate templates of various sizes and shapes (solid-liquid interface) like SiO_2, $CaCO_3$, etc., followed by selective removal of the template core [76-80].

2.1.2. Chemically-assisted oxidative polymerization of dopamine (using exogenous oxidants)

Despite its versatility and simplicity, the auto-oxidative pH-induced method is a relatively slow process demanding at least several hours to overnight incubation times [81], and requires alkaline conditions in order to reach reasonable reactions rates [82]. Besides, dissolved atmospheric oxygen is a critical element contributing to dopamine auto-oxidation and polymerization reactions, *via* hydrogen abstraction [83-85]. Indeed, when oxygen was eliminated from the solution, either by permanent nitrogen gas bubbling or by deoxygenation under vacuum, the incubation of dopamine in alkaline conditions, even at high pH values, did not visibly lead to polydopamine production [37].

Therefore, efforts have been made to overcome these limitations and alternative preparation strategies, based on the use of exogenous oxidants, have been developed to accomplish faster oxidation kinetics and further adjust polydopamine products properties. Such alternatives allowed, potentially, the production of polydopamine under neutral or acidic pH, which would be particularly interesting to expand polydopamine surface coating and one-pot drug/adjuvant co-loading applications to base-sensitive or insoluble substrates and molecules [25].

In fact, under high concentrations of oxygen (up to pure oxygen), the reaction kinetics increased drastically and allowed the deposition of highly homogenous and ultra-smooth PDA layers, achieved in much shorter deposition times [86]. Beside pure oxygen, other water-soluble oxidizing reagents were proven efficient to induce accelerated dopamine polymerization and could trigger polydopamine formation in mild alkaline conditions, but also in neutral or even acidic solutions [24, 41, 87-88]. In this context, various oxidants have been employed including sodium periodate ($NaIO_4$), ammonium peroxydisulfate ($(NH_4)_2S_2O_8$) and potassium permanganate ($KMnO_4$), in addition to multiple other inorganic chemicals and metal ion additives such as Cu(II), Fe(III) and Mn(III) salts, etc. [44, 82, 87-90]. The choice of the used oxidant as well as its concentration has a major impact on the polymerization rates and the pathways favored during polydopamine assembling process [91]. Besides, mixtures of $CuSO_4/H_2O_2$ [92], $FeCl_3/H_2O_2$ [93] or $FeSO_4/H_2O_2$ [94] were also used as oxidants for ultra-fast polydopamine shells or nanoparticles formation. Despite the great enhancement of polydopamine production kinetics, the possible effect of metal ions on the structure and properties of polydopamine should be taken into account. Indeed, polydopamine components (particularly catechol groups) exhibit a high affinity and complexation ability towards various metallic cations, leading to the inevitable incorporation of these latter in polydopamine matrix. Depending on the redox and complexation ability of the metal ion, this would lead to changes in polydopamine chemical composition (loss of nitrogen content, presence of metal content) and consequently to changes in its physico-chemical properties [24, 89, 95].

2.1.3. Radical-, ionization- and microwave-assisted dopamine polymerization

In order to avoid chemical contamination of polydopamine nanomaterials encountered when using exogenous oxidants, alternative strategies have been developed to obtain fast dopamine polymerization kinetics, for the formation of polydopamine under neutral or even acidic conditions. Recently, Wang et al. reported a free radical-mediated strategy allowing further control the size of PDA nanoparticles prepared in a water/ethanol/ammonia mixture, *via*

tuning the free radicals in the reaction medium [96]. Based on the speculation that polydopamine formation process could involve radical coupling pathways related to the generation of semi-quinone radical intermediates *via* dismutation reaction [97-98], two strategies were tested and found effective to control polydopamine formation. The first one consisted in quenching the radical intermediates generated during PDA formation *via* the addition of strong radical scavengers (such as edaravone), which leads to the inhibition of nanoparticles growth. Whereas the second strategy was based on the addition of stable free radicals (such as PTIO•) which facilitates the seed formation process. Both strategies offer an interesting modality to control PDA nanoparticles diameter, while maintaining the characteristic chemical structure and physico-chemical properties of the conventional nanoparticles.

Free radical species triggering polydopamine formation can also be generated by providing external energy to the system *via* UV irradiation [99-100]. This light-induced method allowed the acceleration of dopamine polymerization under alkaline conditions and was also proven effective for polydopamine formation at neutral or acidic conditions (down to pH 2.0) [100]. Polydopamine formation could also be achieved by using visible light, under neutral conditions (pH = 7.0), in presence of 9-mesityl-10-methylacridinium ions as a photocatalyst [101]. Excited, this molecule can activate the solution dissolved oxygen, which triggers dopamine polymerization. The microwave-assisted polymerization is another method found to accelerate polydopamine formation in a chemical-free manner. Using this technique, only 15 minutes were needed to deposit a 18 nm film of PDA under 1000 W versus several hours for the traditional protocol [81]. This enhancement effect of the polymerization kinetics was attributed to an increased radical generation by microwave irradiation and the resulting superheating effect. However, to the best of our knowledge, no previous studies have been reported about using this polymerization process for the preparation of PDA nanoparticles.

A hydrothermal process was also used to trigger dopamine oxidation and self-polymerization and allowed to extend polydopamine production to strong acidic environments (pH 1.0 and at 160 °C) [102]. The efficiency of this strategy was attributed to the pronounced auto-ionization of water under the high temperature and pressure employed, leading to the formation of hydroxyl ions in the bulk solution which are involved in dopamine oxidation reactions.

2.2. Enzymatic dopamine polymerization

The process of melanin biosynthesis in living organisms has inspired the development of a new approach for the preparation of polydopamine nanomaterials based on enzyme-catalyzed

dopamine oxidation and self-polymerization. Several enzymes reported for the oxidation of phenolic and aromatic amines compounds have been employed as catalysts to trigger dopamine oxidative processes. For instance, laccase has been employed for the preparation of polydopamine nanoparticles and coatings (at pH ~ 5.5). In comparison to the conventional polydopamine products, the yielded products were interestingly more stable and uniform [103-105]. Horseradish peroxidase (HRP) was also efficient for rapid oxidation of dopamine in presence of hydrogen peroxide [106]. Also, using an urease catalytic reaction and based on the basification of the reaction medium coupled to urea hydrolysis, Li et al. developed an efficient approach offering control over dopamine polymerization and yielding polydopamine nanoparticles of tunable sizes that increase linearly with the increase of urea concentration [107].

Although it is relatively more complicated than the conventional dopamine auto-oxidative protocol, the enzyme-catalyzed strategy represents an environmentally friendly method that is highly efficient for the preparation of polydopamine nanomaterials. Interestingly, being inspired by melanin biosynthesis, polydopamine produced using this method resembles at best to the naturally occurring melanin [30, 36]. Furthermore, this approach is particularly advantageous for simultaneous immobilization of enzymes with preserved enzymatic activity in a one-pot preparation method.

2.3. Dopamine electro-polymerization strategy

Electropolymerization of dopamine emerged as an alternative approach mainly used for the preparation of polydopamine coatings [108-111]. Rapid polymerization and high deposition rates were obtained on diverse conductive nanostructures (TiO_2 nanotubes [112], Fe_3O_4 nanoparticles [113], nanoporous gold film [114], etc.). Also, PDA-coated magnetite nanoparticles could be electro-synthesized in a one-pot reaction. By varying the time at which dopamine is added to the reaction medium, it was possible to yield nanocomposites with controlled nanoparticles sizes and shell thicknesses [113]. Interestingly, uniform fluorescent polydopamine nanoparticles were obtained by Wang et al. using a novel anodic microplasma electrochemistry method. This technique induced the generation of oxidative species that could trigger the nucleation of polydopamine nanoparticles at the plasma-liquid interface. As the process progressed, the solution pH shifted to acidic values (pH ~ 5) which inhibited the further growth of nanoparticles and allowed the control of their size [115].

Despite its simplicity, efficiency and possibility to be performed in a deoxygenated medium, the main drawback of this method is that polydopamine production can only occur on electrically conductive substrates, thus limiting its extent of applications.

To summarize, a wide variety of approaches have been stablished, to date, for a well-controlled preparation of polydopamine-derived nanomaterials. However, the exact structure and formation mechanisms of polydopamine are still not fully clear, as will be discussed in the following section.

Table1. The major methods used for the preparation of controlled polydopamine particulate nanostructures

Preparation method	Obtained nanostructures	Impact on nanostructures properties	Ref
Basic buffers (Tris, Phosphate, Bicarbonate), in presence of substrates	Preparation of PDA-coated structures, Few nm to few hundreds of nm	Tris buffer is the most used basic buffer, Choice of buffer impacts the polymerization kinetics and thickness, roughness, and paramagnetic properties of PDA layer.	[43]
Sodium hydroxide / Water	Preparation of PDA nanospheres, Few tens to few hundreds of nm	Hydroxide ions concentration impacts the size of PDA nanoparticles.	[37, 45-46]
Ammonium hydroxide / Water / Ethanol	Preparation of monodisperse PDA nanospheres, Few tens to few hundreds of nm	Ammonia concentration impacts the size of PDA nanoparticles, Ethanol used at a volume fraction of 25% to 40% to obtain monodisperse nanoparticles.	[47, 50]
Reverse microemulsion: - Ammonium hydroxide as aqueous phase - Cyclohexane as oil phase - Igepal as surfactant	Preparation of small PDA nanospheres, Few tens of nm	The size of dispersed ammonia droplets impacts the size of PDA nanoparticles.	[56]
Basic conditions, In presence of templating molecules (polymers, polyelectrolytes, surfactants, proteins, etc.)	Preparation of small PDA nanospheres, Nm to few tens of nm	Templates act as confined environments for PDA synthesis, Templates concentration impacts the size of PDA nanoparticles.	[57-58, 116]
Basic conditions, in presence of folic acid (FA)	Preparation of PDA nanospheres/nanotubes, Few tens to few hundreds of nm	FA and dopamine concentrations impact the morphology of PDA nanostructures.	[63, 117]

Basic conditions (mainly buffers), in presence of core templates (soft templates or solid templates selectively removed)	Preparation of PDA nanocapsules, Few tens to few hundreds of nm	The size and shape of the cores define the size and shape of the hollow PDA structures	[72, 75, 77-78, 118]
Acidic, neutral or basic conditions, in presence of oxidants (like $NaIO_4$) Metal ions (like Cu (II))	Preparation of polydopamine nanoparticles and PDA-coated structures, Few nm to few hundreds of nm	Choice of oxidant type and concentration impacts the kinetics of PDA polymerization, Oxidants and metal ions impact the structure of PDA and the thickness and roughness of the coating, Fast polymerization kinetics are obtained in comparison to conventional methods.	[82, 87, 89]
Basic conditions (mainly ammonia), in presence of free radicals or radical scavengers	Preparation of PDA nanospheres, Few tens to few hundreds of nm	These additives allow radical tuning in the solution and a control of PDA polymerization and of the size of PDA nanoparticles.	[96]
Enzymatic polymerization (like laccase-mediated polymerization)	Preparation of PDA nanoparticles or PDA-coated nanostructures, Few tens to few hundreds of nm	Preparation of stable and uniform nanostructures, resembling to melanin materials, Possible simultaneous immobilization of active enzymes on the yielded structures, Green products.	[103, 105-106]
Electro-polymerization / Plasma-mediated electrochemistry	Preparation of PDA-coated nanostructures or PDA nanospheres, Few nm to few hundreds of nm	Exclusively used to coat conductive nanostructures like TiO_2 or Fe_3O_4, Fast polymerization kinetics are obtained in comparison to conventional methods, Ultra-small fluorescent PDA nanospheres were obtained.	[112-113, 115]

3. Polydopamine structural models and formation mechanisms

Since polydopamine discovery, numerous studies devoted to the investigation of polydopamine molecular structure and its buildup mechanism have been reported [42, 119-124]. However, despite the great efforts invested, the detailed chemical composition of polydopamine is not fully understood yet and the elucidation of a definite structural model is still a long-lasting debate that has not yet come to its end. In fact, polydopamine's insoluble nature in common aqueous and organic solvents [119-120, 124] made it difficult to investigate its structure by means of conventional analytical techniques usually applied for polymers molecular weights characterization [124-125]. Besides, it is accepted that polydopamine composition has a marked chemical heterogeneity and can depend on the preparation method and experimental conditions, as explained above [42, 44], which makes the elucidation of an exact structure more challenging.

Various techniques were applied to uncover polydopamine composition, including mainly mass spectroscopic analyses, solid-state nuclear magnetic resonance (ss NMR), X-ray photoelectron spectroscopy (XPS), powder X-ray diffraction (PXRD), and Fourier transform infrared (FTIR) spectroscopy along with other analytical methods. Theoretical approaches based on molecular energies calculations were also employed in order to provide more insights into polydopamine molecular organization [120, 123, 126]. Moreover, as previously stated, polydopamine is commonly considered as a eumelanin-like material and there is a general agreement that polydopamine shares formation steps with eumelanin biosynthesis. Therefore, comparative structural studies were also undertaken to help bring more understanding of polydopamine characteristic molecular features [42, 126-127].

Altogether, structural investigations carried out on PDA products (particles and/or coatings) led to controversial models that fall into three main hypotheses. The first one holds that polydopamine has a polymeric nature wherein dopamine and/or its oxidation derivatives are covalently linked *via* aryl-aryl coupling. The second theory suggests a supramolecular assembly arising from 3-dimensional association of monomeric units held together *via* weak interactions such as π-π stacking, Hydrogen bonding (H-bonding), charge transfer or π -cation interactions. The third structural model on the other hand is based on the contribution of both covalent and non-covalent interactions occurring at different stages of the polymerization process and leading to the black insoluble polydopamine products.

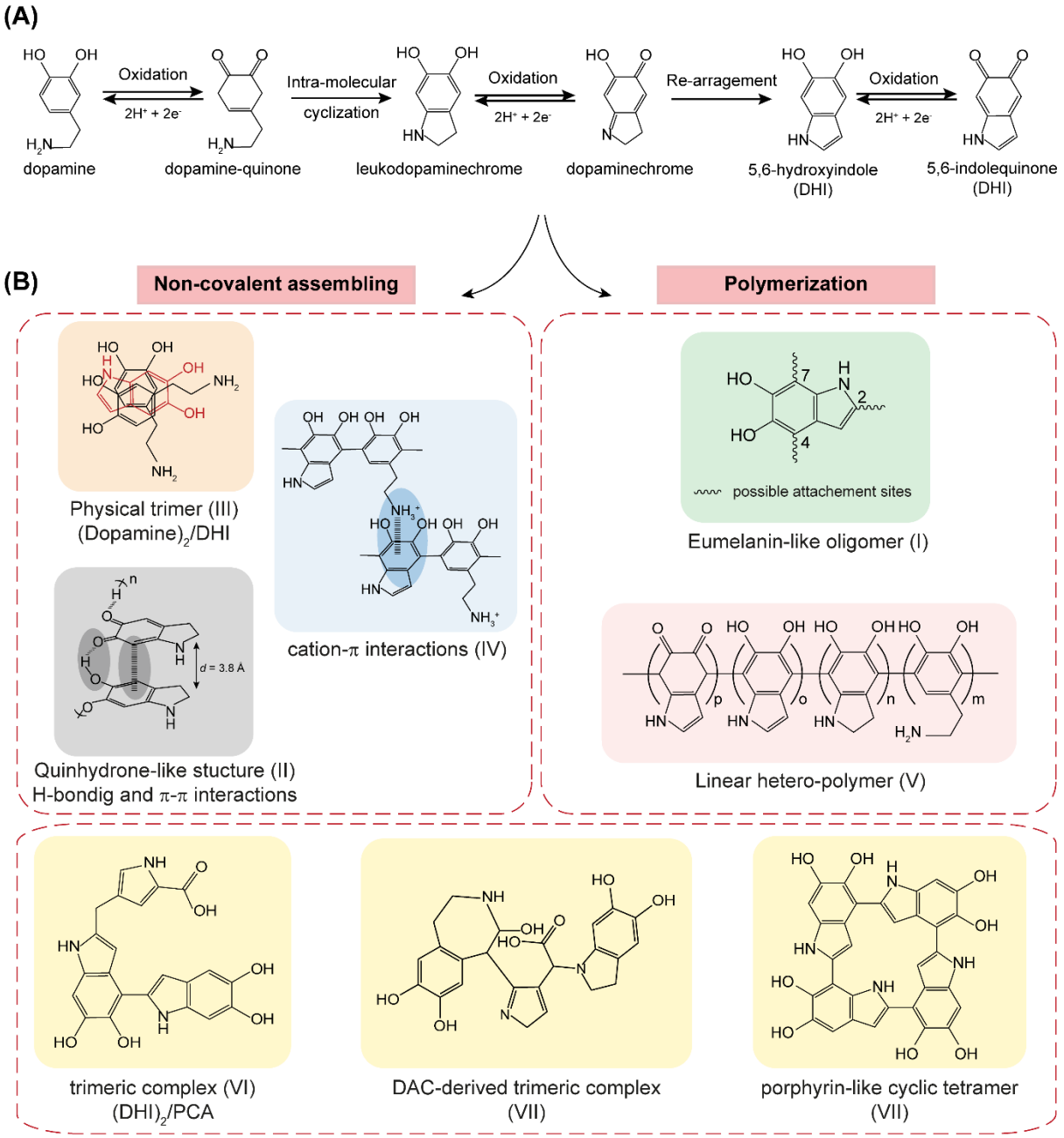

Scheme 1. (A) The generally agreed dopamine auto-oxidation process, leading to the formation of polydopamine building units, (B) Structural models proposed for polydopamine generated from covalent polymerization pathways or physical self-assembling processes.

3.1. Covalent polymerization

While introducing polydopamine, Messersmith's group proposed a chemical structure and a formation mechanism on the basis of a time-of-flight secondary ion mass spectrometry (TOF-SIMS) and XPS data [18]. A major mass peak was detected at m/z 445 and was attributed to a trimer of 5,6-dihydroxyindole (DHI). This trimer was suggested to originate from the fragmentation of a long-chain polymer of similar composition, which led the authors to suggest that polydopamine is a polymeric material arising from a covalent association of DHI

units *via* biphenyl-type covalent bonds (Scheme 1B, structure I). Based on this observation, a polymerization mechanism similar to that of eumelanin biosynthesis was proposed, wherein the initial driving force consists in the oxidation of dopamine monomer under oxidative alkaline conditions leading to dopamine-quinone formation. This component undergoes then an intra-molecular cyclization (by 1,4 Michael-type addition of the amino group to the phenyl-quinone system) which generates a leukodopaminechrome moiety whose further oxidation and rearrangement leads to the formation of the 5,6-dihydroxyindole. The further oxidation of DHI units generates 5,6-indolequinone and induces spontaneous inter-molecular cross-linkages by dehydrogenerative C-C bond formation at positions 2, 4 and 7 of the indole moieties, allowing to yield the black insoluble eumelanin-like polydopamine polymer [18].

However, this polymerization process known as eumelanin-like poly(indole) structural model became later on an active area of investigation. In fact, chemical differences were noticed when polydopamine products were compared to pure DHI-polymer (generated from DHI units as exclusive starting monomers) [42, 128]. Furthermore, mass spectroscopic analyses performed by other groups [128-131] on similarly prepared PDA materials did not reveal the presence of the peak at m/z 445 reported by Messersmith's group, and the wide set of analytical methods employed revealed the existence of diverse functional groups referring to the contribution of various moieties as key structural units in polydopamine buildup. For instance, clear experimental evidence about the presence of primary amines, quinone moieties or carboxylic groups has been widely reported throughout the literature [42, 120, 123]. These observations indicated that PDA would not be solely made of polymerized DHI units as proposed. Indeed, since the overall process of dopamine conversion to DHI was demonstrated to be relatively slow [128, 132], dopamine monomer and the various intermediates derived from its oxidation process are very likely to be concommitly present in the reaction solution. This would suggest that multiple synthesis pathways involving various kinetics key control points and different intermediates and types of connections (covalent or physical) may occur and lead to a more heterogeneous composition for polydopamine materials.

3.2. Non-covalent self-assembling

In this context, a different perspective of polydopamine formation was advanced by Dreyer et al. [119] who highlighted the important contribution of non-covalent interactions in this process. They postulated that polydopamine consists in a supramolecular aggregate of monomers lacking any covalent bond. The monomeric building units, consisting here in 5,6-dihydroxyindoline and its dione derivative primarily, are entirely held together through a

combination of H-bonding, π-π stacking and charge transfer complexation. In fact, a detailed study conducted on PDA aggregates, using a variety of solid-state spectroscopic and crystallographic techniques, indicated the presence of these cyclized nitrogenous indoline-type species where the carbon atoms in position 4 and 7 of the aryl core were rather tertiary (hydrogenated). This observation ruled out the covalent model suggested by Lee et al.[18]. Alternatively, Dreyer et al. proposed a quinhydrone-like assembly that is further connected *via* π-π stacking favored by the *d*-spacing of 3.8 Å consistent with that observed in other π-stacked materials [119, 133]. Such spacing was found to likely facilitate or result from charge transfer between the faces of polydopamine building units (Scheme 1B, structure II).

Another entirely physical structure was identified by Hong et al. wherein dopamine units interfere with DHI moieties to build a supramolecular self-assembled block as a significant component trapped in polydopamine network [120]. In fact, the authors could identify a robust physically self-assembled [$(Dopamine)_2$/DHI] trimeric complex entirely arising from non-covalent interactions probably including H-bonding and π-π interactions (Scheme 1B, structure III). The detection of all the protons from dopamine and DHI species in ^{1}H ss NMR spectra confirmed the non-covalent character of the interactions involved in this complex. However, it was observed that the dissociation of this complex leads to covalent bond-forming oxidation reactions resulting in the formation of a 2,2' linked DHI-DHI dimer which eventually reacts with dopamine to form a covalent dopamine-DHI-DHI oligomer (C5 of dopamine connected to C4 of DHI). Thus, the authors suggested an overall mechanism for polydopamine formation implying two different pathways, (i) the self-assembly of dopamine and DHI to generate the physical trimer [$(Dopamine)_2$/DHI], along with (ii) covalent bonds formation yielding structures like dopamine-DHI-DHI conjugates. More recently, these authors have reported the first experimental evidence that cation-π, a non-covalent interactions mode unexplored so far in polydopamine materials, can be the driving force responsible for oligomers molecular assembly into polydopamine granules [121]. Such interactions were demonstrated to occur between protonated amines of uncyclized dopamine moieties and the π-system of indole species leading to highly cohesive polydopamine structure (Scheme 1B, structure IV).

3.3. Co-contribution of covalent polymerization and non-covalent self-assembling

The aforementioned studies, among multiple others, highlighted that non-covalent interactions would play an important role in polydopamine assembling. So far, the general

consensus favors the contribution of oxidative polymerization leading to covalent oligomers with different molecular weights, as well as the non-covalent interactions probably taking place in the latest stages of polydopamine synthesis, to yield the final insoluble polydopamine product. One of the most accepted models concurring with this theory, is the one illustrated by Liebscher et al. [123] who re-examined the major structural features present in PDA, using an association of a broad range of analytical techniques, including ^{1}H and ^{13}C ss NMR under magic angle spinning (MAS) conditions, electrospray ionization high-resolution mass spectrometry (ES-HRMS) in addition to XPS and FTIR. Their spectra interpretation revealed the presence of indolic moieties along with open-chain aminoethyl containing compounds and enabled the assignment of each C-atom to a moiety to which it belongs. Interestingly, it was observed that the two carbon lines at positions 4 and 7 cannot both be protonated, which was in disagreement with what was postulated by Dreyer et al. [119]. In matrix-assisted laser desorption/ionization mass spectrometry (MALDI-MS), the peaks detected were attributed to oligomers composed of uncyclized dopamine and DHI-related units present under different degrees of (un)saturation and/or oxidation states, which concurred with the NMR and XPS results. The covalent connections between building units were proposed to occur *via* the benzo moieties yielding a linear hetero-polymer (Scheme 1B, structure V). In this model, the contribution of weak interactions was not excluded and was proposed to give rise to a supramolecular assembly of the linear PDA chains. Additionally, their DFT results implied a linear oligomeric chain structure for polydopamine and the stacking between PDA chains was revealed thermodynamically favorable and H-bonds were very likely to occur. Very recently, evidence for the PDA polymeric nature was provided by Messersmith's group [124]. By means of single molecule force spectroscopy (SMFS), the authors could demonstrate directly, for the first time, the presence of high molecular weight polymer chains. So far, the mass spectrometry methods allowed the identification of low molecular weight oligomers (up to the octamer level) [123, 125, 129-130]. The SMFS technique, which enables the study of covalent and non-covalent interactions occurring at the scale of an individual macromolecule, was employed in this study to investigate polydopamine intermolecular and intramolecular interactions. PDA-coated AFM cantilevers were approached to then retracted from PDA coated or uncoated substrates. The analysis of the Force-distance curves obtained revealed the existence of constant force plateaus separated by "steps". The plateaus reflected the entropic resistance to polymer chain extension originating from a single molecule stretching event and the steps were related to the rupture of the connections in one or more PDA chains. Steps heights between the plateaus corresponded to the magnitude of the interaction's force. By

analyzing these plateaus lengths, the authors could investigate PDA chains lengths and their molecular weights. Their results corresponded to a polydisperse polymer having an average molecular weight value of 11.2 kDa with some polymer chains having above 50 kDa. The great resistance of PDA polymer to very high forces that exceed the threshold of rupture for non-covalent interactions was consistent with a polymeric nature where dopamine and its oxidation derivatives are linked together linearly *via* aryl-aryl covalent coupling, in a manner similar to that proposed by Liebscher et al. [123]. However, the authors do not rule out the presence of small oligomeric species in PDA nanomaterials and stated the possible contribution of weak intermolecular interactions between PDA molecules to yield the final polydopamine materials.

Non-linear covalent oligomeric blocks and other building units were also proposed in polydopamine formation. For instance, beside phenylethylamines, indoles and indolines species listed so far, two pyrrolecarboxylic acids (PCA) were recognized for the first time by Della Vecchia et al. as building units of the polydopamine matrix [42]. The authors conducted a set of chemical and spectroscopic experiments, which enabled them to conclude that PDA is rather a mixture of oligomeric building blocks, up to the tetramer level, composed of three main species: uncyclized dopamine or its quinone-derivative monomers, DHI units and pyrrolecarboxylic acid moieties. These latter are likely to derive from partial oxidative cleavage of DHI units under the auto-oxidative conditions related to PDA formation process.

Similarly, Ding et al. [130] indicated the presence of a major mass peak at m/z 402, identified as a trimer complex consisting of two DHI units and one pyrrolecarboxylic acid moiety [$(DHI)_2$/PCA] (Scheme 1B, structure VI); further covalent linkage between these trimers was found to be unlikely. More recently, Luy et al. [129] speculated that the peak at m/z 402 would correspond to a covalent trimer composed of one dopaminechrome (DAC), one DAC degraded unit (2H-pyrrole moiety) and one benzazepine moiety (Scheme 1B, structure VII). It could be noticed that such complex resembles to the dopamine/DHI/PCA-based models reported in the literature [42, 130] and may share physico-chemical properties, allowing the authors to confirm its likelihood. All these authors proposed that covalent interactions occur at the initial stages of the polymerization process, leading to these small blocks, which interact in later stages via non-covalent interactions to build up the supramolecular structure of PDA.

In line with the previous findings, Warren's group studied by means of pump-probe microscopy the role of aggregation in polydopamine nanoparticles assembly [134] and suggested that polydopamine nanostructures result from the formation of covalent

fundamental oligomeric blocks that stack together *via* non-covalent interactions, mainly π-π stacking, to form stacked oligomers, also known as "protomolecules". These stacked oligomers would further aggregate leading to the hierarchical self-assembled structure of polydopamine particles.

Multiple other scenarios regarding dopamine polymerization were proposed in the literature, sometimes without sufficient experimental evidence. As an example, porphyrin-like cyclic tetramers for example can result from oxidative polymerization of DHI units and were indeed found in eumelanin materials (Scheme 1B, structure VIII) [131]. Such compounds were identified as the most stable tetramer generated from oxidized DHI units using the computational structural investigation elaborated by Chen et al. [126].

To summarize, numerous models have emerged concerning polydopamine key components and its buildup mechanisms. However, it is currently agreed that these models should not be considered as mutually exclusive, since polydopamine is very likely to result from the combination of various mechanisms occurring at different stages of the polymerization process, as stated earlier.

4. Physico-chemical properties of polydopamine nanostructures and their implementation in cancer treatment

Polydopamine products display multiple characteristic features arising from their chemical and structural resemblance to naturally occurring eumelanin. The investigation and interpretation of the physico-chemical and functional properties of polydopamine materials were indeed often made in analogy to their natural counterparts to allow a better understanding of their common features. It is important to note however, that PDA nanomaterials properties are highly dependent on their preparation method and may particularly vary when polymerization is achieved in presence of additives that risk interacting with or be entrapped within polydopamine matrix.

4.1. Toxicity, Biocompatibity and Biodegradability

Based on structural and physico-chemical similarities reported between synthetic eumelanin-like polydopamine and naturally occurring melanin, polydopamine materials were anticipated to benefit from the wide distribution of melanin in the human body and show excellent biocompatibility [26, 47]. Numerous *in vitro* and *in vivo* studies performed on PDA-based

nanosystems (PDA nanospheres, PDA nanocapsules, PDA-coated nanoparticles) confirmed their biocompatibility and revealed their great potential as candidates for *in vivo* biomedical applications. However, the presence of dopamine monomers in polydopamine matrix, as revealed in some reports [120], have raised questions regarding the possible cytotoxic effects that could be related to this neurotransmitter. To address this issue, Hong et al. examined the amount of dopamine released from PDA particles. Their findings revealed an extremely low-level release of dopamine, which was attributed to a robust self-assembled structure in which dopamine is well-entrapped. Cytotoxicity assays showed a viability maintained to > 90 % with preserved growth and morphology [120], which was consistent with the excellent biocompatibility of polydopamine widely documented in the literature. Indeed, PDA-based nanosystems showed negligible toxicity on a wide set of cells tested *in vitro* (epithelial cells, endothelial cells, fibroblasts, osteoblasts, neurons, etc.), for which viability and proliferation ability were almost maintained to normal [47, 135-136]. In agreement with these *in vitro* assays, *in vivo* studies confirmed the excellent biocompatibility of PDA-based nanosystems used in various contexts [137-138]. For instance, PDA nanoparticles injected intravenously in rats showed a very low acute toxicity with a very high median lethal dose (about 500 mg/kg), nearly five hundred times the dose used for their photothermal therapeutic applications. Interestingly, long-term *in vivo* toxicity monitored over a one-month period after a single intravenous injection in mice or rats revealed that the animals remained healthy with no sign of behavior abnormalities; complete blood panel tests showed normal biochemical indicators with no detectable interference with the physiological regulation or immune response. Moreover, the histopathological examination did not show any sign of tissue damage, inflammatory, or fibrosis aspect with no detectable change in the cellular structures [47, 56]. These findings were in line with the results reported for melanin showing no noticeable toxicity detected within 30 days, after injection of high doses (up to 100 mg/kg) in mice [139]. Furthermore, multiple evidences indicated that polydopamine coatings, shown to be ultra-stable *in vivo*, can interestingly function as a biocompatible layer allowing to significantly attenuate the intrinsic toxicity of biomaterials in a material-independent manner. Indeed, several reports have highlighted the beneficial role of PDA coatings in reducing the inflammatory and immunological side responses and improving the biocompatibility of various materials including organic materials (like poly-L-lactic acid), metallic nanoparticles (like gold nanoparticles), quantum dots, etc. [52, 140-142]. PDA coatings also showed a beneficial role in promoting hemocompatibility and controlling cell adhesion and proliferation on substrates [143-144]. Increasing the hydrophilicity of the tissue-contacting interfaces was

proposed as an important factor responsible for the reduction of the *in vivo* side responses in PDA-coated biomaterials in contact of tissues or blood.

Beside their high biocompatibility, several findings reported in the literature led to the identification of polydopamine as a biodegradable material. Its naturally occurring analogue, *i. e*. eumelanin, is assumed to be metabolized *in vivo*, although the exact biodegradation pathways are not fully known yet. Langer's group revealed that synthetic melanin implants could be significantly resorbed within 8 weeks, which was attributed here to an uptake of melanin particles by macrophages and giant cells and to a further intracellular degradation process [145]. In fact, it has been demonstrated that both polydopamine and natural melanin undergo a hydrogen peroxide-mediated decomposition related to the oxidative cleavage of o-quinone-indole moieties leading to the formation of pyrrole-2,3-dicarboxilic acids (PDCA) or pyrrole-2,3,5-tricarboxylic acids (PTCA), depending on branching positions in covalent oligomers [42, 47]. This observation is highly interesting for the understanding of the possible biodegradation process of polydopamine, since hydrogen peroxide and other reactive oxygen species are endogenous components that can be produced majorly by NADPH oxidases, which are enzymes largely distributed in phagocytes and many organs [26, 47, 146]. This oxidation-induced process is generally accepted as a likely degradation pathway of polydopamine materials *in vivo*.

These intrinsic biocompatibility and biodegradability of polydopamine materials make them highly suitable for *in vivo* applications.

4.2. Nanomechanical properties

Nanomechanical properties of biomaterials and drug delivery systems are key parameters that influence their biological performance. In particular, nanoparticles elasticity has been recognized to play an essential role in directing nanoparticles biodistribution through impacting their blood circulation, tissue penetration, cell internalization, etc. [147-149]. The evaluation of nanoparticles mechanics is also of great interest for the understanding of their structural and functional properties. However, in the case of polydopamine nanomaterials, only few studies have dealt with the evaluation of polydopamine mechanical behavior, but were limited to PDA films and coatings. Mechanical studies performed on conventional polydopamine coatings revealed relatively high Young's modulus values of few GPa (~ 2 GPa to ~ 4 GPa), as measured *via* AFM nanoindentation or compressive film buckling experiments [150-152]. Such elasticity can reflect the good cohesion of polydopamine nanostructures and the ultra-stability of PDA coatings *in vivo*. Films elasticity was also

investigated using computational approaches. DFT simulations using models based on dimers of dopamine, dopaminochrome and DHI units predicted Young's modulus values ranging from 0.33 to 1.24 GPa, depending on molecules directions [150], while other *in silico* models generated from controllable covalent cross-linking of DHI units provided Young's moduli comprised between 4.1 to 4.4 GPa for the highest covalently cross-linked polymer model (70 %) [152]. Interestingly, increased elastic moduli could be obtained by increasing the inter-unit bonding *in silico*, suggesting that it is possible to enhance the mechanical strength of PDA materials through increasing the polymerization extent. Indeed, knowing that ~ 20 % of polydopamine structure is composed of unpolymerized monomers or partially polymerized oligomers, several relevant experimental studies demonstrated that increased robustness and enhanced mechanical performance of PDA coatings could be achieved through techniques allowing the enhancement of polydopamine cross-linking level and impacting eventually its cohesive structure. For example, the addition of copper ions [151], calcium cations or cross-linkers like genipin [150], heat treatment (up to 600 °C) inducing PDA carbonization [151], or thermal annealing at moderate temperatures (~ 130 °C) [153] resulted in increased Young's modulus values and allowed the production of highly stable PDA coatings resistant to delamination and dissolution, usually occurring under strong alkaline conditions for example. Controlling the experimental conditions of polydopamine synthesis and post-processing methods has thus a great impact on the mechanical properties of PDA materials and consequently on their stability and biological fate, but would considerably impact their physico-chemical properties.

Since it is generally accepted that polymeric nanomaterials would behave differently from their bulk counterparts, the investigation of the nanomechanical properties of PDA nanoparticles is of great interest for a better comprehension of their structural characteristics, but the first report investigating PDA nanoparticles nanomechanical properties has only been published very recently by our group [54] (Figure 4). In this study, we have evaluated the elasticity of polydopamine nanospheres and examined the impact of nanoparticles size on their Young's modulus, using AFM nanoindentation method. Interestingly, we found that the elastic modulus exhibited by PDA nanoparticles depended on their size, with average values of 188±42 MPa, 313±76 MPa, 365±59 MPa and 480±108 MPa for nanoparticles having average hydrodynamic diameters of 106±2 nm, 131±2 nm, 161±2 nm and 290±2 nm, respectively. The increased elasticity obtained when the nanoparticles size increases could be interpreted by the geometric packing order model described in details in the section 4.4. Indeed, based on this model and on pump-probe microscopy analyses, Warren's group [134]

suggested that bigger polydopamine nanoparticles would have higher geometric packing order between the stacked oligomers forming the core of the nanoparticles, which could interpreter the higher Young's modulus obtained for bigger nanoparticles in our study. Compared to other polymeric nanosystems such as PMMA, PS and PLGA nanoparticles, PDA nanoparticles showed Young's moduli of about one order of magnitude lower. This difference may be attributed to the different structures, intra-particulate interactions and assembly modes, and would be expected to correlate with a better biological performance, owing to less macrophages uptake and greater tumor accumulation [148-149].

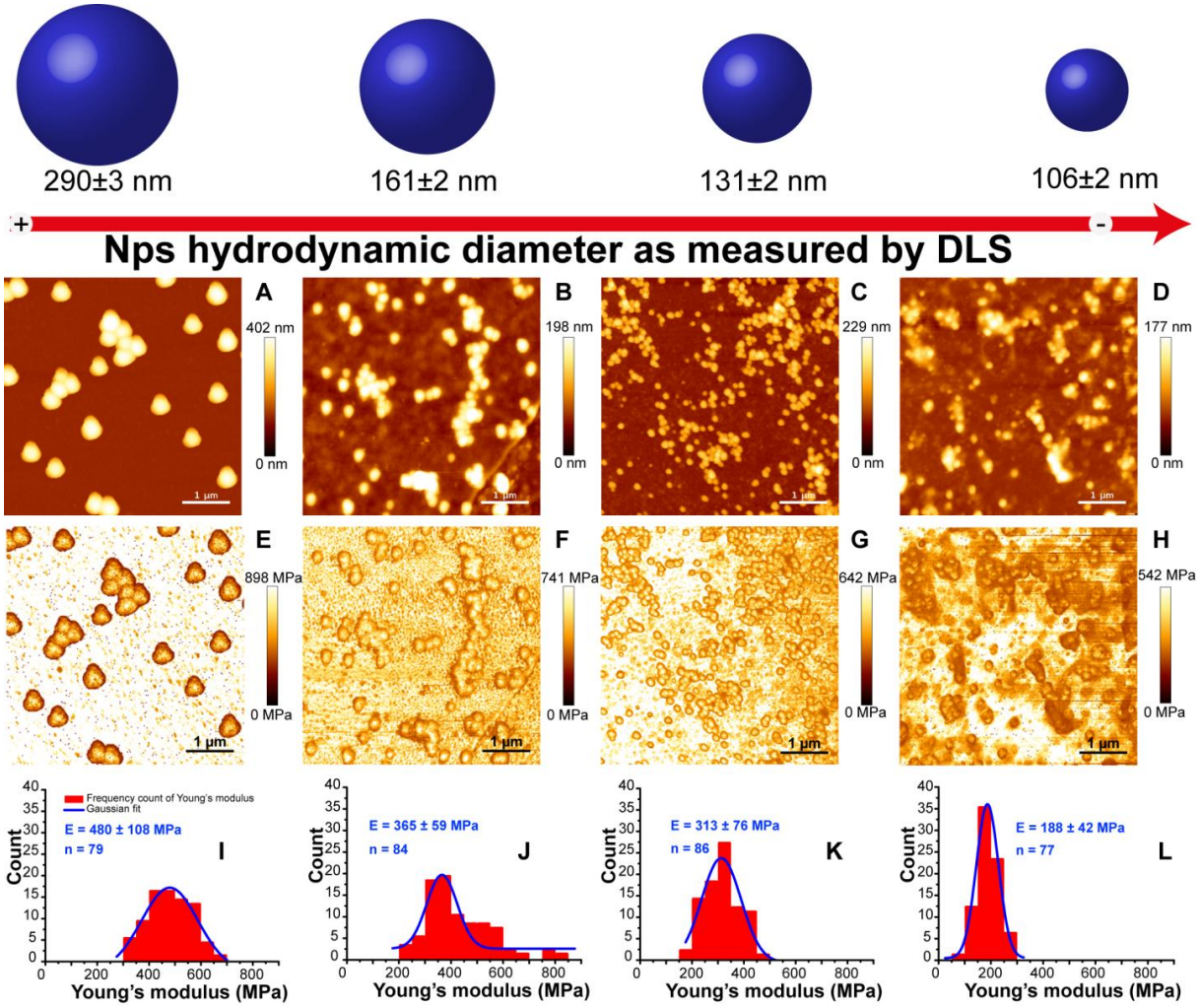

Figure 4. Nanomechanical study performed on PDA nanoparticles, (A-D) AFM height images in Tris buffer of covalently attached PDA NPs with different sizes on silanized mica substrates with their corresponding Young's modulus maps (E-H) obtained with JPK Quantitative imaging (QI) mode at a force setpoint of 35 nN and an indentation speed of 50 µm s^{-1}, (I-L) represent the histograms distribution of the Young's modulus of NPs with Gaussian fits [54].

4.3. Polydopamine chemical reactivity

As detailed in section 3, polydopamine is composed of heterogenous building units, which expose various reactive sites prone to a wide set of covalent, non-covalent and coordinate couplings with different types of materials and molecules (Figure 5) [23]. The catechol and amine functions, abundant in polydopamine, have been recognized as key features responsible for the high reactivity and strong adhesion of this material [154]. The major interactions reported for polydopamine adhesion mechanism and its reactivity will be discussed below.

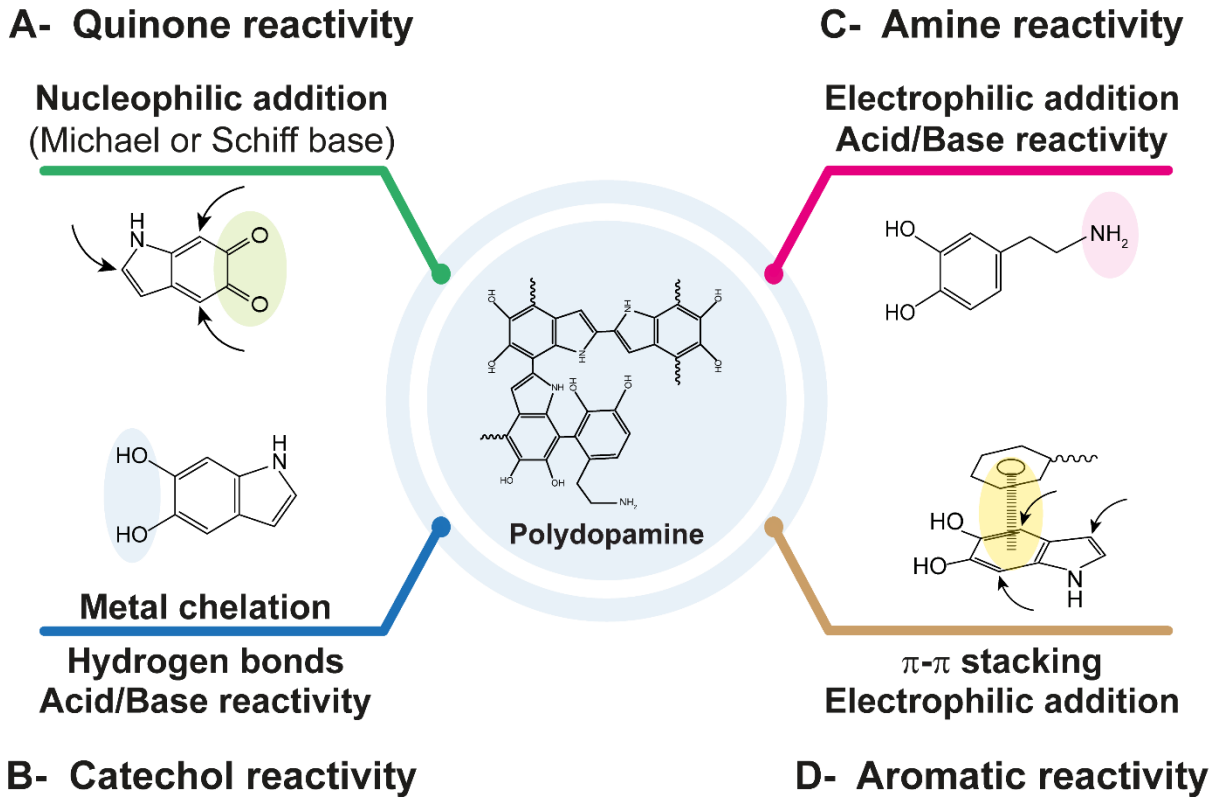

Figure 5. Most common interactions (covalent, non-covalent and coordination) involved in polydopamine functionalization.

4.3.1. Adhesive properties

Polydopamine is the first reported material that can strongly adhere to virtually all types, shapes and sizes of substrates, including noble metals, oxides, polymers, semiconductors, ceramics, low energy surface materials and superhydrophobic surfaces, etc. [18, 23]. It can interestingly form a firmly adherent layer likely owing to numerous extremely close anchoring points, which can be used to coat porous materials including metal organic frameworks (MOFs) and mesoporous nanostructures usually difficult to coat [24].

This strong interfacial adhesion allowed the design of diverse core@PDA shell nanocomposites (inorganic or organic nanoparticles, liposomes, etc.) in which the polydopamine layer, highly stable *in vivo*, can be used to enhance biomaterials

biocompatibility, serve as a bridge for secondary functionalization steps, or also be used for its therapeutic or theranostic potential as will be described later. Table 2 illustrates few examples of PDA-coated nanoparticles applied in cancer therapy and the role of PDA shell in the cited systems.

Table 2. Examples of nanosystems types modified by polydopamine and the role PDA shell in the proposed system

Coated core		Preparation method of PDA layer	Properties / Functionality of PDA layer	Application	Ref
Inorganic cores	Gold nanostructures, like gold nanorods	Tris buffer (10 mM, pH 8.5), [DA] = 1 $mg.ml^{-1}$, Vortex and sonication for 35 min	Thickness = 30 nm. Photothermal effects, Drug carrier for PDT (methylene blue) or CT (Doxorubicin).	PDT-PTT	[155]
	Au-Ag branched NPs	Tris buffer (10 mM, pH 8.5), [DA] = 0.04-0.22 $mg.ml^{-1}$, 3 h	Thickness = 6-34 nm. Photothermal effects, Prevention of the release of toxic metals from the NPs core, Enhancement of NPs biocompatibility, Preservation of the branched structure of the NPs.	Synergistic PTT	[156]
	Fe_3O_4 NPs	PBS buffer (10 mM, pH 8.5), [DA] = 0.12 $mg.ml^{-1}$, Shaking for 4 h	Thickness = 4 nm. Photothermal effects, Adsorption of dye-labeled single-stranded DNA (ssDNA), for the detection of mRNA for cancer diagnosis, Fluorescence quenching of the probe, hindering its off-target activation.	MRI and PA imaging-guided PTT	[157]
	MnO_2 NPs (Mesoporous NPs)	Tris buffer (10 mM, pH 8.5), [DA] = 1 $mg.ml^{-1}$, 6 h	Prevention of drug pre-leakage during circulation, pH-responsive drug release in the tumor acidic microenvironment, Anchoring of NH_2-PEG-FA (for anti-fouling properties and active targeting of tumor).	PDT-PTT	[158]
	$CaCO_3$ NPs	NH_4HCO_3 decomposed into CO_2 and NH_3 gas, ethanol, solution of Ca^{2+} and dopamine, Dopamine/$CaCl_2$ = 2/150 (m/m), 24 h	Thickness = 44 nm. Preparation of hollow PDA-$CaCO_3$ nanoparticles, Immobilization of a lipid bilayer of DOPA, DPPC, cholesterol and DSPE-PEG, Loading of the PS Ce6 and prevention of its photobleaching, pH-responsive drug release in the tumor acidic microenvironment,	Imaging-guided PDT	[78]

	Silica NPs (Mesoporous NPs)	Tris buffer (10 mM, pH 8.0), [DA] = 1.5 $mg.ml^{-1}$, 2.5 h	Photothermal effects, pH- and NIR-responsive drug release in the tumor microenvironment, Anchoring of SH-PEG-FA (for anti-fouling properties and active targeting of tumor)	Targeted Chemo/Gene/PTT	[159]
Organic cores	PLGA-TPGS NPs	Tris buffer (10 mM, pH 8.5), [DA] = 0.1 $mg.ml^{-1}$, 6 h	Thickness ~ 15 nm. Anchoring of SH-terminated aptamer (for active targeting of tumor and enhanced cellular uptake)	Targeted chemotherapy	[160]
	Liposomes (POPC)	Tris buffer (10 mM, pH 8.5), [DA] = 0.2 $mg.ml^{-1}$, 4 h, 40 °C	pH-responsive drug (5-FU) release in the tumor microenvironment, Stable and biocompatible coating	Chemotherapy	[161]
	DSPE-PEG micelles	Tris buffer (10 mM, pH 8.5), [DA] -, 6 h	Thickness ~ 4 nm. Photothermal effects, Conjugation of chemotherapeutic drug (Bortezomib), pH- and NIR-responsive drug release in the tumor microenvironment	Chemo/Photothermal therapy	[162]
	Polypeptides micelles (PEG_{45}-b-poly(L-cysteine)$_{20}$)	Tris buffer [DA] = 0.75 $mg.ml^{-1}$, 4 h	Thickness ~ 45 nm. Photothermal effects, NIR-responsive drug (Doxorubicin) release in the tumor microenvironment	Chemo/Photothermal therapy	[163]
Soft cores	Emulsion droplets (DMDES)	Emulsion of DMDES, Ammonia and SDS, Tris buffer, [DA] = 1.4 $mg.ml^{-1}$, 24 h, Ethanol for DMDES removal	Photothermal effects, Preparation of PDA nanocapsules, pH and NIR-responsive drug (doxorubicin) release in the tumor microenvironment	Imaging-guided chemo/Photothermal therapy	[74]
Drug assemblies	Doxorubicin NPs (DNPs)	PBS buffer (pH 8.5) [DA] = 0.75 $mg.ml^{-1}$, Overnight	Photothermal effects, Prolong blood circulation of DNPs and Prevent doxorubicin pre-leakage, pH and NIR-responsive drug release in the tumor microenvironment	Chemo/Photothermal therapy	[164]

PLGA: poly(lactide-*co*-glycolide), TPGS: d-α-tocopheryl polyethylene glycol 1000 succinate, PEG: polyethylene glycol, 5-FU: 5-fluorouracile.

This unique property is most likely the result of an interplay of chemical interactions involving two vital motifs present in polydopamine, *i. e*. catechol and amine functions, which represent also the major functionalities present in mussel adhesive proteins [95, 165]. Various covalent and non-covalent interactions can be engaged depending on the surface to coat. The catechol function is able to interact with a wide variety of substrates mainly *via* coordination bonding, bidentate chelating or bridged bonding and hydrogen bonding, etc. [27, 166]. More recently, the primary amine group has gained increasing attraction in the understanding of polydopamine strong adhesion. The vital role of primary amines was highlighted by Klosterman et al. who revealed that the addition of primary amines while forming polydopamine coatings increased this latter's adhesion properties [150]. Another evidence was brought by the observations revealing that mature particles do not exhibit a high adhesion capacity to surfaces, which was ascribed to the fewer amount of primary amines [25, 42], in comparison to the strong adhesion obtained when surface coating is performed during the early stages of polydopamine formation [25, 42]. Besides, it was found that poly(catecholamine) coatings exhibited a significantly higher adhesive strength (30-times) than that of poly(catechol) ones [154]. These findings suggest that polydopamine coatings grow progressively from the surface of the coated structure and the high cooperative adhesive action of these functional groups contribute to the resulting cohesive stable layer.

4.3.2. Metal binding ability

Catechol function is the major responsible of PDA affinity to several metal cations, including Fe^{2+}, Fe^{3+}, Cu^{2+}, Mn^{2+}, Pb^{2+} and multiple others. It can indeed strongly bind to multivalent metal cations through the *o*-diphenol functionality, and it exhibits a higher binding affinity compared to o-quinone [167]. This chemistry depends however on several conditions including the pH [56] or the affinity of catechol towards the metal ion. It should be noted that other functional groups present in polydopamine would also participate in metal chelating properties, such as amine, carboxylic and phenolic groups [30]. The polydopamine-metal coordination ability was explored for the preparation of diverse metal-organic frameworks (MOFs)[168-170] and has been considered of particular interest for the design of novel PDA-based theranostic systems. For instance, several magnetic resonance imaging (MRI)-guided nanoplatforms have been described in tumor imaging and were obtained through interaction of polydopamine with paramagnetic metal ions like Gd^{3+} [171], Fe^{3+} [56] or Mn^{2+} [172], leading to efficient MRI contrast nanoagents exhibiting high longitudinal relaxivity values in comparison to conventional contrast agents [30]. Such theranostic systems could be in fact

achieved either by loading/anchoring the metal cations onto PDA nanostructures [56, 173] or *via* coating metal oxide cores (like Fe_3O_4 or Mn_3O_4) with a PDA shell [138, 174].

It was found that the chelation of metal ions would induce their reduction and subsequent transformation into metallic nanoparticles bound to PDA surface, this was used for the *in situ* growth of Au [175] or Ag [176] nanoparticles on polydopamine surface. In addition, the catechol reactivity towards metal cations has been largely explored in polydopamine synthesis process as described in the section 1 and could be also used for the complexation of de-assembled PDA aggregates as a strategy to form cohesive robust PDA coatings [177]. Furthermore, it has been recently discovered that polydopamine nanoparticles can selectively kill cancer cells through a ferroptosis mechanism involving this metal complexation ability [135-136]. *In vivo*, biological melanins are also well-known for their affinity towards metal ions [178], which is used for instance for the sequestration of potentially cytotoxic transition metals [9].

4.3.3. Chemical reactivity

The high chemical reactivity of polydopamine is particularly interesting for the design of multifunctional nanosystems and can serve to extend polydopamine nanomaterials applications.

4.3.3.1. Covalent interactions

Catechol / Quinone reactivity (Figure 5A, B)

The catechol group, a central element in polydopamine reactivity, is in fact present in a chemical equilibrium with its corresponding quinone [95], and the reduced/oxidized state of the catechol/o-quinone system is of great importance to direct polydopamine reactivity. This equilibrium can be impacted by the solution pH, the presence of oxidants/reductants, or by exposition to relatively high temperature under air.

O-quinone systems, owing to the carbonyl function and Michael acceptor character, are prone to addition reactions of nucleophilic groups such as thiols and amines, *via* Michael addition (for thiols and amines) or Schiff-base condensation (for amines). The most favorable positions for such addition reactions depend on the type of the engaged nucleophile and on the quinone system (dopamine-quinone or indole-quinone). For instance, Michael addition of thiols or amines occurs preferentially *via* 1,4-addition while carbonyl reactivity with amines is preferentially a 1,2-addition type yielding the Schiff-base [25]. This chemistry is one of the most explored strategies used for the immobilization of (bio)molecules, such as polymers

[179-180], proteins [181-182] or small molecules [183], on the surface of polydopamine nanoparticles or shells (Table 3). This is mainly attributed to its simplicity (since the reaction can be simply conducted under mild alkaline aerobic conditions) and to its versatility (since amines and thiols are present in numerous molecules or can be easily introduced into them) [25]. Poly(ethylene glycol) (PEG) chains grafting is for instance often achieved using this o-quinone reactivity, allowing the formation of a hydrophilic antifouling coating on the surface of polydopamine nanoparticles or PDA-coated nanosystems, permitting to improve their colloidal stability, reduce their uptake by the reticuloendothelial system and prolong their blood circulation times [45, 184-185]. Also, tumor targeting molecules like folic acid [186], galactosamine [187] or EGFR antibody [188] could be grafted on PDA surface *via* this chemical route, in order to improve tumor accumulation for enhanced treatment efficiency and reduced side effects [30]. Few examples of the implementation of this chemistry are illustrated in table 3.

Table 3. Examples of Michael addition and/or Schiff base condensation reactions explored for the development of PDA-based nanosystems

Grafted molecule	PDA-based system	Reaction conditions	Applications	Ref
Thiolated poly(methacrylic acid) (SH-PMA) – pH cleavable hydrazine bond – Doxorubicin (DOX)	PDA NCs	pH 8.0 Overnight incubation In presence of TCEP (to prevent the oxidation of thiol groups)	Immobilization of DOX, Preparation of a stimuli-responsive DDS for an intracellular delivery of the anti-cancer drug	[179]
Thiol- or amine-terminated poly(ethylene glycol)	PDA NPs	≥ pH 8.0 Overnight incubations	Improvement of PDA NPs colloidal stability for i*n vivo* applications	[184, 189]
Thiol-terminated hydroxyethyl starch (HES)	PDA NPs	pH 10.0 24 h incubation	Improvement of the PDA NPs colloidal stability for i*n vivo* applications, using a coating with a favorable biocompatibility and biodegradability (superior to PEG-modified PDA NPs)	[180]
SH- PEG - folic acid (FA)	PDA-modified mesoporous silica NPs	pH 8.5 In presence of TCEP (to prevent the oxidation of thiol groups)	Grafting of a cancer targeting moiety for enhanced anti-tumor therapy efficiency	[190]
Folic acid (FA)	PDA-coated Au-Zein nanocomplexes	pH 8.5 1 h incubation	Grafting of a cancer targeting moiety for enhanced anti-tumor therapy efficiency	[183]
Galactosamine (amin-bearing tumor targeting moiety)	PDA NPs	pH 8.5 2 h incubation	Grafting of a tumor targeting moiety for specific liver tumor targeting	[187]

EGFR antibody	PDA-coated mesoporous silica nanoparticles	--	Grafting of a tumor targeting moiety for specific tumor targeting	[188]
Ovalbumin (amin-bearing tumor model antigen)	PDA NPs	Neutral conditions 5 h incubation	Grafting of a tumor antigen on PDA NPs for antigen delivery in tumor immunotherapy	[181]
Bovine serum albumin (BSA)	Graphene oxide/PDA hybrid nanosystem	pH 8.5 24 h incubation	Immobilization of BSA, serving as a molecular carrier for paramagnetic agents	[182]
Arginine	PDA NPs	Tris buffer 72 h incubation	Attachment and packing of *in situ* formed PDA nanoparticles on the surface of linoleic acid-arginine nanoemulsion droplets, used as templates for the preparation of PDA nanocapsules	[191]
Polyethyleneimine (PEI)	*In situ* formed polydopamine nanoparticles	--	Co-polymerization of dopamine and PEI for the preparation of fluorescent polydopamine nanoparticles, through the reduction of π-π interactions	[192]

NPs: nanoparticles, NCs: nanocapsules

Amine reactivity (Figure 5C)

In addition to the catechol/o-quinone system, the amine groups also contribute to the chemical reactivity of polydopamine through interaction with electrophilic moieties or exhibiting an acid/base reactivity [25]. For instance, amine functions present in PDA can interact with carboxylic groups to form an amide function *via* conventional carbodiimide chemistry reported as a drug coupling strategy [193], or serve as a reactive site for facile coupling of isothiocyanate-containing molecules that can be particularly used for PDA nanoparticles labelling. Moreover, an amine-mediated acylation reaction was employed to immobilize an ATRP initiator on PDA-coated particles allowing for a surface-initiated polymerization and controlled growth of polymer brushes from the particles surface [194]. Amines are also involved in aza-Michael-type addition which was used for polydopamine functionalization using acrylate/acrylamide molecules [195].

4.3.3.2. Non-covalent interactions (Figure 5B, D)

Due to the presence of catechol groups and pyrrolcarboxylic acids (acidic) on one hand and amines groups (basic) on the other hand, polydopamine displays a zwitterionic character with an isoelectric point of ~ 4 [45, 196]. Polydopamine can hence expose positive or negative charges depending on the medium's pH. This functionality was explored for the highly selective pH-responsive uptake and release of charged small molecules into PDA capsules [196], and represented an interesting approach for controlled drug loading and release in the drug delivery applications.

Beside electrostatic interactions, polydopamine assemblies are able to interact with diverse molecules through other non-covalent interactions, namely π-π stacking, hydrophobic effects and Van der Waals interactions and H-bonding. Indeed, the abundance of π-conjugated, aromatic and phenolic structures in polydopamine network allowed for multiple drugs, including doxorubicin [66, 197] and paclitaxel [198] or photosensitizing molecules like chlorin e6 [199] and indocyanine green [185, 197], to be loaded in the polydopamine matrix [66, 199] or bound onto polydopamine surface [197], affording thus PDA-based therapeutic platforms working as promising candidates for efficient cancer treatment.

4.4. UV-visible-NIR absorption properties

Unlike common organic products, synthetic eumelanin-like polydopamine displays a broad-band absorption extending over the whole UV-visible-NIR regions, and increasing monotonically towards high energies [9]. This unique profile has been reported before as a

characteristic optical feature for natural melanins (eu-, neuro-, allo- and pheo- melanins) [200-202]. The extinction coefficients calculated for the wavelengths ranging from 300 to 1000 nm for both polydopamine nanoparticles and melanin granules were found to be very close, especially for the smallest nanoparticles [45]. Based on these spectral similarities, analogies were made between the two resembling materials for a better interpretation of polydopamine optical properties.

For eumelanin, contrary to what has been though at first, the broad-band absorption does not originate from scattering phenomena [203] but corresponds effectively to an intrinsic light absorption. Indeed, based on accurate measurements of the optical scattering coefficient, it was found that the contribution of Rayleigh scattering is lower than 6 % of the total optical attenuation in the 210 to 325 nm region and is undetectable for the wavelengths ranging between 325 and 800 nm [201]. Similarly, Warren et al. confirmed recently that, for polydopamine also, the optical spectrum reflects real absorption and is not significantly altered by scattering effects [134].

The "chemical disorder model" is accordingly one well-accepted explanation of this broad absorption band characterizing eumelanin and synthetic eumelanin-like materials, particularly polydopamine [202, 204]. In this model, the monotonic absorption profile is the consequence of the overlapping of different absorption bands associated to ensembles of chemically distinct species present in the material network [202].

Although the chemical disorder model can be used for the understanding of the broad absorption, the structural complexity at the origin of such absorption can not only be related to the chemical heterogeneity at the level of fundamental building units but also to the hierarchical assembly configurations (at secondary/supramolecular level), which produce a wide series of Highest Occupied Molecular Orbital (HOMO) – Lowest Unoccupied Molecular Orbital (LUMO) gap energies, resulting in the monotonic featureless broad absorption band [26, 204]. In this context, few models have been suggested to interpret the unique absorption profile of natural or synthetic eumelanins. Indeed, the oxidation/reduction dynamics among eumelanin-like oligomers and the aggregation-dependent interchromophoric interactions were presented as important factors perturbing π-electron delocalization [205-206], resulting in different HOMO-LUMO gaps. The oxidized forms were admitted to have lower HOMO-LUMO gap energy, thus leading to a broadening of eumelanin absorption band.

More recently, the geometric order / disorder model emerged as another key factor to consider in the interpretation of the broad absorption of eumelanin and polydopamine. The significant contribution of non-covalent interactions in the assembly process of polydopamine, including

π-π stacking, π-cation interactions and charge transfer, has been well-established using experimental and computational structural investigations. Since π-electron density of eumelanin-like oligomers is an important parameter impacting their absorption profiles, the proximity between oligomers but also the packing between stacked oligomers would impact the absorption spectrum of the assembled structure [134, 206-208]. Chen et al. showed that the excitonic effects of the eumelanin aggregated stacked oligomers (protomolecules) has a great role in the broad-band absorption. The protomolecules being in different sizes and randomly oriented, the interplay of the geometric order / disorder in the aggregated eumelanin structures would result in random and significant excitonic couplings through the formation of electron-photon pairs, leading to the broadening of the absorption chromophore band along with the enhancement of the absorption towards higher energies [207]. The contribution of aggregation and structural scaffold disorder, as well as the redox dynamics, in the eumelanin chromophore broad band were also investigated and confirmed by Micillo et al. [208].

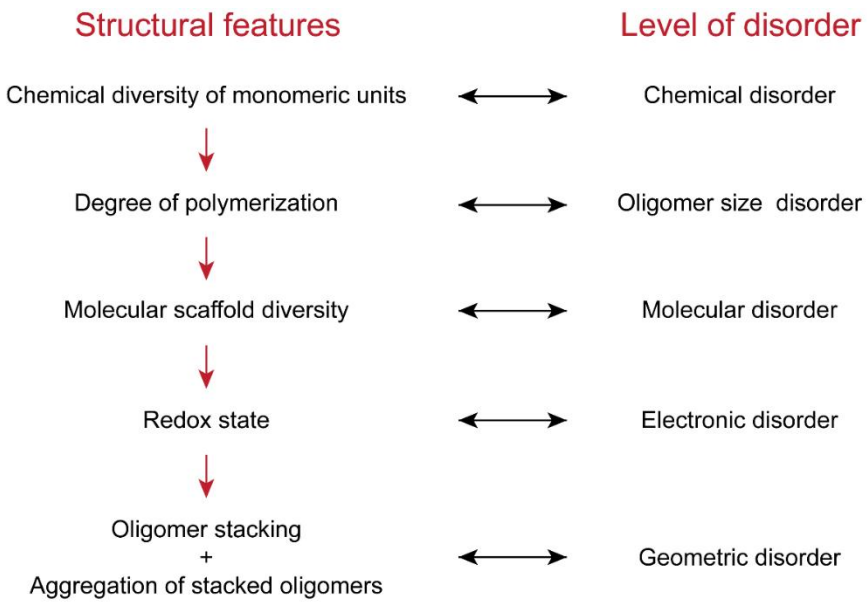

Figure 6. Simplified scheme of chemical disorder levels in eumelanins realized through structural definitions at multiple length-scales in the hierarchy of the material (adapted from [127])

These findings were reinforced very recently by Warren's group [134] who conducted an in-depth investigation of the optical properties of eumelanin-like nanoparticles, originating from dopamine or DOPA, by means of pump-probe microscopy technique, which allowed to reveal features of individual absorption bands. Considering that polydopamine nanoparticles originate from a multi-step process consisting in (i) the formation of oligomeric building blocks, (ii) their consecutive stacking followed by (iii) the aggregation of these stacked

oligomers, the authors examined the absorption features at these different assembly levels (Figure 7). It was found here that low molecular weight (LMW) subunits present higher UV absorption compared to larger fragments, while high molecular weight (HMW) fractions showed an enhanced absorption at the visible and NIR wavelengths compared to LMW units. A possible explanation suggested that HWM fractions would be composed of higher MW oligomers, leading to more extended π-electron delocalization within oligomers and thus to a lower HOMO-LUMO gap energy. A higher stacking order between oligomers of different HOMO-LUMO gaps would enhance the absorption at low energies [134, 209]. Interestingly, the authors revealed that HMW fragments exhibited different absorption behavior compared to their parental nanoparticles. This implied that a change in the electronic structure would occur when the stacked oligomers aggregated to form the nanoparticle. A size-dependent absorption was also found for PDA nanoparticles; larger nanoparticles displayed higher absorption at longer wavelengths compared to smaller ones. Based on these observations, Warren's group concluded that, in addition to the chemical diversity model and the fundamental oligomers' π-electron delocalization, the geometric packing order of the protomolecules in eumelanin-like systems is a key determinant in the broad-band absorption of the final aggregated assembly; it may impact the interactions between oligomers changing thus the absorption behavior. The number of stacked oligomers would impact the geometric preference, which results in the size-dependent absorption profiles. The higher absorption observed at longer wavelengths for large nanoparticles in comparison to smaller ones was also reported by Wang et al. [96]. It should be noted, that the geometric packing order model detailed by Warren's group is well-adapted to interpreter the size-dependent properties of PDA nanoparticles, namely the nanomechanical [54] and photothermal properties [96], as will be discussed later.

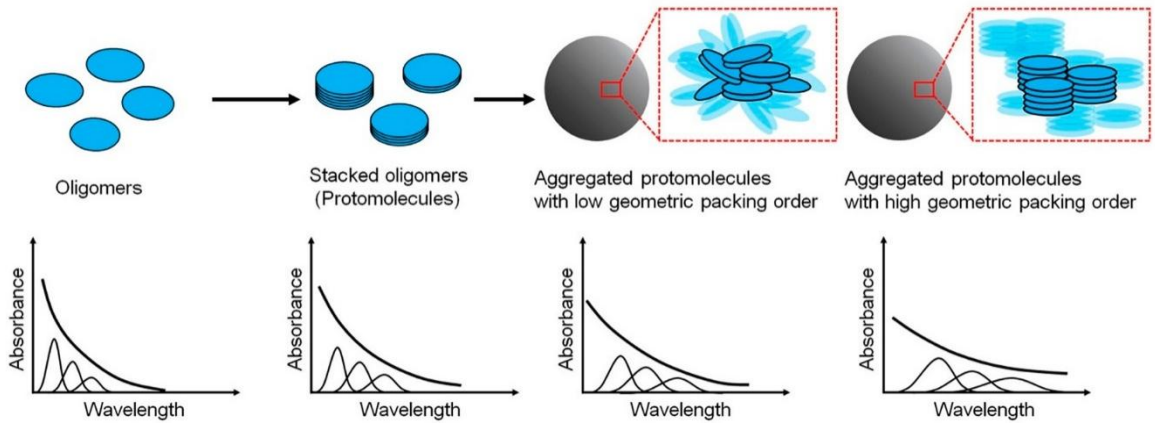

Figure 7. Structure-property relationship proposed by Warren's group for melanin-like materials including polydopamine, based on the geometric disorder model. The hierarchical assembly would play a role to extend the broad absorption band to low energies (adapted with permission from [134]).

4.5. Fluorescence emission properties

An investigation of the absolute radiative quantum yields of synthetic eumelanin was performed by Meredith et al. and showed that more than 99.9 % of the absorbed light in the UV and visible regions was dissipated through non-radiative relaxation mode [210], which concurred with previously reported findings revealing an extremely low emission quantum yield (Φ_r as low as 0.003) [211-212]. Comparably to other synthetic eumelanins, very weak emission spectra were reported for conventionally-prepared polydopamine nanoparticles [213]. Similar to self-assembled organic chromophore systems, the stacking of fundamental oligomers and the subsequent aggregation in PDA nanomaterials were proposed to be at the origin of the observed self-quenching effects [213].

Interestingly, although very weak, the emission of synthetic eumelanins showed a clear dependency of the position, width, intensity and quantum yield on the excitation energy, which is an uncommon feature for organic materials. Lower excitation energies led to lower radiative emission, with for example a four-fold increase of the quantum yield at a 250 nm excitation compared to 500 nm [210, 214]. A 3D map of specific quantum yields variation as a function of excitation and emission wavelengths was developed to help understand the photophysical and structural properties of eumelanin-like materials [214]. The photoluminescence was proposed to arise from different HOMO-LUMO gap energies related to oligomers of chemically distinct species, supporting hence the chemical disorder model described above [210]. This hypothesis was supported in other reports which related eumelanins emission properties to the chemically distinct oligomeric units that can be selectively excited at different excitation wavelengths [214-215]. These interpretations can be also applied to polydopamine [26].

Furthermore, size-dependent emission spectra and yields were obtained for eumelanin samples [211]. The small eumelanin aggregates exhibited higher emission yields with longer emission decay times (> 1 ns for < 1000 Da) compared to larger ones (< 1 ns for > 10000 Da). Also, it was found that energy transfer occurs both within but also between the fundamental building units. Thus, the aggregation state, responsible for eumelanin-like materials buildup, was proposed as another determinant factor in this photophysical property [211-212].

Interestingly, several groups have shown that fluorescent polydopamine nanomaterials can be made by tailoring polydopamine synthesis or post-processing conditions. Endowing polydopamine products with luminescence properties can be indeed of great utility for the development of nanosystems used in medical imaging or fluorescence bioimaging-guided therapies. Different fabrication strategies have been developed in order to achieve the desirable photoluminescence properties of polydopamine and were categorized, by Yang et al. [216], into four strategies consisting in polydopamine (i) chemical oxidation [217], (ii) degradation [218], (iii) conjugation [192] or (iv) carbonization [219]. These strategies were mainly based on the reduction/weakening of the π-π interactions present in polydopamine scaffold or on the reduction of dopamine polymerization degree, hindering hence the aggregation-caused quenching effect, or also on the creation of distinct sp^2 and sp^3 hybridized carbon atoms, introducing thus the fluorescence properties.

For instance, the oxidation of polydopamine particles using hydrogen peroxide has emerged as a facile novel method allowing the synthesis of fluorescent organic nanoparticles with a tunable fluorescence emission [220-222]. Interestingly, the obtained PDA nanoparticles displayed two-photon fluorescence properties under NIR light excitation, which permits to reach a superior penetration depth during tissue bio-imaging. The same route was also reported for the preparation of fluorescent PDA shells and the development of fluorescent PDA nanocapsules [35]. Besides, based on the high ROS rates, and particularly H_2O_2, in the tumor microenvironment in comparison to normal tissues, PDA oxidation-mediated fluorescence generation can be explored for tumor diagnosis / operation applications [221].

4.6. Photothermal and Photoacoustic properties

Due to their intrinsic fluorescence self-quenching effect, polydopamine products are able to generate heat when they are photo-excited. This is because the repopulation of the ground electronic state occurs predominantly through non-radiative relaxation and the majority of the absorbed energy is released as heat via vibrational relaxation [95]. Indeed, a transient pump-probe analysis performed on eumelanin-like samples showed a very rapid ground-state bleaching with about 90 % of the absorbed energy dissipated as heat, within a relaxation time of 20 ps [212].

This characteristic feature, together with the broad light absorption band, paved the way for the eumelanin-like polydopamine nanomaterials to be investigated as potential agents used in hyperthermia-mediated therapy called “photothermal therapy” (PTT). This therapeutic approach is in fact based on the administration of a light-heat converting agent followed by

the illumination of the targeted site with a localized laser. The heat generated locally by the photothermal agent, upon its photo-excitation, is used to kill abnormal cells nearby. PTT has been largely explored in the past years as a minimally invasive therapeutic method showing promising results in efficient tumor ablation, but also in other applications such as multi-resistant bacterial infections treatment. This method is recognized as a particularly advantageous treatment modality, compared to the conventional cancer therapies owing notably to the spatio-temporal controllability which allows improved target selectivity and minimal side effects, with subsequent efficiency enhancement [30]. The photothermal agents currently available are mainly consisting in metallic nanoparticles, particularly Au nanoparticles, and few carbon-based nanosystems. However, these nanoagents usually suffer from long-term biosafety, compromising their clinical implementation [47]. The application of biocompatible and biodegradable materials in photothermal therapies is hence of great interest for the *in vivo* biomedical applications.

Liu et al. have introduced, for the very first time, melanin-like polydopamine nanoparticles as a powerful photothermal agent fulfilling all the requirements for an *in vivo* PTT application [47]. Colloidal PDA nanospheres displayed a strong NIR photo-absorption, with a molar extinction coefficient of $\varepsilon_{808\ nm} = 7.3\ 10^8\ M^{-1}.cm^{-1}$ (for a nanoparticles size of 70 nm), which is relatively high in comparison to values reported for multiple photothermal agents such as carbon nanotubes ($\varepsilon_{808\ nm} = 7.9\ 10^6\ M^{-1}.cm^{-1}$) [47]. A strong absorption in the so-referred-to "photo-therapeutic window" (650 nm – 850 nm) is in fact highly interesting for clinically relevant photothermal applications. In this optical window, there is a minimal interference of biological chromophores absorption or scattering effects and a maximal penetration depth of the incident light is enabled [31, 223].

The photothermal conversion efficiency is another key parameter indicative of the photothermal agents' efficiency. In the case of PDA nanospheres of 70 nm, the photothermal conversion efficiency was found to be about 40 % [47]. This value is interestingly high compared to the most common PTT agents, such as gold nanorods, widely reported for cancer treatment, which exhibit a photothermal conversion efficiency of 22 % [47]. Indeed, upon 500 s of illumination with an 808 nm laser at 2 $W.cm^{-2}$, these PDA nanospheres dispersed at 200 µg/ml induced a temperature increase of the suspension of almost 34 °C. This result is very satisfying for high-temperature hyperthermia-mediated tumor ablation, since it is accepted that cancer cells, which are more sensitive to hyperthermia than normal cells [224], can be killed when the surrounding temperature increases to values > 50 °C for 4-6 minutes, or 42-45 °C for 15-60 min [225].

These findings were later confirmed by several groups who reported a temperature increase of a similar order of magnitude. The generated temperature increased in a concentration- and laser power-dependent manner [56, 66, 193, 226-227]. Similar to the colloidal nanospheres, multiple PDA-based nanostructures, such as PDA shells [228-230], polydopamine dots [231] and mesoporous polydopamine nanostructures [232], showed excellent photothermal properties relevant to polydopamine nanostructure. In the case of core@PDA shell systems, an improved photothermal effect could be obtained by increasing polydopamine shell thickness [228-229].

Although the photothermal properties of polydopamine materials have been demonstrated by several groups, a full understanding of this photothermal conversion ability is still lacking. Particularly, to the best of our knowledge, no work has yet studied in depth the impact of PDA nanoparticles size on their photothermal conversion efficiency. In one recent study, Wang et al. have briefly revealed a dependency of the solution temperature increase on the size of PDA nanoparticles; larger nanoparticles induced higher temperature increase compared to smaller ones. This result was attributed here to the higher absorption in the NIR region (808 nm) observed for larger nanoparticles [96]. A similar result was also reported for mesoporous polydopamine nanoparticles [232]. These findings could be interpreted by the geometric packing order / disorder model and the aggregation state of the stacked oligomers forming PDA nanoparticles, as explained before: bigger polydopamine particles would exhibit a higher geometric packing order [134], and thus higher excitonic effects, NIR absorption and quenching effects, leading to the stronger heat generation.

Interestingly, when PDA nanoparticles were subjected to a long-time laser illumination (2 $W.cm^{-2}$ for 1 h) [47, 56] or repeated illumination-cooling cycles (up to five cycles) [189, 226] they showed a high photo-stability as evidenced by the stable temperature increase obtained at the different cycles, by the stable absorption features and by the absence of morphological changes before and after illumination. Such property is crucial for the maintenance of efficient light absorption during NIR irradiation, and renders polydopamine-based nanostructures superior to gold nanoparticles, largely reported in PTT applications, which undergo morphological changes resulting in decreased light absorption during NIR activation [47].

The excellent photothermal stability during cyclic irradiation, along with the strong light absorption and great photothermal activity and conversion efficiency, suggested that PDA nanoparticles would be of a great potential in photoacoustic imaging (PAI) applications. This technique is in fact an emerging bio-imaging method allowing to dynamically monitor the

biodistribution and tumor retention of injected systems and offering a high tissue penetration depth, spatial resolution and sensitivity. It relies on pulsed illumination of a photo-thermal converting agent, the heat generated by this latter would thermo-elastically generate pressure waves detected using an ultrasound transducer [30, 233]. The combination of photoacoustic and photothermal effects in a single system would be highly interesting for photoacoustic imaging-guided cancer photothermal therapy applications, offering hence a desirable theranostic platform [234]. Aqueous PDA nanoparticles suspensions exhibited a concentration-dependent photoacoustic performance and interestingly photoacoustic signals could be detected even at concentrations as low as 15 $\mu g.ml^{-1}$. *In vivo* assays revealed the excellent photoacoustic contrast generated by polydopamine nanoparticles and tumor-targeted PDA nanoparticles enabled significant illumination of the tumor site with a clear margins delineation. Several other studies followed and confirmed the great potential of polydopamine-based nanosystems for PAI applications [137, 232, 235-236]. PDA-coated nanostructures were also proven to exhibit excellent photoacoustic properties. For instance, 200 nm-sized PDA hollow nanocapsules dispersed at 200 $\mu g.ml^{-1}$ exhibited a slightly higher photothermal conversion efficiency (40.4% versus 37.1%) and over two-folders higher photoacoustic imaging ability in comparison to PDA nanospheres of similar size and at similar concentration [74]. The higher photoacoustic signals were attributed to the higher photothermal conversion ability, but also to the hollow structure favorable for harmonic imaging enforcing the ultrasonic signals.

5. Application of PDA nanomaterials in cancer therapy

5.1. Drug delivery applications

The administration of free anti-cancer drugs usually encounters several limitations, including particularly solubility issues or a non-specific biodistribution leading to a poor drug bioavailability and severe side effects [30]. In order to overcome these limitations, diverse drug delivery nanosystems have been developed with several successful clinical implementations, benefiting from their passive tumor accumulation *via* the EPR effect [237]. In this context, owing to its high chemical reactivity resulting in high drug payloads and its multi-drug loading ability, PDA-based nanostructures have received considerable attention as drug carriers allowing drug/gene delivery for efficient cancer treatment. Moreover, when the anti-cancer drug is physically loaded on the nanocarrier, the H-bonding and π–π interactions generally established between polydopamine and the loaded drugs tend to be disrupted or weakened under acidic, oxidative or also reductive conditions. Therefore, PDA nanostructures

would benefit from the intrinsic tumor microenvironment characteristics (*i. e.* weakly acidic pH, high amounts of hydrogen peroxide and of glutathione) and function as stimuli-responsive drug delivery systems [30]. Moreover, taking advantage of the endocytosis-mediated internalization process of PDA nanoparticles demonstrated by Ding et al. [238], drug release can be triggered in the acidic endosomal and lysosomal compartments allowing the intracellular delivery of the anti-cancer drug. Additionally, the hyperthermia generated by polydopamine upon its NIR illumination could also be explored to achieve an on-demand NIR-triggered drug delivery, as a result of weakened interactions with the loaded drug under heat [239].

In view of such features, PDA-based nanomaterials have been largely explored as drug nanocarriers, few examples are cited in table 4. They showed excellent results in preventing the premature drug release during circulation and inducing enhanced release rates after tumor internalization, compared to pristine or other nanoparticles. PDA nanocapsules and mesoporous PDA nanoparticles are particularly promising candidates for drug delivery applications, owing to their high payload capacity [191]. Regarding the PDA-coated structures, polydopamine coatings can serve either as the drug nanocarrier composite [240], controlling the thickness of PDA shell allows here to control the drug loading rate, or serve as a "gate keeper" for a controlled drug delivery, owing to its stimuli-responsiveness [241].

PDA-based nanomaterials were in fact not only applied for the delivery of chemotherapeutic drugs, but were also extended to antigen delivery for anti-tumor immunotherapy [181]. They have emerged also as nanocarriers for photosensitizing agents used in photodynamic therapy (PDT).

Table 4. Examples of PDA-based nanoplatforms used for mono- or multi-modal cancer therapy

Nanosystem configuration	Targeting moiety	Cargo	Applications	Properties	Testing stages	Ref
PDA NPs	Ovalbumin (tumor model antigen)	--	Immunotherapy	vaccine delivery	*in vitro:* C57BL/6 (murine colon cancer) *in vivo:* colon-cancer model	[181]
Fe_3O_4-PDA NPs	Bortezomib (BTZ)	--	CT, MRI guidance	pH-responsive drug release: -at pH 7.4: 1.7 μM in 10 h -at pH 5.5: 4.7 μM in 10 h -at pH 4.0: 5.0 μM in 10 h	--	[242]
Magnetic Nanocrystal Clusters (MNCs) @ PDA shell	Cisplatin	--	CT, Magnetic guidance	pH-responsive drug release: -at pH 7.0: 38% in 24 h -at pH 5.0: abrupt release	*in vitro*: HeLa cells (human cervical cancer), MCF-7 cells (human breast adenocarcinoma)	[240]
Mn / SS /PEG-PDA NPs	Doxorubicin (DOX)	--	CT MRI guidance	pH and redox-responsive DOX release -at pH 7.4: 20% in 24 h -at pH 5. : 40% in 24 h -at pH 7.4 + GSH: 45% in 24 h -at pH 5.5 + GSH: 70% in 24 h	*in vitro*: 4T1 cells (breast cancer), HeLa cells, K7M2 (murine osteosarcoma) *in vivo*: 4T1-bearing tumor mice (breast cancer model)	[243]
PDA-modified MSNs	DOX	Folic acid (FA)	Targeted CT	pH-responsive DOX release: -at pH 7.4: 28.5% in 190 h -at pH 5.6: 38.3% in 190 h -at pH 2.0: 49.5% in 190 h	*in vitro*: HeLa cells *in vivo*: HeLa-bearing tumor mice (cervical cancer model)	[190]

PEG-PDA NPs	Doxorubicin (DOX)	Triphenyl-phosphonium	Targeted CT	Mitochondria-targeted drug delivery for overcoming cancer drug resistance	*in vitro*: MDA-MB-231 cells (human breast adenocarcinoma)	[244]
PDA-coated CPT nanocrystals	Camptothecin (CPT)	Peptide XQ1	Targeted CT	Improved solution dispersion and stability of CPT nanocrystals, Rapid cross-membrane translocation and high intracellular drug delivery pH-dependent drug release	*in vitro*: A549 cells (human adenocarcinoma lung), HeLa cells	[245]
PDA-PEG NPs	DOX, 7-ethyl-10-hydroxycamptothecin (SN38)	--	CT, PTT	pH-responsive drug release: *DOX & SN38, respectively: -at pH 7.0: 5.2% & low in 12 h -at pH 5.0: 14.5% & 25.3% in 12h NIR irradiation-responsive drug release: *DOX & SN38, respectively: -No laser: 5.2% & 12.2% -30 min irradiation: 23.1% & 58.6% H_2O_2-responsive drug release	*in vitro*: MCF-7 cells, PC-9 (non-small-cell lung cancer) *in vivo*: PC-9 cells-bearing mice	[239]

CT: Chemotherapy, NPs: nanoparticles

5.2. Light-mediated cancer therapies

Considering their outstanding photophysical properties, their colloidal stability and their superior biocompatibility and biodegradability, polydopamine-based nanosystems are emerging as attractive photothermal converting and photoacoustic-contrast agents and gaining an increasingly growing interest for efficient tumor ablation in PTT-based cancer therapy. Coupling PDA nanoparticles to photoactive molecules also known as photosensitizer, would present several advantages for cancer therapy. Indeed, PDA nanoparticles may play the role of nanocarriers of the photosensitizers with a high payload. Moreover, this enables the design of bifunctional light activated nanoplatforms with subsequent photothermal effect (PPT) and photodynamic effect (PDT). Such combination would allow a more efficient and synergistic treatment modality of cancer. In the following section, we will first introduce the photothermal therapy and photodynamic therapy, and then we will develop the various strategies that can be adopted for the design of PDA based nanoparticles with bifunctional PTT/PDT applications. In addition, the interests and limits of the bifunctional nanoplatforms in cancer therapy will be also emphasized and discussed.

5.2.1. PDA nanoparticles for photothermal therapy

Liu et al. demonstrated the high photothermal efficiency of PEGylated PDA nanoparticles *in vitro* and *in vivo*, on a colon cancer model [56]. Significant tumor growth suppression was obtained following NPs intravenous injection into SW620-bearing mice and illumination using an 808 nm laser at 1.3 $W.cm^{-2}$ for 6 min.

Various strategies have been employed to further enhance the photothermal effects obtained with polydopamine for an improved therapeutic efficacy.

Light absorbing molecules like indocyanine green (ICG) or IR820, can act as “thermal-enhancement agents” [246]. They would result in an increased NIR absorption and their association to PDA nanomaterials has been described in several studies and resulted in enhanced photothermal performance and therapeutic outcomes. For instance, the association of the FDA-approved photosensitizing molecule ICG with polydopamine has been investigated for PAI-guided photothermal cancer treatment [235, 247]. The loading of ICG into polydopamine allowed to significantly increase the system’s NIR light absorption, up to 13 times higher at 780 nm. In return, polydopamine quenched the fluorescence of ICG and prevented its photobleaching, and lead to an improved stability under its laser irradiation. The hybrid nanoplatform exhibited an amplified photothermal effect with a temperature increment

exceeding 14 °C in presence of ICG in comparison to the pristine system (after illumination at 808 nm, 0.6 W.cm^{-2} for 5 min, 20 µg.ml^{-1}), as well as an improved photoacoustic contrast (Figure 8). The nanosystem represented hence a promising phototheranostic nanoagent achieving a complete tumor suppression with a low laser density, as evidenced by *in vivo* experiments.

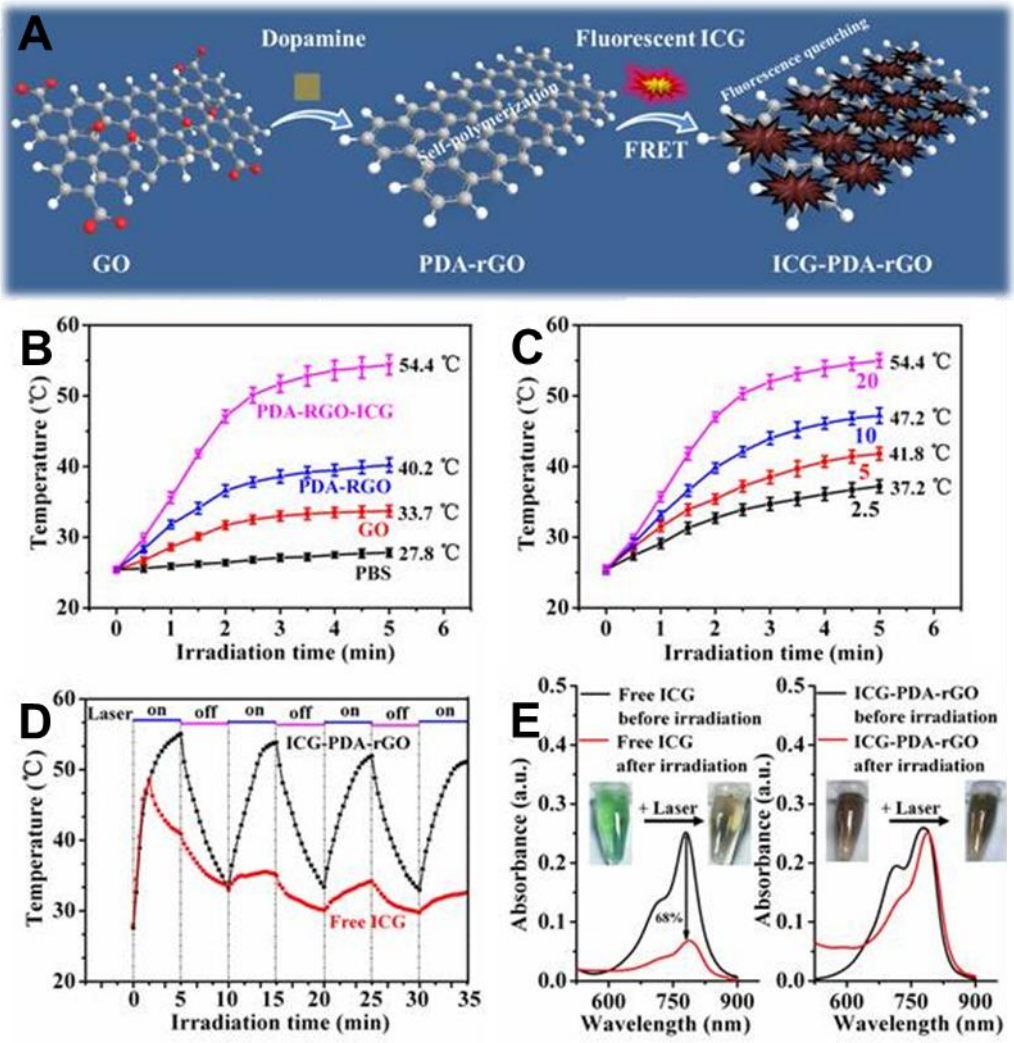

Figure 8. ICG-loaded polydopamine-reduced graphene oxide (rGO) nanocomposites with amplified photothermal and photoacoustic effects for cancer theranostics, (A) Schematic illustration of the preparation process of ICG-PDA-rGO, (B) Photothermal heating curves of PBS, GO, PDA-rGO and ICG-PDA-rGO solutions, CGO=CPDA-rGO=CICG-PDA-rGO=20 mg.l^{-1}, (C) Photothermal heating curves of ICG-PDA-rGO solutions of different concentrations , (D) Temperature evaluation of ICG-PDA-rGO and equal free ICG solutions over four laser ON/OFF cycles. (laser ON time: 5 min, laser OFF time: 5 min), (E) UV-vis absorption spectra of free ICG and ICG-PDA-rGO solutions before and after four cycles of laser irradiation at 808 nm and 0.6 W.cm^{-2}. (Printed with permission from [235]).

The coupling of metal ions, like Cu^{2+} and Mn^{2+}, to PDA nanostructures allows not only to perform bio-imaging but also to achieve amplified photothermal effects [34, 248]. Cu^{2+}-loaded PDA nanoparticles were proposed by Ge. et al. as an efficient MRI-guided therapeutic

nanoagent [248]. Indeed, in presence of Cu^{2+}, a four-fold increase in PDA nanoparticles molar extinction coefficient was obtained, accompanied with a significantly enhanced photothermal conversion efficiency reaching 54.8 % for CuPDA against 37.6 % for PDA nanoparticles of a similar size (51 nm). Laser irradiation of a 75 $\mu g.ml^{-1}$ nanoparticles suspension at 808 nm and 3.5 $W.cm^{-2}$ induced a temperature increase of 51.5 °C for CuPDA versus 42.2 °C for PDA nanoparticles. Interestingly, the nanocomposite displayed a pH-responsive release of copper ions allowing their efficient delivery in the tumor tissue. The released ions exhibited a synergistic chemotherapeutic cancer cells killing effect.

Enhanced photothermal effects could also be obtained through the combination of PDA nanostructures to other photothermal converting agents. In this perspective, PDA-Au nanohybrids represent promising materials that benefit from the plasmonic photothermal activity of gold nanosystems along with the interesting photothermal conversion properties of polydopamine. For instance, Wu et al. fabricated an injectable thermoresponsive poly(N-acryloyl glycinamide-co-acrylamide) hydrogel containing PDA-coated gold nanoparticles and the anti-cancer drug doxorubicin, and serving as a breast filler for efficient prevention of breast cancer recurrence [249]. This nanocomposite exhibited an intriguing photothermal activity arising from the combination of both gold nanoparticles and polydopamine coating. Interestingly, a red shifting was observed in the gold nanoparticles absorption spectra upon modification with polydopamine, suggesting a higher photothermal efficiency. A pronounced temperature increase was obtained, with a ΔT reaching 43 °C after a 5 min irradiation with a 808 nm laser at 2 $W.cm^{-2}$.

In another example, the biocompatible graphene oxide (GO) was utilized in association to polydopamine, owing to its "intrinsic high NIR light absorption" and photothermal conversion ability. It was suggested that polydopamine would restore a part of π conjugation in GO through the reduction of this latter, generating stable reduced GO (rGO), characterized by its higher NIR light absorption and enhanced photothermal activity. This association is thereby very suitable for PTT applications, explaining the interesting temperature increase revealed in several studies for the PDA/GO nanohybrids [188, 235, 250].

5.2.2. PDA as nanocarriers of photosensitizers for photodynamic therapy (PDT) applications

PDT is a potent light-based therapeutic modality clinically approved for cancer treatment [251] and is based on the use of a photosensitizer (PS), a light-absorbing compound, which photo-activation at an appropriate wavelength, leads eventually to the generation of reactive

oxygen species (ROS) that are cytotoxic. Indeed, following the PS administration, the near infrared (NIR) irradiation of the tumor site induces the photo-excitation of the PS to an excited singlet state. The excited PS can then re-gain its fundamental state either directly through fluorescence emitting or *via* conversion to a triplet state, a lower energy excited state, through an intersystem crossing. At this state, the PS can interact either with nearby substrates through electron transfer to eventually produce free radicals (type I PDT reactions) or with molecular oxygen through energy transfer to generate singlet oxygen that is highly cytotoxic (type II PDT reactions) [233]. Although highly promising, PSs usually suffer from poor water solubility limiting their bioavailability and therapeutic efficacy, which renders interesting their encapsulation and administration using nanocarriers. These latter allow to considerably improve the biodistribution of photosensitizers and enhance their membrane permeability, resulting in enhanced therapeutic efficacy and minimal side effects. In this context, PDA-based nanostructures have emerged as promising nanocarriers for photosensitizing agents and have thus been largely applied in anti-cancer PDT. For example, taking advantage of the negative charge of polydopamine, Yan et al. synthesized a highly positively charged zinc-phthalocyanine, the $ZnPc(TAP)_4^{12+}$, which allowed the physical adsorption, of this water-soluble phthalocyanine derivative, on the surface of PDA nanoparticles *via* electrostatic interactions. The nanosystem was further modified with a tumor targeting moiety, folic acid (FA), which offered a high tumor accumulation and resulted in specific and efficient cancer cells eradication [186]. A resembling system was previously proposed by the same group of researchers in which both $ZnPc(TAP)_4^{12+}$and nocodazole (NOC), a cell cycle inhibitor, were immobilized on PDA nanoparticles surface using electrostatic interactions for an enhanced synergistic anti-cancer therapy [252].

Another promising nanomedicine was proposed by Liu et al. who developed an innovative oxygen-self supplied platform composed of a photosensitizer, methylene blue, carried by polydopamine-hemoglobin complexes encapsulated inside a bio-vesicle engineered from recombined red blood cells (RBCs) membranes and serving as oxygen carrier and supplier [253]. In fact, with oxygen being crucial for the photodynamic effects, tumors extreme hypoxia represents a major mechanism of resistance to the photodynamic therapy. To bypass this bio-barrier, the corpuscular hemoglobin in this nanosystem was about ten-fold higher than that of natural RBCs, thanks to the abundant catechol functions present in polydopamine. Beside its role as a drug carrier, the anti-oxidation property of polydopamine, which is ascribed to the strong anti-oxidation ability of polyphenols, allowed it to mimic the anti-oxidative enzymes in RBCs, preventing hence the oxidative degradation of oxygen-

transporting hemoglobin. This platform demonstrated its high potential in inducing a strong PDT effect against normoxic or extremely hypoxic tumors leading to a complete tumor ablation. It can interestingly serve as a universal platform for other oxygen-involved therapies such as radiotherapy.

5.2.3. PDA/PS as synergistic photothermal / photodynamic nanoplatforms

PTT/PDT bi-modal therapy has emerged as a promising non-invasive bimodal approach that has shown encouraging results in the cancer treatment field. In fact, this combination is based on the generally accepted synergistic effects obtained by associating both modalities. On one hand, the hyperthermia generated by the photothermal converting agent can enhance blood flow into the illuminated tumor site, which leads to an improved tumor oxygenation and consequently an enhanced concurred oxygen-mediated PDT effect [246]. Moreover, the local hyperthermia would induce membrane permeabilization, thus increasing cellular uptake of the photosensitizing agent or generated singlet oxygen [250]. On the other hand, the oxygen depletion taking place in the tumor microenvironment during PDT renders the cells more sensitive to heat, enhancing thereby the efficacy of PTT [254].

In this perspective, beside serving as simple nanocarriers for PS, an increasing number of papers have demonstrated the great potential of PDA nanomaterials conjugated to PS in inducing enhanced therapeutic outcomes through photothermal and photodynamic effects respectively. Curiously, based on the broad absorption band of PDA, single-wavelength activation protocols were applied in several studies in this combinational therapeutic approach [199], which facilitates the illumination procedure by reducing the needed equipment, and would lead to enhanced therapeutic efficacy due to the synchronized PTT/PDT activities [30]. Nevertheless, PDA activation for PTT usually uses longer wavelength irradiations (808 nm) in comparison to conventional wavelengths used in PDT, which permits to reach higher photothermal conversion and a higher tissue-penetration depth and eradicate deeper tumoral tissues.

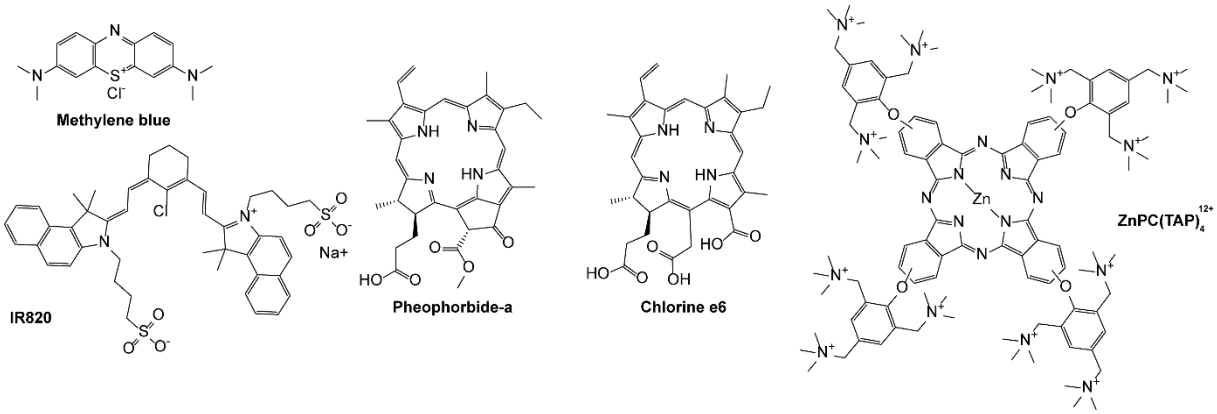

Scheme 2. Structures of photosensitizers used for the design of PDA-based nanoparticles for synergistic photothermal/photodynamic therapy.

Several PSs have been coupled (scheme 2) to PDA nanoconstructs for the development of PDA-based bifunctional nanoplatforms. This can be done by using various strategies of PS couplings depending on the therapeutical application. Indeed, the PS can be (i) loaded inside the PDA matrix, (ii) physically adsorbed on the surface of nanoparticles or (iii) covalently bound to their surface (figure 9).

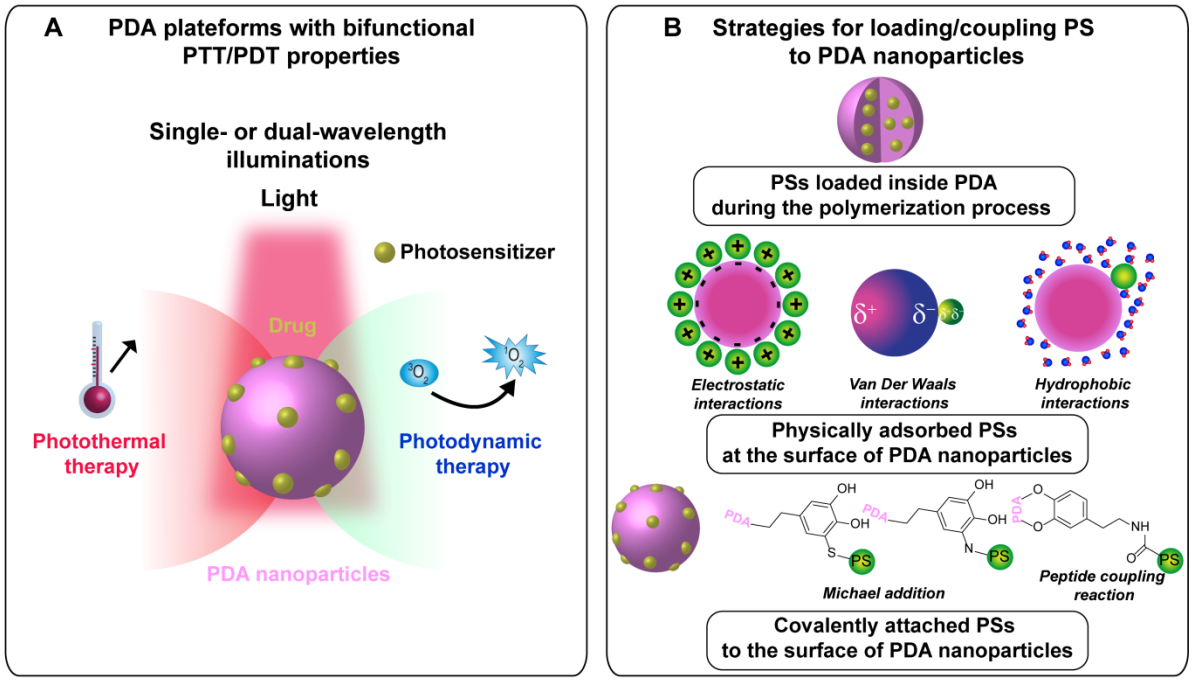

Figure 9. (A) PDA/PS nanoplatforms for synergistic photothermal/photodynamic therapy, (B) Strategies of PS coupling to PDA nanostructures.

5.2.3.1. PS loaded inside PDA matrix

Taking advantage of the abundance of aromatic groups in PDA, Poinard et al. developed a photothermal/photodynamic therapeutic nanoagent based on PDA nanoparticles encapsulating

the hydrophobic PS chlorin e6 (Ce6) within the polymeric core, *via* π-π stacking interactions [199]. This strategy allowed to load unprecedently high amounts of Ce6 in the PDA-based nanocarrier and offered an enhanced cellular uptake (over 8-fold higher) with a sustained drug release up to 5 days. Under a single laser irradiation at 665 nm and at a relatively low power density of 250 $mW.cm^{-2}$, this nanosystem showed improved additive cell killing effects in comparison to PTT or PDT alone.

Due to the fluorescence quenching and ROS scavenging abilities of polydopamine [26], the encapsulation of the photosensitizing drug in the core of the nanoparticles would prevent its degradation and limit its undesirable activation under day light. However, ROS generation and subsequently the anti-cancer photodynamic effect is only correlated to the amounts of released PS [199]; the unreleased PS remains inactive. Moreover, although this encapsulation strategy allows to preserve the surface properties of the nanosystem and despite the high PS loading amounts and the efficient drug delivery to the tumor, drug embedment in PDA matrix may induce changes in the stacking ang aggregation of PDA oligomeric building units, which would consequently impact the photophysical properties of PDA nanosystems and their nanomechanics, compromising hence their biological performance and therapeutic efficacy.

5.2.3.2. PS adsorbed onto the surface of PDA nanomaterials

Diverse physical interactions could be deployed for the loading of PS on polydopamine, particularly *via* π-π interactions, hydrophobic interactions, hydrogen bonding or electrostatic interactions. Multiple PS-bearing polydopamine nanosystems have been described for this category.

Wang et al. proposed a multifunctional drug delivery platform, based on PDA-coated gold nanorods (GNRs), for multi-modal cancer theranostics [155]. The nanohybrid was further functionalized with PEG which increased its colloidal stability and a photosensitizer, methylene blue (MB), was then adsorbed on the surface of polydopamine *via* electrostatic and π-π interactions. The association of GNRs to PDA resulted in an improved PTT performance which allowed an efficient tumor ablation, as demonstrated *in vitro* and *in vivo*. The combination of hyperthermia and ROS generation associated to MB, promoted the anti-cancer therapeutic efficacy.

Similarly, IR820, a NIR light absorber with a great potential in photodynamic and photothermal therapies but also in photoacoustic imaging, was used in association to polydopamine after being adsorbed on the surface of PEGylated PDA nanoparticles *via* π-π

and electrostatic interactions [255]. The combination of both photothermal agents offered a considerable enhancement in the light-heat conversion efficiency of the nanoagent with a great photostability, which together with the ROS generation ability of the PS, IR820, allowed an efficient cancer treatment following a single laser irradiation at 808 nm with a power density of 1 $W.cm^{-2}$. Moreover, given the interesting PA properties of PDA nanoparticles and IR820, this system showed a great potential as a multifunctional nanoplatform for cancer theranostic applications.

A tumor targeting PDT-PTT platform was developed by Han et al. for improved therapeutic specificity and consisted in a novel photomedicine composed of a polydopamine core and a pheophorbide a-hyaluronic acid shell as an efficient anti-cancer agent displaying negligible side effects [256]. While hyaluronic acid acts as the tumor-targeting moiety, polydopamine acts as a quencher hindering the fluorescence and singlet oxygen generation of the conjugated PS. However, in the presence of cancer-specific enzymes, particularly hyaluronidase, the PS is released and its photo-mediated activity is restored, leading to a localized photodynamic effect. Following a single laser irradiation at 607 nm, the nanosystem exhibited a synergistic PTT/PDT anti-tumoral activity and showed promising results *in vitro* and *in vivo*.

In a more recent study, Chen et al. proposed a novel PDA-based PDT-PTT dual platform in which aggregation-induced emission (AIE) gens were used as efficient photosensitizing agents [257]. Herein, a mitochondria-targeting AIE PS conjugate was attached to the surface of polydopamine nanoparticles *via* π-π interactions, H-bonding and electrostatic attraction, and showed an unprecedently high loading capacity with a low leakage rate. A synergistic PDT/PTT-mediated tumor inhibition was indeed obtained *in vitro* and *in vivo* and was associated to a low IC_{50} of 71 $\mu g.ml^{-1}$ versus 170 $\mu g.ml^{-1}$ or 105 $\mu g.ml^{-1}$ for PDT (white light, 100 $mW.cm^{-2}$) or PTT (808 nm laser, 1 $W.cm^{-2}$) alone, respectively. The nanohybrid system displayed a positive surface charge which resulted in pronounced cytotoxic effects.

The physical adsorption of the photosensitizing molecules on the surface of PDA nanoparticles or shells uses relatively simple chemical procedures for molecules immobilization, in comparison to covalent conjugation. Although such interactions are energetically weak, studies have demonstrated their relative stability under physiological conditions. They are on the other hand easily weakened under the acidic, reductive or oxidative conditions characterizing the tumor microenvironment or under NIR irradiation, which offers an efficient PS delivery in the targeted site. Undesired pre-leakage of the PS from PDA surface could however be observed limiting consequently the therapeutic

efficiency and increasing the side effects. Improved stability may hence be achieved through covalent coupling of the PS to the nanostructure.

5.2.3.3. PS covalently bound to the surface of PDA nanomaterials

Zhang et al. reported the preparation of Ce6-carrying PDA nanospheres *via* covalent binding between the carboxylic acid of the PS and the amine groups exposed on polydopamine surface, using carbodiimide chemistry [193]. The combined photothermal and ROS-mediated effects, associated to PDA and Ce6 respectively, resulted in a significantly enhanced anti-cancer therapeutic efficacy as demonstrated through *in vitro* and *in vivo* studies, following a dual-wavelength laser irradiation (808 nm for PDA activation and 670 nm for Ce6) [193].

This carbodiimide-mediated conjugation strategy has been later employed by Wang et al. for the immobilization of the PS Ce6 on the surface of PDA nanoparticles. However, in order to improve the selectivity and therapeutic efficacy of this nanomedicine, the authors decorated herein the Ce6-bearing PDA nanospheres with a tumor targeting moiety, hyaluronic acid (HA), which offered a remarkably higher tumor penetration and resulted in a superior synergistic anti-tumor effect in comparison to the non-targeting platform [254].

In an another approach, Yang et al. [258] selected black phosphorus (BP) nanosheets (NSs), biocompatible and biodegradable inorganic materials, as the nanocarrier for Ce6 delivery, taking advantage of its high surface area that offers considerably high loading amounts of the PS. PDA was used here to coat the NSs and served as a bridge to enable the covalent anchoring of Ce6 and triphenyl phosphonium (TPP), a mitochondria-targeting moiety, using carbodiimide chemistry for both reactions. Under a single 660 nm irradiation, the combination of PDA and BP in the nanosystem resulted in an increased photothermal conversion efficiency, with 33.2 % for PDA@BP NSs versus 26.6 % for BP NSs alone, while Ce6 induced efficient ROS generation and photodynamic effect. The as-prepared platform exhibited a selective localization in mitochondria which further promoted the phototherapeutic efficiency, as demonstrated in *in vitro* and *in vivo* cancer models.

Other covalent interactions were engaged for the design of similar bimodal photoactivatable nanoagents. For instance, Hu et al. have developed C_{60}-PDA-graphene nanohybrids as a promising anti-cancer candidate for synergistic PT/PD therapies [250]. In this study, fullerene C_{60}, a promising photodynamic agent, was conjugated to the targeting moiety folic acid (FA), and the resulting conjugate was anchored on PDA-rGO nanohybrid using nucleophilic Michael addition or Schiff base reaction of the amine-terminated FA on the o-quinone function of polydopamine. The covalent attachment of C_{60}-FA conjugate on the nanohybrid

structure limited the aggregation of the former observed in previous studies, preserving its photodynamic activity. As mentioned above, the association of PDA to rGO results in enhanced NIR light absorption and subsequently in improved heat generation upon light activation. Interestingly, the C_{60}-FA conjugate contributed to the global photothermal activity of the nanosystem, with an induced temperature elevation of 7.5 °C versus 17.5 °C for PDA-rGO hybrid after irradiation with a Xe lamp at 2 $W.cm^{-2}$ for 15 min at a concentration of 50 $\mu g.ml^{-1}$. After a single irradiation using the Xe lamp, the as-prepared nanoplatform showed efficient photo-induced apoptotic effects related to a synergistic PTT/PDT anti-tumoral activity.

In order to achieve a superior treatment efficacy and ensure its biosafety, it is highly desirable to design smart nanocarriers that specifically deliver the PS to the targeted tumor tissue and in a controlled manner. In this context, a smart PDT/PTT controllable platform was proposed by Zhan et al. based on the complementary base pairing rules [259]. A thymine-modified zinc phtalocyanine (T-ZnPc) was bound to adenine-modified PDA nanoparticles *via* the base pairing rules. The hyperthermia induced by polydopamine photo-activation will break the base pairing resulting in a NIR-triggered release of the ZnPc. Synergistic photodynamic/photothermal effects allowed the efficient cancer ablation.

The covalent conjugation of the PS offers a higher stability and biosafety to the nanomedicine and allows an efficient delivery of the molecule to the targeted site. The design of smart stimuli-responsive delivery systems allows to further control the release behavior of the PS for a higher efficiency. Nonetheless, more efforts are still needed for the development of such systems, through exploring the potential of diverse smart cleavable linkers, which would offer a spatio-temporally controlled release under external stimuli.

Although the excellent activity of these systems has been largely demonstrated through *in vitro* and *in vivo* models, the direct immobilization of the PS on polydopamine results in a partial decrease in the PS-mediated ROS generation [250, 258], due to the redox activity of PDA and its ROS scavenging capacity. This issue should be considered by coupling the PS to PDA nanoplatforms through hydrophilic polymers, such as polyethylene glycol.

Table 5. PDA-based nanoplatforms applied in light-mediated cancer therapy, PDT and/or PTT

Nanosystem configuration	Targeting moiety	Loaded PS	Properties	Applications	Illumination conditions	Testing stages	Ref
Ce6-PDA NPs	--	Ce6	High loading amounts of Ce6	PTT-PDT	PTT/PDT: 665 nm, 250 $mW.cm^{-2}$, 15 min	*in vitro*: T24 cells (bladder cancer)	[199]
Ce6-PDA NPs	--	Ce6	Increased photostability	PTT-PDT	PTT: 808 nm, 2 $W.cm^{-2}$, 5 min for *in vitro* and 10 min for *in vivo* tests; PDT: 670 nm, 50 $mW.cm^{-2}$, 5 min for *in vitro* and 10 min for *in vivo* tests	*in vitro:* HepG2 cells (liver cancer) *in vivo:* HepG2 - bearing mice	[193]
Ce6-PDA NPs	Hyaluronic acid (HA)	Ce6	Enhanced cellular internalization (CD44-mediated endocytosis)	PTT-PDT	PTT: 808 nm, 2.5 $W.cm^{-2}$, 5 min for *in vitro* and 10 min for *in vivo* tests; PDT: 670 nm, 50 $mW.cm^{-2}$, 5 min (for *in vitro* tests) or 10 min (for *in vivo* tests)	*in vitro:* HCT-116 cells and 3D tumor spheroids (colorectal cancer) *in vivo:* HCT116 - bearing mice	[254]
PDA-Ce6-GSH-Au nanoflowers (NFs)	--	Ce6 (conjugated to the Au *via* GSH)	Induced a significant red shift of ~80 nm and amplified the photothermal conversion efficiency of AuNFs, Lower dark toxicity	Synergistic PTT effects - PDT	PTT: 808 nm, 2 $W.cm^{-2}$, 10 min (for *in vitro* and *in vivo* tests); PDT: 660 nm, 100 $mW.cm^{-2}$, 5 min (for *in vitro* tests) or 10 min (for *in vivo* tests)	*in vitro:* HeLa cells (cervical cancer) *in vivo:* HeLa - bearing mice	[260]

Ce6-TPP-PDA@Black phosphorus	Triphenyl phosphonium (TPP)	Ce6	Mitochondria-targeting system	PTT/PDT	PTT/PDT: 660 nm, 0.5 $W.cm^{-2}$, 5 min (for *in vitro* tests) or 10 min (for *in vivo* tests)	*in vitro*: HeLa cells *in vivo*: HeLa-bearing mice	[258]
ZnO-Ce6@PDA	--	Ce6		PTT/PDT	PTT: 780 nm, 2.9 $W.cm^{-2}$, 10 min (for *in vitro* tests); PDT: 660 nm, 100 $mW.cm^{-2}$, 10 min (for *in vitro* tests)	*in vitro*: HeLa cells	[261]
ZnP@PDA NPs	--	ZnP (Zinc Porphyrin)	Fluorescence-guided imaging	PTT/PDT	PTT/PDT: 660 nm, 0.8 $W.cm^{-2}$ for 5 min (for *in vitro* tests) or 0.75 $W.cm^{-2}$ for 5 min (for *in vivo* tests)	*in vitro*: HeLa cells *in vivo*: HeLa-bearing mice	[262]
C_{60}-PDA-GO nnaohybrids	FA	C_{60} (fullerene)		Targeted PDT/PTT	PTT/PDT: Xe lamp, 660 nm, 2 $W.cm^{-2}$, 9 min (for *in vitro* tests)	*in vitro*: HeLa cells	[250]
Ce6-MnO_2-PDA-FA NPs	FA	Ce6	pH-responsive drug release, O_2-generating system	Targeted and O_2-strengthened PDT/PTT	PTT: 808 nm, 1 $W.cm^{-2}$, 10 min (for *in vitro* and *in vivo* tests); PDT: 660 nm, 400 $mW.cm^{-2}$, 5 min (for *in vitro* and *in vivo* tests)	*in vitro*: MCF-7 cells (Breast cancer) *in vivo*: MCF-7-bearing mice	[158]
AIEgen-PDA-PEG NPs	Indolium group	AIEgens (TPE-Methoxyl-indolium)	Mitochondria-targeting	Imaging-guided PDT-PTT	PTT: 808 nm, 1 $W.cm^{-2}$, 5 min (for *in vitro* and *in vivo* tests); PDT: white light, 100 $mW.cm^{-2}$, 10 min (for *in vitro* and *in vivo* tests)	*in vitro*: HeLa cells *in vivo*: HeLa-bearing mice	[257]

ICG-Laponite-PDA-PEG-RGD NPs	Arginine-Glycine-Aspartic acid (RGD)	Indocyanine green (ICG)	Improved photostability of ICG, Enhanced photothermal conversion ability	Targeted and imaging-guided PDT-PTT	PTT/PDT: 808 nm, 1.2 $W.cm^{-2}$, 5 min (for *in vitro* tests);	*in vitro*: MDA-MB-231 cells (breast cancer)	[263]
Gold nanorods (GNRs) @ PDA shell – MB – PEG NPs	--	Methylene blue (MB)	Synergistic PTT effects due to PDA and GNRs combination	PTT/PDT	PTT: 808 nm, 2 $W.cm^{-2}$, 5 min (for *in vitro* and *in vivo* tests); PDT: 671 nm, 30 $mW.cm^{-2}$, 3 min (for *in vitro* and *in vivo* tests)	*in vitro*: HeLa cells *in vivo*: HeLa-bearing mice	[155]
IR820/Fe^{3+}-PDA-PEG NPs	--	IR820	Dual imaging: PA and MR imaging	Imaging-guided PDT-PTT	PTT/PDT: 808 nm, 1 $W.cm^{-2}$, 10 min (for *in vitro* tests)	*in vitro*: HeLa cells	[255]
PDA @ PS-HA shell	Hyaluronic acid (HA)	Pheophorbide a (Pheo a)	Hyaluronisase-responsive Pheo a release	Targeted PDT, PTT	PTT/PDT: 670 nm laser, 3 $J.cm^{-2}$ (for *in vitro* tests) and 100 $J.cm^{-2}$ (for *in vivo* tests)	*in vitro:* MDA-MB-231 cells (breast cancer) *in vivo:* MDA-MB-231-bearing mice	[256]
TPGS micelles @ PDA nanoclusters	--	IR780	Overcoming tumor drug resistance, Sequential system activation under consecutive light irradiations, NIR light-responsive DOX release	PDT-PTT-CT	PTT/PDT: 808 nm, 0.5 $W.cm^{-2}$, 10 min (for *in vitro* tests) and 5min (for *in vivo* tests)	*in vitro:* MCF-7 /ADR cells (breast cancer) *in vivo:* MCF-7 /ADR -bearing mice	[264]

ZnPc-FA-PDA NPs	Folic acid (FA)	ZnPc	pH-responsive release of the PS	Targeted PDT	PDT: 680 nm, 5 $J.cm^{-2}$ for 2 min (for *in vitro* tests) or 75 $J.cm^{-2}$ for 10 min (for *in vivo* tests)	*in vitro*: HeLa cells, MCF-7 cells *in vivo*: HeLa or MCF-7-bearing mice	[186]
ZnPc-NOC-PDA NPs	--	ZnPc, Nocodazole (NOC)	pH-responsive release of the PS and NOC, Enhanced nuclear uptake, Fluorescent molecular tomography imaging capability	Cell proliferation inhibition, PDT	PDT: 680 nm, 7.5 $J.cm^{-2}$ for 3 min (for *in vitro* tests) or 50 $J.cm^{-2}$ for 5 min (for *in vivo* tests)	*in vitro*: MCF-7 cells *in vivo*: MCF-7-bearing mice	[252]
$CaCO_3$-PDA-PEG NCs	--	Ce6	pH-responsive of the PS	PDT, MRI-guidance	PDT: 660-nm light emitting diode (LED), 5 mW cm^{-2}, 1 h (for *in vivo* tests)	*in vitro*: 4T1 cells *in vivo*: 4T1 cells-bearing mice	[78]
PDA NPs	--	--	ΔT = 34 °C for 200 $\mu g.ml^{-1}$ under 808 nm, 2 $W.cm^{-2}$, 500 s	PTT	PTT: 808 nm, 2 $W.cm^{-2}$, for 5 min (for *in vivo* tests)	*in vitro*: HeLa cells, 4T1 cells *in vivo*: 4T1 cells-bearing mice	[47]
PDA-Fe^{3+}-PEG NPs	--	--	ΔT ~ 30 °C for 250 $\mu g.ml^{-1}$ under 808 nm, 1.3 $W.cm^{-2}$, for 10 min pH-activatable MRI contrast	PTT, MRI-guidance	PTT: 808 nm, 1.3 $W.cm^{-2}$, for 6 min (for *in vivo* tests)	*in vitro*: SW620 cells (colon cancer) *in vivo*: SW620-bearing mice	[56]

PEG-PDA/mesoporous Ca phosphate hollow JNPs	DOX, ICG	--	pH- and NIR irradiation-responsive release	CT, synergistic PTT, PAI guidance	PTT: 808 nm NIR laser, 1 $W.cm^{-2}$ (for *in vivo* tests)	*in vitro*: HepG2 cells *in vivo*: HepG2-bearing mice	[67]
PNAm / PDA-coated AuNPs supramolecular polymer nanocomposite hydrogel	DOX	--	pH- and heat-responsive drug release	CT, synergistic PTT	PTT: 808 nm NIR laser, 2 $W.cm^{-2}$ (for *in vitro* and *in vivo* tests)	*in vitro*: L929 cells (murine fibroblast cells) *in vivo*: 4T1-bearing mice (breast cancer model)	[249]
Cu/PDA NPs	Cu^{2+}	--	ΔT = 42.2 °C for 75 $\mu g.ml^{-1}$, under 808 nm, 3.5 $W.cm^{-2}$, for 20 min pH-responsive Cu^{2+} release	PTT, CT MRI-guidance	PTT: 808 nm, 1 $W.cm^{-2}$, for 10 min (for *in vitro* tests), 0.33 $W.cm^{-2}$, 20 min (for *in vivo* tests)	*in vitro*: KB cells (epidermal cancer) *in vivo*: KB-bearing mice	[248]
PDA-coated selenide molybdenum ($MoSe_2$) nanosheets	DOX	--	pH- and heat-responsive drug release	CT, synergistic PTT	PTT: 808 nm, 2 $W.cm^{-2}$, for 5 min (for *in vitro* and *in vivo* tests)	*in vitro*: HeLa cells *in vivo*: U14-bearing mice (cervical cancer model)	[265]
PDA-modified black phosphorus nanosheets	DOX, P-gp SiRNA	--	pH- and heat-responsive drug release	CT, gene therapy, PTT	PTT: 808 nm, 1.5 $W.cm^{-2}$, for 5 min (for *in vivo* tests)	*in vitro*: MCF-7 cells *in vivo*: MCF-7-bearing mice	[266]

ZnP: Zinc Porphyrin, JNPs: Janus nanoparticles, NCs: nanocapsules, PNAm; Poly(N-acryloyl glycinamide-co-acrylamide), TPGS: D-α-tocopheryl poly(ethylene glycol) 1000 succinate

5.3. Multi-modal cancer therapy

In order to reach better therapeutic outcomes, multi-modal cancer therapy is widely adopted for cancer treatment. Diverse all-in-one innovative PDA-based platforms have been described in the literature as multifunctional/multi-modal therapeutic or theranostic nanoagents [159] [264, 267]. Numerous reviews published over the recent years have cited in great details the diverse therapeutic approaches and associations described regarding PDA-mediated anti-cancer treatment [29-32, 165, 268].

6. Other catecholamines-derived melanin-like materials

The outstanding properties of PDA-based materials and their remarkable potential in diverse biomedical applications, particularly in the cancer therapy field, have boosted the research of new melanin-like materials for the design of novel therapeutic agents. Catecholamines like 3,4-dihydroxy-L-phenylalanine (L-DOPA) or norepinephrine, and other related molecules like serotonin, have been considered for the development of bio-inspired advanced functional materials. Other naturally occurring catechols or dopamine chemical derivatives [23-24, 166] were also described in the literature for the preparation of polydopamine-resembling materials. Natural melanin granules have also gained interest as photothermal and photoacoustic agents showing high photothermal conversion efficiency (about 40 %) and excellent activity revealed through in *vitro* and *in vivo* assays [269-271].

The small structural differences between precursor monomers may result in a divergence in the functional properties and biological performance of the corresponding polymerized structures, which would offer a rich repertoire of melanin-mimicking materials of tailored characteristics.

Here, we will describe the ability of three main precursors, namely L-DOPA, norepinephrine and serotonin, to give rise to polydopamine-like "polymers" following their oxidation

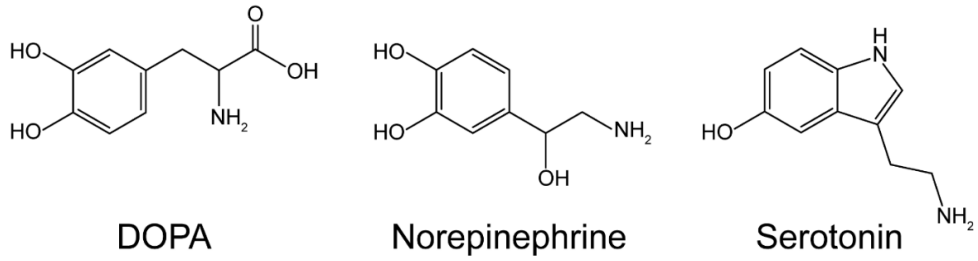

Scheme 3. Structures of the main monomers explored for the synthesis of polydopamine-resembling materials

6.1. Poly(L-DOPA), PDOPA

3,4-dihydroxy-L-phenylalanine or L-DOPA is decarboxylated *in vivo* to generate dopamine. As the natural precursor of eumelanin in vivo [272], L-DOPA is the first obvious material that can be considered for the preparation of synthetic melanin structures.

Inspired by the large advancements achieved for polydopamine development, poly(L-DOPA) (PDOPA) coating materials and colloidal nanoparticles were successfully prepared using the solution oxidation method [273], the enzyme-catalyzed polymerization process [274-275] or also the electro-polymerization method [276]. Nevertheless, the formation of PDOPA can be less successful than PDA, probably because of to the electrostatic repulsion occurring between neighboring carboxylic acid groups, hindering the stacking and the aggregation of oligomeric units. This limitation could be however overcome under high ionic strength conditions [277]. Differences in the oxidation and polymerization rates were found for L-DOPA in comparison to dopamine, which lead to different deposition rates and particles formation kinetics [278].

Adding to the reactive sites described for polydopamine in section (4-2-1), the chemical reactivity of PDOPA takes advantage of the carboxylic acid group available for diverse secondary reactions including with amine or hydroxyl-bearing molecules [278-279]. Also, bridging the carboxylic functions of L-DOPA monomers *via* a disulfide bond allowed to prepare novel PDOPA coatings offering an on-demand degradation in presence of reducing agents like glutathione and was applied for the delivery of doxorubicin in tumor microenvironment [278, 280].

PDOPA coatings were in fact successfully deposited on diverse surfaces such as metals, polymers, oxides and emulsion droplets [118, 277], and were used for diverse biomedical purposes, including cancer therapy. For instance, novel magnetic-guided PDOPA-coated Fe_3O_4 nanoparticles were recently developed for targeted delivery of the anti-cancer drug taxol and showed a promising tumor growth inhibition effect *in vivo*, with a more uniform drug release profile in comparison to polydopamine-coated analogue structures [281].

In comparison to PDA nanoparticles, PDOPA counterparts displayed a stronger NIR light absorption and exhibited an enhanced photothermal conversion efficiency under laser illumination at 808 nm and a power density of 2 $W.cm^{-2}$ [273]. These properties can be advanced to develop photothermal therapeutic nanoagents with a great potential in cancer treatment applications.

6.2.Poly(norepinephrine), PNE

Norepinephrine is another endogenous catecholamine that, similarly to the parent dopamine and L-DOPA, can spontaneously polymerize under ambient alkaline conditions. The synthesis of poly(norepinephrine) (PNE) was first reported in 2009 after polydopamine discovery [282]. PNE was at first mostly reported as a versatile coating material applied to coat substrates of different types and shapes including nanoparticles [283], nanotubes [284] and nanofibers [285] and could deposit on the surface of several organic and inorganic substrates including polymers, metals, silicates and graphene oxides [286-287].

Following the protocols described for polydopamine formulation, spherical monodisperse PNE nanoparticles were successfully prepared, using a NaOH solution [288] or an alkaline Tris buffer / ethanol mixture [289]. Their size and morphology were tunable by varying the monomer or solvent amounts. For instance, increasing the monomer amount led to the increase of nanoparticles size. The increase of ethanol concentration allowed the obtention of nanoparticles of smaller size, while the use of ethanol at very low concentrations (0.1 mM) induced a loss in their spherical shape and monodispersity, which was attributed to the Hansen solubility parameter theory, as for polydopamine formation.

Similar to polydopamine, PNE materials expose multiple reactive sites serving as anchors for the immobilization of diverse biomolecules (enzymes [284, 290-291], antibodies [292], etc.) and for nanoparticles functionalization using PEG chains [288].

In comparison to its polydopamine analogue, conventional PNE present an ultra-smooth and a highly homogenous surface, due to the presence of 3,4-dihydroxybenzaldehyde, an intermediate generated during the polymerization of norepinephrine [293]. This property is advantageous for biomedical applications and allows to overcome limited surface regularity encountered in polydopamine [286]. Indeed, PNE nanoparticles showed increased hydrophilicity and enhanced anti-fouling properties in comparison to their PDA counterparts suggesting a superior potential in biological applications [289] and PNE coatings served as an interesting bio-interface used to endow coated biomaterials with high hydrophilic and anti-fouling properties [289]. Moreover, following the immobilization of an enzyme on the PDA or PNE surfaces, higher enzyme loading rates were obtained for PDA due to this latter's rougher surface, however a decreased enzyme activity was observed and attributed to a reduced accessibility of its active sites [284]. The higher hydrophilicity of PNE counterparts allowed on the other hand to promote the activity of the immobilized enzyme.

Owing to its bio-inspired nature and this highly hydrophilic character, PNE nanoparticles exhibited excellent biocompatibility as demonstrated in *in vitro* and *in vivo* studies and

showed no immune response or long-term toxic effects during *in vivo* studies [288-289, 294-295].

Considering all these aspects, PNE nanomaterials have gained increasing attention for biomedical applications, including tissue engineering [296] and gene delivery [297] applications, and have recently emerged as smart thermal and/or pH responsive drug delivery platforms and excellent photothermal nano-agents, applied for combined chemo-PTT cancer therapy.

Indeed, due to its composition rich in aromatic rings, PNE nanoparticles are able to load compounds with aromatic rings, like doxorubicin, and hold a great potential as anti-cancer drugs nanocarriers [288, 298]. Interestingly, PNE nanoparticles showed excellent drug loading ability with a maximum loading capacity of DOX that exceeded greatly that of PDA counterparts. Besides, PNE nanoparticles exhibited a higher cellular uptake efficiency, which resulted in a significantly enhanced intracellular DOX accumulation in comparison to polydopamine, confirming hence their superior potential in drug delivery applications. Similar to polydopamine, PNE nanomaterials showed a pH-sensitivity leading to a reduced leakage during blood circulation and to an enhanced drug release in acidic tumor microenvironment and cytolysosome compartments, due to the protonation of the amine functions in PNE causing the disruption of the π-π interactions.

Moreover, very recently, PNE nanomaterials were revealed to be a promising photothermal converting nanoagent of a great potential in cancer therapy. Indeed, PNE nanoparticles displayed a high NIR light absorption and an excellent photothermal conversion efficiency of 67% for nanoparticles of ~ 100 nm, following their irradiation at 808 nm, which is a 1.63-fold higher than that of their PDA analogues (41%), and higher than most available PTT nanoagents [288]. A great photostability was also observed in the case of PNE nanoparticles upon repeated laser illumination. The therapeutic efficacy of PNE nanoparticles was demonstrated through *in vitro* cells and *in vivo* experiments. Interestingly, under nanoparticles illumination, increased release of encapsulated DOX was obtained, probably due to nanoparticles thermal expansion. This NIR-responsive drug release offered a further control of the site-specific delivery of anti-cancer drugs and results in a synergistic chemo-photothermal effect for an efficient tumor ablation.

Similarly, PNE coatings have shown promising photothermal activity and drug loading ability and were explored for the development of novel artemisinin-loaded PNE-coated FeOOH nanoparticles for efficient cancer photothermal-chemical combination therapy [298].

6.3. Poly(serotonin), PST

Poly(serotonin) (PST) is a less explored class of melanin-like material obtained from the oxidative self-polymerization of serotonin, an indoleamine neurotransmitter derived from the hydroxylation and decarboxylation of the amino acid tryptophan.

The polymerization process, conducted under alkaline conditions, generated monodisperse nanoparticles, whose formation occurred with significantly slower kinetics compared to polydopamine, as monitored using absorption spectroscopy [299].

The drug loading ability, stimuli-responsiveness and photothermal activity of PST nanoparticles have been recently investigated. The anticancer drug DOX was tested and could be efficiently loaded on the surface of PST nanoparticles via π-π and hydrophobic interactions and through hydrogen bonds formation. However, the drug loading efficiency was found to be lower than that of PDA nanoparticles. A controlled pH-induced release of the chemotherapeutic drug was depicted, confirming the interest of PST-based nanosystems in drug delivery applications for tumor therapy.

Moreover, the illumination of PST nanoparticles suspensions at 808 nm and 1.5 $W.cm^{-2}$ induced a solution temperature increase of > 20 °C for nanoparticles concentrations > 100 $\mu g.ml^{-1}$. The temperature increase generated by PST nanoparticles was however lower than that obtained for their PDA counterparts.

Nevertheless, although the photothermal activity and drug loading capability of PST nanoparticles were limited compared to polydopamine materials, the former represent promising anticancer nanoagent candidates. Particularly, PST nanoparticles showed a greater biocompatibility, and a reduced protein corona formation in comparison to polydopamine, which is highly interesting for *in vivo* applications. Indeed, at the nano-bio-interface polyserotonin nanoparticles showed reduced interactions with proteins corona as suggested by quantum mechanics computations, which was attributed to the four-folds lower adhesion obtained for PST nanoparticles compared to PDA during peak-force AFM experiments.

Based on these findings, PST-based nanoparticles can be used as a multifunctional cancer therapeutic nanoagent working as a photothermal agent and a drug nanocarrier for efficient anticancer therapy with a minimal toxicity.

7. Summary and outlooks

In summary, polydopamine represents a successful example of nature-inspired materials. Considering its diverse inherent properties, including the excellent biocompatibility, the high

chemical reactivity and the remarkable photothermal conversion ability, PDA is acknowledged as a robust element that can be considered for the development of innovative "all in one" platforms, in order to provide an efficient cancer treatment and diagnosis.

Nevertheless, despite the rapidly increasing implementation of polydopamine and catecholamines derivatives in nanomedicines research field, several remaining challenges still have to be overcome to achieve advancements towards future clinical translation.

- Regarding the complicated formation mechanisms, thorough investigation based on advanced techniques should be undertaken for a better understanding of the molecular organization and assembly modes. This would offer a full control of the morphological and functional features of polydopamine materials, allowing consequently the expansion of their applications scope.
- The purification methods described so far to separate PDA nanoparticles from the oligomeric and unpolymerized counterparts are mostly based on dialysis or centrifugal filtration. However, these latter seem to be inefficient to separate all of the oligomeric structures from PDA nanoparticles and especially when it comes to nanoparticles with a hydrodynamic diameter less than 100 nm. The presence of such oligomeric structures in PDA nanoparticles suspension would affect their physicochemical properties and their in vivo outcomes.
- As the preparation method leads to different chemical structures of PDA assemblies, this may affect their physicochemical properties and thus their interaction with biological environment. Hence, the preparation procedures should be harmonized between the different studies in order to get a relevant comparative set of data regarding the in vitro or in vivo studies.
- Full comprehensive studies of the photothermal conversion efficiencies of polydopamine nanostructures as a function of particles size and preparation procedures are also still lacking.
- Moreover, due to the high chemical reactivity and sensitivity of polydopamine structures, precautions need to be taken during formulation, use and storage, in order to avoid undesired side reactions.
- As for the biosafety of such materials in humans, the biocompatibility of polydopamine was established based on observations made on cells and animal models (mice or rats). A better understanding of the pharmacokinetics profiles, the behavior towards physiological barriers, and the biodegradation pathways needs to be fulfilled.

References

1. Evangelopoulos M, Tasciotti E 2017 Bioinspired approaches for cancer nanotheranostics *Nanomedicine* **12** 5-7.
2. Li A, Zhao J, Fu J, Cai J, Zhang P 2019 Recent advances of biomimetic nano-systems in the diagnosis and treatment of tumor *Asian Journal of Pharmaceutical Sciences*
3. Yang G, Chen S, Zhang J 2019 Bioinspired and Biomimetic Nanotherapies for the Treatment of Infectious Diseases *Frontiers in Pharmacology* **10**
4. Nosanchuk J D, Casadevall A 2003 The contribution of melanin to microbial pathogenesis *Cellular Microbiology* **5** 203-23.
5. Eisenman H, Casadevall A 2011 Synthesis and assembly of fungal melanin *Applied microbiology and biotechnology* **93** 931-40.
6. Glagoleva A, Shoeva O, Khlestkina E 2020 Melanin Pigment in Plants: Current Knowledge and Future Perspectives *Frontiers in Plant Science* **11** 770.
7. Naaz I, Ali S 2018 Biochemical aspects of mammalian melanocytes and the emerging role of melanocyte stem cells in dermatological therapies *International journal of health sciences* **12**
8. Nunes C S, Vogel K, Chapter 20 - Tyrosinases—physiology, pathophysiology, and applications. In *Enzymes in Human and Animal Nutrition*, Nunes, C. S.; Kumar, V., Eds. Academic Press: 2018; pp 403-12.
9. Xie W, Pakdel E, Liang Y, Kim Y J, Liu D, Sun L, Wang X 2019 Natural Eumelanin and Its Derivatives as Multifunctional Materials for Bioinspired Applications: A Review *Biomacromolecules* **20** 4312-31.
10. Miranda M, Zarivi O, Bonfigli A, Amicarelli F, Aimola P, Ragnelli A M, Pacioni G 1997 Melanogenesis, tyrosinase expression, and reproductive differentiation in black and white truffles (Ascomycotina) *Pigment cell research* **10** 46-53.
11. Jiang Q, Liu Y, Guo R, Yao X, Sung S, Pang Z, Yang W 2019 Erythrocyte-cancer hybrid membrane-camouflaged melanin nanoparticles for enhancing photothermal therapy efficacy in tumors *Biomaterials* **192** 292-308.
12. Li J, Liu X, Zhou Z, Tan L, Wang X, Zheng Y, Han Y, Chen D-F, Yeung K W K, Cui Z, Yang X, Liang Y, Li Z, Zhu S, Wu S 2019 Lysozyme-Assisted Photothermal Eradication of Methicillin-Resistant Staphylococcus aureus Infection and Accelerated Tissue Repair with Natural Melanosome Nanostructures *ACS Nano* **13** 11153-67.
13. Young W J 1921 The Extraction of Melanin from Skin with Dilute Alkali *Biochem J* **15** 118-22.
14. Sedo J, Saiz-Poseu J, Busque F, Ruiz-Molina D 2013 Catechol-based biomimetic functional materials *Advanced materials (Deerfield Beach, Fla.)* **25** 653-701.
15. Yu M, Deming T J 1998 Synthetic Polypeptide Mimics of Marine Adhesives *Macromolecules* **31** 4739-45.
16. Dalsin J L, Hu B H, Lee B P, Messersmith P B 2003 Mussel adhesive protein mimetic polymers for the preparation of nonfouling surfaces *Journal of the American Chemical Society* **125** 4253-8.
17. Statz A R, Meagher R J, Barron A E, Messersmith P B 2005 New peptidomimetic polymers for antifouling surfaces *Journal of the American Chemical Society* **127** 7972-3.
18. Lee H, Dellatore S M, Miller W M, Messersmith P B 2007 Mussel-Inspired Surface Chemistry for Multifunctional Coatings *Science* **318** 426.
19. Waite J H 1999 Reverse engineering of bioadhesion in marine mussels *Annals of the New York Academy of Sciences* **875** 301-9.
20. Yu M, Hwang J, Deming T J 1999 Role of l-3,4-Dihydroxyphenylalanine in Mussel Adhesive Proteins *Journal of the American Chemical Society* **121** 5825-26.
21. Waite J H, Qin X 2001 Polyphosphoprotein from the adhesive pads of Mytilus edulis *Biochemistry* **40** 2887-93.

22. Binns F, King J A G, Mishra S N, Percival A, Robson N C, Swan G A, Waggott A 1970 Studies related to the chemistry of melanins. Part XIII. Studies on the structure of dopamine-melanin *Journal of the Chemical Society C: Organic* 2063-70.
23. Ryu J H, Messersmith P B, Lee H 2018 Polydopamine Surface Chemistry: A Decade of Discovery *ACS Appl Mater Interfaces* **10** 7523-40.
24. Lee H A, Ma Y, Zhou F, Hong S, Lee H 2019 Material-Independent Surface Chemistry beyond Polydopamine Coating *Accounts of Chemical Research* **52** 704-13.
25. Liebscher J 2019 Chemistry of Polydopamine – Scope, Variation, and Limitation *European Journal of Organic Chemistry* **2019** 4976-94.
26. Liu Y, Ai K, Lu L 2014 Polydopamine and its derivative materials: Synthesis and promising applications in energy, environmental, and biomedical fields *Chem. Rev.* **114** 5057.
27. Ye Q, Zhou F, Liu W 2011 Bioinspired catecholic chemistry for surface modification *Chemical Society Reviews* **40** 4244-58.
28. Lynge L E, Van der Westen R, Postma A, Stadler B 2011 Polydopamine-a nature-inspired polymer coating for biomedical science *Nanoscale* **3** 4916.
29. Tran H Q, Batul R, Bhave M, Yu A 2019 Current Advances in the Utilization of Polydopamine Nanostructures in Biomedical Therapy *Biotechnology Journal* **14** 1900080.
30. Liu H, Yang Y, Liu Y, Pan J, Wang J, Man F, Zhang W, Liu G 2020 Melanin-Like Nanomaterials for Advanced Biomedical Applications: A Versatile Platform with Extraordinary Promise *Advanced Science* **7** 1903129.
31. Cheng W, Zeng X, Chen H, Li Z, Zeng W, Mei L, Zhao Y 2019 Versatile Polydopamine Platforms: Synthesis and Promising Applications for Surface Modification and Advanced Nanomedicine *ACS Nano* **13** 8537-65.
32. Mrówczyński R 2018 Polydopamine-Based Multifunctional (Nano)materials for Cancer Therapy *ACS Applied Materials & Interfaces* **10** 7541-61.
33. Huang L, Liu M, Huang H, Wen Y, Zhang X, Wei Y 2018 Recent Advances and Progress on Melanin-like Materials and Their Biomedical Applications *Biomacromolecules* **19** 1858-68.
34. Park J, Moon H, Hong S 2019 Recent advances in melanin-like nanomaterials in biomedical applications: a mini review *Biomaterials Research* **23** 24.
35. Liu M, Zeng G, Wang K, Wan Q, Tao L, Zhang X, Wei Y 2016 Recent developments in polydopamine: an emerging soft matter for surface modification and biomedical applications *Nanoscale* **8** 16819-40.
36. Batul R, Tamanna T, Khaliq A, Yu A 2017 Recent progress in the biomedical applications of polydopamine nanostructures *Biomaterials science* **5** 1204-29.
37. Ju K Y, Lee Y, Lee S, Park S B, Lee J K 2011 Bioinspired polymerization of dopamine to generate melanin-like nanoparticles having an excellent free-radical-scavenging property *Biomacromolecules* **12** 625.
38. Cho S, Kim S H 2015 Hydroxide ion-mediated synthesis of monodisperse dopamine-melanin nanospheres *Journal of colloid and interface science* **458** 87-93.
39. Ball V, Del Frari D, Toniazzo V, Ruch D 2012 Kinetics of polydopamine film deposition as a function of pH and dopamine concentration: Insights in the polydopamine deposition mechanism *J. Colloid Interface Sci.* **386** 366.
40. Ho C-C, Ding S-J 2013 The pH-controlled nanoparticles size of polydopamine for anti-cancer drug delivery *Journal of Materials Science: Materials in Medicine* **24** 2381-90.
41. Ponzio F, Barthès J, Bour J, Michel M, Bertani P, Hemmerlé J, d'Ischia M, Ball V 2016 Oxidant Control of Polydopamine Surface Chemistry in Acids: A Mechanism-Based Entry to Superhydrophilic-Superoleophobic Coatings *Chemistry of Materials* **28** 4697-705.
42. Della Vecchia N F, Avolio R, Alfe M, Errico M E, Napolitano A, d'Ischia M 2013 Building-block diversity in polydopamine underpins a multifunctional eumelanin-type platform tunable through a quinone control point *Adv. Funct. Mater.* **23** 1331.

43. Della Vecchia N F, Luchini A, Napolitano A, D'Errico G, Vitiello G, Szekely N, d'Ischia M, Paduano L 2014 Tris Buffer Modulates Polydopamine Growth, Aggregation, and Paramagnetic Properties *Langmuir* **30** 9811-18.
44. Bernsmann F, Ball V, Addiego F, Ponche A, Michel M, de Almeida Gracio J J, Toniazzo V, Ruch D 2011 Dopamine-melanin film deposition depends on the used oxidant and buffer solution *Langmuir* **27** 2819.
45. Amin D R, Sugnaux C, Lau K H A, Messersmith P B 2017 Size Control and Fluorescence Labeling of Polydopamine Melanin-Mimetic Nanoparticles for Intracellular Imaging *Biomimetics (Basel, Switzerland)* **2**
46. Ho C C, Ding S J 2013 The pH-controlled nanoparticles size of polydopamine for anti-cancer drug delivery *J. Mater. Sci.: Mater. Med.* **24** 2381.
47. Liu Y, Ai K, Liu J, Deng M, He Y, Lu L 2013 Dopamine-Melanin Colloidal Nanospheres: An Efficient Near-Infrared Photothermal Therapeutic Agent for In Vivo Cancer Therapy *Advanced Materials* **25** 1353-59.
48. Ai K, Liu Y, Ruan C, Lu L, Lu G 2013 Sp2 C-Dominant N-Doped Carbon Sub-micrometer Spheres with a Tunable Size: A Versatile Platform for Highly Efficient Oxygen-Reduction Catalysts *Advanced Materials* **25** 998-1003.
49. Yan J, Yang L, Lin M F, Ma J, Lu X, Lee P S 2013 Polydopamine spheres as active templates for convenient synthesis of various nanostructures *Small* **9** 596-603.
50. Jiang X, Wang Y, Li M 2014 Selecting water-alcohol mixed solvent for synthesis of polydopamine nano-spheres using solubility parameter *Scientific reports* **4** 6070.
51. You I, Jeon H, Lee K, Do M, Seo Y C, Lee H A, Lee H 2017 Polydopamine coating in organic solvent for material-independent immobilization of water-insoluble molecules and avoidance of substrate hydrolysis *Journal of Industrial and Engineering Chemistry* **46** 379-85.
52. Liu X, Cao J, Li H, Li J, Jin Q, Ren K, Xu J-P 2013 Mussel-Inspired Polydopamine: A Biocompatible and Ultrastable Coating for Nanoparticles in Vivo *ACS nano* **7**
53. Liu X S, Cao J M, Li H, Li J Y, Jin Q, Ren K F, Ji J 2013 Mussel-inspired polydopamine: A biocompatible and ultrastable coating for nanoparticles in vivo *ACS Nano* **7** 9384.
54. Zmerli I, Michel J-P, Makky A 2020 Bioinspired polydopamine nanoparticles: synthesis, nanomechanical properties, and efficient PEGylation strategy *Journal of Materials Chemistry B*
55. Jiang J, Zhu L, Zhu L, Zhu B, Xu Y 2011 Surface Characteristics of a Self-Polymerized Dopamine Coating Deposited on Hydrophobic Polymer Films *Langmuir* **27** 14180-87.
56. Liu F, He X, Zhang J, Chen H, Zhang H, Wang Z 2015 Controllable synthesis of polydopamine nanoparticles in microemulsions with pH-activatable properties for cancer detection and treatment *Journal of Materials Chemistry B* **3** 6731-39.
57. Ponzio F, Bertani P, Ball V 2014 Role of surfactants in the control of dopamine-eumelanin particle size and in the inhibition of film deposition at solid-liquid interfaces *Journal of colloid and interface science* **431** 176-9.
58. Mateescu M, Metz-Boutigue M-H, Bertani P, Ball V 2016 Polyelectrolytes to produce nanosized polydopamine *Journal of Colloid and Interface Science* **469** 184-90.
59. Zhang Y, Thingholm B, Goldie K N, Ogaki R, Stadler B 2012 Assembly of poly(dopamine) films mixed with a nonionic polymer *Langmuir* **28** 17585-92.
60. Chassepot A, Ball V 2014 Human serum albumin and other proteins as templating agents for the synthesis of nanosized dopamine-eumelanin *Journal of colloid and interface science* **414** 97-102.
61. Bergtold C, Hauser D, Chaumont A, El Yakhlifi S, Mateescu M, Meyer F, Metz-Boutigue M H, Frisch B, Schaaf P, Ihiawakrim D, Ersen O, Monnier C A, Petri-Fink A, Rothen-Rutishauser B, Ball V 2018 Mimicking the Chemistry of Natural Eumelanin Synthesis: The KE Sequence in Polypeptides and in Proteins Allows for a Specific Control of Nanosized Functional Polydopamine Formation *Biomacromolecules* **19** 3693-704.
62. El Yakhlifi S, Ball V 2020 Polydopamine as a stable and functional nanomaterial *Colloids and Surfaces B: Biointerfaces* **186** 110719.

63. Fan H, Yu X, Liu Y, Shi Z, Liu H, Nie Z, Wu D, Jin Z 2015 Folic acid–polydopamine nanofibers show enhanced ordered-stacking via π–π interactions *Soft Matter* **11** 4621-29.
64. Chyasnavichyus M, Young S L, Tsukruk V V 2014 Probing of Polymer Surfaces in the Viscoelastic Regime *Langmuir* **30** 10566-82.
65. Chen F, Xing Y, Wang Z, Zheng X, Zhang J, Cai K 2016 Nanoscale Polydopamine (PDA) Meets π–π Interactions: An Interface-Directed Coassembly Approach for Mesoporous Nanoparticles *Langmuir* **32** 12119-28.
66. Xing Y, Zhang J, Chen F, Liu J, Cai K 2017 Mesoporous polydopamine nanoparticles with co-delivery function for overcoming multidrug resistance via synergistic chemo-photothermal therapy *Nanoscale* **9** 8781-90.
67. Zhang M, Zhang L, Chen Y, Li L, Su Z, Wang C 2017 Precise synthesis of unique polydopamine/mesoporous calcium phosphate hollow Janus nanoparticles for imaging-guided chemo-photothermal synergistic therapy *Chemical Science* **8** 8067-77.
68. Shang B, Wang Y, Peng B, Deng Z 2020 Bioinspired polydopamine coating as a versatile platform for synthesizing asymmetric Janus particles at an air-water interface *Applied Surface Science* **509** 145360.
69. Xu H, Liu X, Su G, Zhang B, Wang D 2012 Electrostatic repulsion-controlled formation of polydopamine-gold Janus particles *Langmuir* **28** 13060-5.
70. Sheng Y, Sun G, Ngai T 2016 Dopamine Polymerization in Liquid Marbles: A General Route to Janus Particle Synthesis *Langmuir* **32** 3122-29.
71. Qu Y, Huang R, Qi W, Su R, He Z 2015 Interfacial Polymerization of Dopamine in a Pickering Emulsion: Synthesis of Cross-Linkable Colloidosomes and Enzyme Immobilization at Oil/Water Interfaces *ACS Applied Materials & Interfaces* **7** 14954-64.
72. Cui J W, Wang Y J, Postma A, Hao J C, Hosta-Rigau L, Caruso F 2010 Monodisperse polymer capsules: Tailoring size, shell thickness, and hydrophobic cargo loading via emulsion templating *Adv. Funct. Mater.* **20** 1625.
73. Xu L, Liu X, Wang D 2011 Interfacial Basicity-Guided Formation of Polydopamine Hollow Capsules in Pristine O/W Emulsions-Toward Understanding of Emulsion Template Role *Chem. Mater.* **23** 5105.
74. Zhuang H, Su H, Bi X, Bai Y, Chen L, Ge D, Shi W, Sun Y 2017 Polydopamine Nanocapsule: A Theranostic Agent for Photoacoustic Imaging and Chemo-Photothermal Synergistic Therapy *ACS Biomaterials Science & Engineering* **3** 1799-808.
75. Ni Y-Z, Jiang W-F, Tong G-S, Chen J-X, Wang J, Li H-M, Yu C-Y, Huang X-h, Zhou Y-F 2015 Preparation of polydopamine nanocapsules in a miscible tetrahydrofuran–buffer mixture *Organic & Biomolecular Chemistry* **13** 686-90.
76. Postma A, Yan Y, Wang Y, Zelikin A N, Tjipto E, Caruso F 2009 Self-Polymerization of Dopamine as a Versatile and Robust Technique to Prepare Polymer Capsules *Chemistry of Materials* **21** 3042-44.
77. Xue J, Zheng W, Wang L, Jin Z 2016 Scalable Fabrication of Polydopamine Nanotubes Based on Curcumin Crystals *ACS Biomaterials Science & Engineering* **2** 489-93.
78. Dong Z, Feng L, Hao Y, Chen M, Gao M, Chao Y, Zhao H, Zhu W, Liu J, Liang C, Zhang Q, Liu Z 2018 Synthesis of Hollow Biomineralized CaCO3–Polydopamine Nanoparticles for Multimodal Imaging-Guided Cancer Photodynamic Therapy with Reduced Skin Photosensitivity *Journal of the American Chemical Society* **140** 2165-78.
79. Tran H Q, Bhave M, Xu G, Sun C, Yu A 2019 Synthesis of Polydopamine Hollow Capsules via a Polydopamine Mediated Silica Water Dissolution Process and Its Application for Enzyme Encapsulation *Frontiers in Chemistry* **7**
80. Yan D, Xu P, Xiang Q, Mou H, Xu J, Wen W, Li X, Zhang Y 2016 Polydopamine nanotubes: bio-inspired synthesis, formaldehyde sensing properties and thermodynamic investigation *Journal of Materials Chemistry A* **4** 3487-93.
81. Lee M, Lee S-H, Oh I-K, Lee H 2017 Microwave-Accelerated Rapid, Chemical Oxidant-Free, Material-Independent Surface Chemistry of Poly(dopamine) *Small* **13** 1600443.

82. Salomäki M, Marttila L, Kivelä H, Ouvinen T, Lukkari J 2018 Effects of pH and Oxidants on the First Steps of Polydopamine Formation: A Thermodynamic Approach *J Phys Chem B* **122** 6314-27.
83. Ball V, Gracio J, Vila M, Singh M K, Metz-Boutigue M H, Michel M, Bour J, Toniazzo V, Ruch D, Buehler M J 2013 Comparison of synthetic dopamine-eumelanin formed in the presence of oxygen and Cu2+ cations as oxidants *Langmuir* **29** 12754.
84. Lee H, Dellatore S M, Miller W M, Messersmith P B 2007 Mussel-inspired surface chemistry for multifunctional coatings *Science* **318** 426-30.
85. Hong S, Schaber C F, Dening K, Appel E, Gorb S N, Lee H 2014 Air/Water Interfacial Formation of Freestanding, Stimuli-Responsive, Self-Healing Catecholamine Janus-Faced Microfilms *Advanced Materials* **26** 7581-87.
86. Kim H W, McCloskey B D, Choi T H, Lee C, Kim M-J, Freeman B D, Park H B 2013 Oxygen Concentration Control of Dopamine-Induced High Uniformity Surface Coating Chemistry *ACS Applied Materials & Interfaces* **5** 233-38.
87. Wei Q, Zhang F, Li J, Li B, Zhao C 2010 Oxidant-induced Dopamine Polymerization for Multifunctional Coatings *Polym. Chem.* **1** 1430.
88. Ball V, Gracio J, Vila M, Singh M K, Metz-Boutigue M-H, Michel M, Bour J, Toniazzo V, Ruch D, Buehler M J 2013 Comparison of Synthetic Dopamine–Eumelanin Formed in the Presence of Oxygen and Cu2+ Cations as Oxidants *Langmuir* **29** 12754-61.
89. Salomäki M, Ouvinen T, Marttila L, Kivelä H, Leiro J, Mäkilä E, Lukkari J 2019 Polydopamine Nanoparticles Prepared Using Redox-Active Transition Metals *J Phys Chem B* **123** 2513-24.
90. Zhao Y, Li H, Gao W, Ren F 2019 Biopolymer-Assisted Manufacturing of Aluminum–Copper Nanoparticle Composites with Enhanced Sinterability *ACS Applied Nano Materials* **2** 5688-94.
91. Lee B P, Dalsin J L, Messersmith P B 2002 Synthesis and gelation of DOPA-modified poly(ethylene glycol) hydrogels *Biomacromolecules* **3** 1038-47.
92. Zhang C, Ou Y, Lei W X, Wan L S, Ji J, Xu Z K 2016 CuSO4/H2O2-Induced Rapid Deposition of Polydopamine Coatings with High Uniformity and Enhanced Stability *Angewandte Chemie (International ed. in English)* **55** 3054-7.
93. Zhu J, Tsehaye M T, Wang J, Uliana A, Tian M, Yuan S, Li J, Zhang Y, Volodin A, Van der Bruggen B 2018 A rapid deposition of polydopamine coatings induced by iron (III) chloride/hydrogen peroxide for loose nanofiltration *Journal of colloid and interface science* **523** 86-97.
94. Jiao L, Xu Z, Du W, Li H, Yin M 2017 Fast Preparation of Polydopamine Nanoparticles Catalyzed by Fe(2+)/H2O2 for Visible Sensitive Smartphone-Enabled Cytosensing *ACS Appl Mater Interfaces* **9** 28339-45.
95. Ball V 2014 Physicochemical perspective on "polydopamine" and "poly(catecholamine)" films for their applications in biomaterial coatings *Biointerphases* **9** 030801.
96. Wang X, Chen Z, Yang P, Hu J, Wang Z, Li Y 2019 Size control synthesis of melanin-like polydopamine nanoparticles by tuning radicals *Polymer Chemistry* **10** 4194-200.
97. Wang W, Li R, Tian M, Liu L, Zou H, Zhao X, Zhang L 2013 Surface Silverized Meta-Aramid Fibers Prepared by Bio-inspired Poly(dopamine) Functionalization *ACS Applied Materials & Interfaces* **5** 2062-69.
98. Wang L, Hu L, Gao S, Zhao D, Zhang L, Wang W 2015 Bio-inspired polydopamine-coated clay and its thermo-oxidative stabilization mechanism for styrene butadiene rubber *RSC Advances* **5** 9314-24.
99. Du X, Li L, Behboodi-Sadabad F, Welle A, Li J, Heissler S, Zhang H, Plumeré N, Levkin P A 2017 Bio-inspired strategy for controlled dopamine polymerization in basic solutions *Polymer Chemistry* **8** 2145-51.
100. Du X, Li L, Li J, Yang C, Frenkel N, Welle A, Heissler S, Nefedov A, Grunze M, Levkin P A 2014 UV-Triggered Dopamine Polymeization: Control of Polymerization, Surface Coating, and Photoppaterning *Adv. Mater.* **26** 8029.
101. Wang J, Ma G, Huang W, He Y 2018 Visible-light initiated polymerization of dopamine in a neutral environment for surface coating and visual protein detection *Polymer Chemistry* **9** 5242-47.

102. Zheng W, Fan H, Wang L, Jin Z 2015 Oxidative Self-Polymerization of Dopamine in an Acidic Environment *Langmuir* **31** 11671.
103. Li F, Yu Y, Wang Q, Yuan J, Wang P, Fan X 2018 Polymerization of dopamine catalyzed by laccase: Comparison of enzymatic and conventional methods *Enzyme and microbial technology* **119** 58-64.
104. Tan Y, Deng W, Li Y, Huang Z, Meng Y, Xie Q, Ma M, Yao S 2010 Polymeric Bionanocomposite Cast Thin Films with In Situ Laccase-Catalyzed Polymerization of Dopamine for Biosensing and Biofuel Cell Applications *The Journal of Physical Chemistry B* **114** 5016-24.
105. Zhang C, Gong L, Mao Q, Han P, Lu X, Qu J 2018 Laccase immobilization and surface modification of activated carbon fibers by bio-inspired poly-dopamine *RSC Advances* **8** 14414-21.
106. Cheng H, Hu M, Zhai Q, Li S, Jiang Y 2018 Polydopamine tethered CPO/HRP-TiO2 nano-composites with high bio-catalytic activity, stability and reusability: Enzyme-photo bifunctional synergistic catalysis in water treatment *Chemical Engineering Journal* **347** 703-10.
107. Li N, Wang H-B, Thia L, Wang J-Y, Wang X 2015 Enzymatic-reaction induced production of polydopamine nanoparticles for sensitive and visual sensing of urea *Analyst* **140** 449-55.
108. Kim S, Jang L K, Park H S, Lee J Y 2016 Electrochemical deposition of conductive and adhesive polypyrrole-dopamine films *Scientific Reports* **6** 30475.
109. Li S, Wang H, Young M, Xu F, Cheng G, Cong H 2019 Properties of Electropolymerized Dopamine and Its Analogues *Langmuir* **35** 1119-25.
110. Hongfei S, Huaixiang L, Wei H In *Porous polydopamine and para-aminobenzoic acid complex membrane formed by electrochemical codeposition/degradation*, 2017 6th International Conference on Measurement, Instrumentation and Automation (ICMIA 2017), 2017/06; Atlantis Press: 2017; pp 11-16.
111. Stöckle B, Ng D Y W, Meier C, Paust T, Bischoff F, Diemant T, Behm R J, Gottschalk K-E, Ziener U, Weil T 2014 Precise Control of Polydopamine Film Formation by Electropolymerization *Macromolecular Symposia* **346** 73-81.
112. Cai J, Huang J, Ge M, Iocozzia J, Lin Z, Zhang K Q, Lai Y 2017 Immobilization of Pt Nanoparticles via Rapid and Reusable Electropolymerization of Dopamine on TiO2 Nanotube Arrays for Reversible SERS Substrates and Nonenzymatic Glucose Sensors *Small* **13**
113. Mazario E, Sánchez-Marcos J, Menéndez N, Herrasti P, García-Hernández M, Muñoz-Bonilla A 2014 One-pot electrochemical synthesis of polydopamine coated magnetite nanoparticles *RSC Advances* **4** 48353-61.
114. Sukeri A, Arjunan A, Bertotti M 2020 New strategy to fabricate a polydopamine functionalized self-supported nanoporous gold film electrode for electrochemical sensing applications *Electrochemistry Communications* **110** 106622.
115. Wang Z, Xu C, Lu Y, Wei G, Ye G, Sun T, Chen J 2018 Microplasma electrochemistry controlled rapid preparation of fluorescent polydopamine nanoparticles and their application in uranium detection *Chemical Engineering Journal* **344** 480-86.
116. Chassepot A, Ball V 2014 Human serum albumin and other proteins as templating agents for the synthesis of nanosized dopamine-eumelanin *J. Colloid Interface Sci.* **414** 97.
117. Yu X, Fan H, Wang L, Jin Z 2014 Formation of Polydopamine Nanofibers with the Aid of Folic Acid *Angewandte Chemie International Edition* **53** 12600-04.
118. Xu H, Liu X, Wang D 2011 Interfacial Basicity-Guided Formation of Polydopamine Hollow Capsules in Pristine O/W Emulsions – Toward Understanding of Emulsion Template Roles *Chemistry of Materials* **23** 5105-10.
119. Dreyer D R, Miller D J, Freeman B D, Paul D R, Bielawski C W 2012 Elucidating the structure of poly(dopamine) *Langmuir* **28** 6428.
120. Hong S, Na Y S, Choi S, Song I T, Kim W Y, Lee H 2012 Non-covalent self-assembly and covalent polymerization co-contribute to polydopamine formation *Adv. Funct. Mater.* **22** 4711.
121. Hong S, Wang Y, Park S Y, Lee H 2018 Progressive fuzzy cation-π assembly of biological catecholamines *Science Advances* **4** eaat7457.

122. Kang X, Cai W, Zhang S, Cui S 2017 Revealing the formation mechanism of insoluble polydopamine by using a simplified model system *Polymer Chemistry* **8** 860-64.
123. Liebscher J, Mrowczynski R, Scheidt H A, Filip C, Hadade N D, Turcu R, Bende A, Beck S 2013 Structure of polydopamine: A never-ending story? *Langmuir* **29** 10539.
124. Delparastan P, Malollari K G, Lee H, Messersmith P B 2019 Direct Evidence for the Polymeric Nature of Polydopamine *Angewandte Chemie (International ed. in English)* **58** 1077-82.
125. Cîrcu M, Filip C 2018 Closer to the polydopamine structure: new insights from a combined 13C/1H/2H solid-state NMR study on deuterated samples *Polymer Chemistry* **9** 3379-87.
126. Chen C-T, Buehler M J 2018 Polydopamine and eumelanin models in various oxidation states *Physical Chemistry Chemical Physics* **20** 28135-43.
127. d'Ischia M, Napolitano A, Ball V, Chen C T, Buehler M J 2014 Polydopamine and Eumelanin: From Structure-Property Relationships to a Unified Tailoring Strategy *Acc. Chem. Res.* **47** 3541.
128. Lyu Q, Hsueh N, Chai C L L 2019 Direct Evidence for the Critical Role of 5,6-Dihydroxyindole in Polydopamine Deposition and Aggregation *Langmuir* **35** 5191-201.
129. Lyu Q, Hsueh N, Chai C L L 2019 Unravelling the polydopamine mystery: is the end in sight? *Polymer Chemistry* **10** 5771-77.
130. Ding Y, Weng L T, Yang M, Yang Z, Lu X, Huang N, Leng Y 2014 Insights into the Aggreagation/Deposition and Structure of a Polydopamine Film *Langmuir* **30** 12258.
131. Alfieri M L, Micillo R, Panzella L, Crescenzi O, Oscurato S L, Maddalena P, Napolitano A, Ball V, d'Ischia M 2018 Structural Basis of Polydopamine Film Formation: Probing 5,6-Dihydroxyindole-Based Eumelanin Type Units and the Porphyrin Issue *ACS Applied Materials & Interfaces* **10** 7670-80.
132. Lyu Q, Song H, Yakovlev N L, Tan W S, Chai Christina L L 2018 In situ insights into the nanoscale deposition of 5,6-dihydroxyindole-based coatings and the implications on the underwater adhesion mechanism of polydopamine coatings *RSC Advances* **8** 27695-702.
133. Liao F, Yin S, Toney M F, Subramanian V 2010 Physical discrimination of amine vapor mixtures using polythiophene gas sensor arrays *Sensors and Actuators B: Chemical* **150** 254-63.
134. Ju K-Y, Fischer M C, Warren W S 2018 Understanding the Role of Aggregation in the Broad Absorption Bands of Eumelanin *ACS Nano* **12** 12050-61.
135. Nieto C, Vega M A, Marcelo G, Martín del Valle Eva M 2018 Polydopamine nanoparticles kill cancer cells *RSC Advances* **8** 36201-08.
136. Nieto C, Vega M A, Enrique J, Marcelo G, Martin Del Valle E M 2019 Size Matters in the Cytotoxicity of Polydopamine Nanoparticles in Different Types of Tumors *Cancers* **11**
137. Ju K Y, Kang J, Pyo J, Lim J, Chang J H, Lee J K 2016 pH-Induced aggregated melanin nanoparticles for photoacoustic signal amplification *Nanoscale* **8** 14448-56.
138. Cheng Y, Zhang S, Kang N, Huang J, Lv X, Wen K, Ye S, Chen Z, Zhou X, Ren L 2017 Polydopamine-Coated Manganese Carbonate Nanoparticles for Amplified Magnetic Resonance Imaging-Guided Photothermal Therapy *ACS Appl Mater Interfaces* **9** 19296-306.
139. Kunwar A, Adhikary B, Jayakumar S, Barik A, Chattopadhyay S, Raghukumar S, Priyadarsini K I 2012 Melanin, a promising radioprotector: Mechanisms of actions in a mice model *Toxicology and Applied Pharmacology* **264** 202-11.
140. Hong S, Kim K, Wook H, Park S, Lee K, Lee D Y, Lee H 2011 Attenuation of the in vivo toxicity of biomaterials by polydopamine surface modification *Nanomedicine (London, England)* **6** 793-801.
141. Nie S, Qin H, Cheng C, Zhao W, Sun S, Su B, Zhao C, Gu Z 2014 Blood activation and compatibility on single-molecular-layer biointerfaces *Journal of Materials Chemistry B* **2** 4911-21.
142. Cheng C, Sun S, Zhao C 2014 Progress in heparin and heparin-like/mimicking polymer-functionalized biomedical membranes *Journal of Materials Chemistry B* **2** 7649-72.
143. Ding Y, Yang Z, Bi C W C, Yang M, Zhang J, Xu S L, Lu X, Huang N, Huang P, Leng Y 2014 Modulation of protein adsorption, vascular cell selectivity and platelet adhesion by mussel-inspired surface functionalization *Journal of Materials Chemistry B* **2** 3819-29.

144. Luo R, Tang L, Zhong S, Yang Z, Wang J, Weng Y, Tu Q, Jiang C, Huang N 2013 In vitro investigation of enhanced hemocompatibility and endothelial cell proliferation associated with quinone-rich polydopamine coating *ACS Appl Mater Interfaces* **5** 1704-14.
145. Bettinger C J, Bruggeman J P, Misra A, Borenstein J T, Langer R 2009 Biocompatibility of biodegradable semiconducting melanin films for nerve tissue engineering *Biomaterials* **30** 3050-7.
146. Cave A C, Brewer A C, Narayanapanicker A, Ray R, Grieve D J, Walker S, Shah A M 2006 NADPH oxidases in cardiovascular health and disease *Antioxidants & redox signaling* **8** 691-728.
147. Hui Y, Yi X, Hou F, Wibowo D, Zhang F, Zhao D, Gao H, Zhao C X 2019 Role of Nanoparticle Mechanical Properties in Cancer Drug Delivery *ACS Nano* **13** 7410-24.
148. Hui Y, Yi X, Wibowo D, Yang G, Middelberg A P J, Gao H, Zhao C-X 2020 Nanoparticle elasticity regulates phagocytosis and cancer cell uptake *Science Advances* **6** eaaz4316.
149. Guo P, Liu D, Subramanyam K, Wang B, Yang J, Huang J, Auguste D, Moses M 2018 Nanoparticle elasticity directs tumor uptake *Nature Communications* **9**
150. Klosterman L, Ahmad Z, Viswanathan V, Bettinger C J 2017 Synthesis and Measurement of Cohesive Mechanics in Polydopamine Nanomembranes *Advanced Materials Interfaces* **4** 1700041.
151. Li H, Xi J, Zhao Y, Ren F 2019 Mechanical properties of polydopamine (PDA) thin films *MRS Advances* **4** 405-12.
152. Lin S, Chen C-T, Bdikin I, Ball V, Grácio J, Buehler M J 2014 Tuning heterogeneous poly(dopamine) structures and mechanics: in silico covalent cross-linking and thin film nanoindentation *Soft Matter* **10** 457-64.
153. Malollari K G, Delparastan P, Sobek C, Vachhani S J, Fink T D, Zha R H, Messersmith P B 2019 Mechanical Enhancement of Bioinspired Polydopamine Nanocoatings *ACS Applied Materials & Interfaces* **11** 43599-607.
154. Alfieri M L, Panzella L, Oscurato S L, Salvatore M, Avolio R, Errico M E, Maddalena P, Napolitano A, D'Ischia M 2018 The Chemistry of Polydopamine Film Formation: The Amine-Quinone Interplay *Biomimetics (Basel)* **3** 26.
155. Wang S, Zhao X, Wang S, Qian J, He S 2016 Biologically Inspired Polydopamine Capped Gold Nanorods for Drug Delivery and Light-Mediated Cancer Therapy *ACS Applied Materials & Interfaces* **8**
156. Hao M, Kong C, Jiang C, Hou R, Zhao X, Li J, Wang Y, Gao Y, Zhang H, Yang B, Jiang J 2019 Polydopamine-coated Au-Ag nanoparticle-guided photothermal colorectal cancer therapy through multiple cell death pathways *Acta Biomaterialia* **83** 414-24.
157. Lin L-S, Cong Z-X, Cao J-B, Ke K-M, Peng Q-L, Gao J, Yang H-H, Liu G, Chen X 2014 Multifunctional Fe3O4@Polydopamine Core–Shell Nanocomposites for Intracellular mRNA Detection and Imaging-Guided Photothermal Therapy *ACS Nano* **8** 3876-83.
158. Zeng W, Zhang H, Deng Y, Jiang A, Bao X, Guo M, Li Z, Wu M, Ji X, Zeng X, Mei L 2020 Dual-response oxygen-generating MnO2 nanoparticles with polydopamine modification for combined photothermal-photodynamic therapy *Chemical Engineering Journal* **389** 124494.
159. Cheng W, Nie J, Gao N, Liu G, Tao W, Xiao X, Jiang L, Liu Z, Zeng X, Mei L 2017 A Multifunctional Nanoplatform against Multidrug Resistant Cancer: Merging the Best of Targeted Chemo/Gene/Photothermal Therapy *Advanced Functional Materials* **27** 1704135.
160. Tao W, Xu G, Yu X, Zhang J, Sheng Y, Liu G, Mei L 2016 Robust aptamer–polydopamine-functionalized M-PLGA–TPGS nanoparticles for targeted delivery of docetaxel and enhanced cervical cancer therapy *Int J Nanomedicine* **11** 2953.
161. Zong W, Hu Y, Su Y, Luo N, Zhang X, Li Q, Han X 2016 Polydopamine-coated liposomes as pH-sensitive anticancer drug carriers *Journal of Microencapsulation* **33** 1-6.
162. Zhang R, Su S, Hu K, Shao L, Deng X, Sheng W, Wu Y 2015 Smart micelle@polydopamine core–shell nanoparticles for highly effective chemo–photothermal combination therapy *Nanoscale* **7** 19722-31.
163. Wu X, Zhou L, Su Y, Dong C-M 2016 A polypeptide micelle template method to prepare polydopamine composite nanoparticles for synergistic photothermal–chemotherapy *Polymer Chemistry* **7** 5552-62.

164. Li M, Sun X, Zhang N, Wang W, Yang Y, Jia H, Liu W 2018 NIR-Activated Polydopamine-Coated Carrier-Free "Nanobomb" for In Situ On-Demand Drug Release *Advanced Science* **5** 1800155.
165. Kwon I S, Bettinger C J 2018 Polydopamine nanostructures as biomaterials for medical applications *Journal of Materials Chemistry B* **6** 6895-903.
166. Lyu Q, Hsueh N, Chai C L L 2019 The Chemistry of Bioinspired Catechol(amine)-Based Coatings *ACS Biomaterials Science & Engineering* **5** 2708-24.
167. Jin Z, Fan H 2016 The modulation of melanin-like materials: methods, characterization and applications *Polymer International* **65** 1258-66.
168. Chen Y, Ai K, Liu J, Ren X, Jiang C, Lu L 2016 Polydopamine-based coordination nanocomplex for T1/T2 dual mode magnetic resonance imaging-guided chemo-photothermal synergistic therapy *Biomaterials* **77** 198-206.
169. Yao A, Jiao X, Chen D, Li C 2020 Bio-Inspired Polydopamine-Mediated Zr-MOF Fabrics for Solar Photothermal-Driven Instantaneous Detoxification of Chemical Warfare Agent Simulants *ACS Applied Materials & Interfaces* **12** 18437-45.
170. Wang D, Wu H, Zhou J, Xu P, Wang C, Shi R, Wang H, Wang H, Guo Z, Chen Q 2018 In Situ One-Pot Synthesis of MOF–Polydopamine Hybrid Nanogels with Enhanced Photothermal Effect for Targeted Cancer Therapy *Advanced Science* **5** 1800287.
171. Cho S, Park W, Kim D H 2017 Silica-Coated Metal Chelating-Melanin Nanoparticles as a Dual-Modal Contrast Enhancement Imaging and Therapeutic Agent *ACS Appl Mater Interfaces* **9** 101-11.
172. Miao Z-H, Wang H, Yang H, Li Z-L, Zhen L, Xu C-Y 2015 Intrinsically Mn2+-Chelated Polydopamine Nanoparticles for Simultaneous Magnetic Resonance Imaging and Photothermal Ablation of Cancer Cells *ACS Applied Materials & Interfaces* **7** 16946-52.
173. Li Y, Xie Y, Wang Z, Zang N, Carniato F, Huang Y, Andolina C M, Parent L R, Ditri T B, Walter E D, Botta M, Rinehart J D, Gianneschi N C 2016 Structure and Function of Iron-Loaded Synthetic Melanin *ACS nano* **10** 10186-94.
174. Deng X, Cao S, Li N, Wu H, Smith T J, Zong M, Lou W 2016 A magnetic biocatalyst based on mussel-inspired polydopamine and its acylation of dihydromyricetin *Chinese Journal of Catalysis* **37** 584-95.
175. Subair R, Tripathi B P, Formanek P, Simon F, Uhlmann P, Stamm M 2016 Polydopamine modified membranes with in situ synthesized gold nanoparticles for catalytic and environmental applications *Chemical Engineering Journal* **295** 358-69.
176. Liu L, Cai R, Wang Y, Tao G, Ai L, Wang P, Yang M, Zuo H, Zhao P, He H 2018 Polydopamine-Assisted Silver Nanoparticle Self-Assembly on Sericin/Agar Film for Potential Wound Dressing Application *Int J Mol Sci* **19** 2875.
177. Zhang P, Hu W, Wu M, Gong L, Tang A, Xiang L, Zhu B, Zhu L, Zeng H 2019 Cost-Effective Strategy for Surface Modification via Complexation of Disassembled Polydopamine with Fe(III) Ions *Langmuir* **35** 4101-09.
178. Hong L, Simon J D 2007 Current Understanding of the Binding Sites, Capacity, Affinity, and Biological Significance of Metals in Melanin *The Journal of Physical Chemistry B* **111** 7938-47.
179. Cui J, Yan Y, Such G K, Liang K, Ochs C J, Postma A, Caruso F 2012 Immobilization and Intracellular Delivery of an Anticancer Drug Using Mussel-Inspired Polydopamine Capsules *Biomacromolecules* **13** 2225-28.
180. Wu H, Hu H, Wan J, Li Y, Wu Y, Tang Y, Xiao C, Xu H, Yang X, Li Z 2018 Hydroxyethyl starch stabilized polydopamine nanoparticles for cancer chemotherapy *Chemical Engineering Journal* **349** 129-45.
181. Wang N, Yang Y, Wang X, Tian X, Qin W, Wang X, Liang J, Zhang H, Leng X 2019 Polydopamine as the Antigen Delivery Nanocarrier for Enhanced Immune Response in Tumor Immunotherapy *ACS Biomaterials Science & Engineering* **5** 2330-42.
182. Karimi Shervedani R, Samiei Foroushani M, Kefayat A, Torabi M, Rahnemaye Rahsepar F 2018 Construction and characterization of a theranostic system based on graphene/manganese chelate *Biosensors and Bioelectronics* **117** 794-801.

183. Wang H, Zhu W, Huang Y, Li Z, Jiang Y, Xie Q 2017 Facile encapsulation of hydroxycamptothecin nanocrystals into zein-based nanocomplexes for active targeting in drug delivery and cell imaging *Acta Biomaterialia* **61** 88-100.
184. Zhu Z, Su M 2017 Polydopamine Nanoparticles for Combined Chemo- and Photothermal Cancer Therapy *Nanomaterials (Basel, Switzerland)* **7**
185. Sun L, Li Q, Zhang L, Xu Z, Kang Y, Xue P 2018 PEGylated Polydopamine Nanoparticles Incorporated with Indocyanine Green and Doxorubicin for Magnetically Guided Multimodal Cancer Therapy Triggered by Near-Infrared Light *ACS Applied Nano Materials* **1** 325-36.
186. Yan S, Huang Q, Chen J, Song X, Chen Z, Huang M, Xu P, Zhang J 2019 Tumor-targeting photodynamic therapy based on folate-modified polydopamine nanoparticles *Int J Nanomedicine* **14** 6799-812.
187. Zhu D, Tao W, Zhang H, Liu G, Wang T, Zhang L, Zeng X, Mei L 2016 Docetaxel (DTX)-loaded polydopamine-modified TPGS-PLA nanoparticles as a targeted drug delivery system for the treatment of liver cancer *Acta biomaterialia* **30** 144-54.
188. Tran A-V, Shim K, Vo Thi T-T, Kook J-K, An S S A, Lee S-W 2018 Targeted and controlled drug delivery by multifunctional mesoporous silica nanoparticles with internal fluorescent conjugates and external polydopamine and graphene oxide layers *Acta Biomaterialia* **74** 397-413.
189. Mu X, Zhang F, Kong C, Zhang H, Zhang W, Ge R, Liu Y, Jiang J 2017 EGFR-targeted delivery of DOX-loaded Fe(3)O(4)@ polydopamine multifunctional nanocomposites for MRI and antitumor chemo-photothermal therapy *International journal of nanomedicine* **12** 2899-911.
190. Cheng W, Nie J, Xu L, Liang C, Peng Y, Liu G, Wang T, Mei L, Huang L, Zeng X 2017 pH-Sensitive Delivery Vehicle Based on Folic Acid-Conjugated Polydopamine-Modified Mesoporous Silica Nanoparticles for Targeted Cancer Therapy *ACS Applied Materials & Interfaces* **9** 18462-73.
191. Ding T, Wang L, Zhang J, Xing Y, Cai K 2018 Interfacially active polydopamine for nanoparticle stabilized nanocapsules in a one-pot assembly strategy toward efficient drug delivery *Journal of Materials Chemistry B* **6** 1754-63.
192. Zhao C, Zuo F, Liao Z, Qin Z, Du S, Zhao Z 2015 Mussel-Inspired One-Pot Synthesis of a Fluorescent and Water-Soluble Polydopamine–Polyethyleneimine Copolymer *Macromolecular Rapid Communications* **36** 909-15.
193. Zhang D, Wu M, Zeng Y, Wu L, Wang Q, Han X, Liu X, Liu J 2015 Chlorin e6 Conjugated Poly(dopamine) Nanospheres as PDT/PTT Dual-Modal Therapeutic Agents for Enhanced Cancer Therapy *ACS Appl Mater Interfaces* **7** 8176-87.
194. Song Y, Ye G, Wu F, Wang Z, Liu S, Kopeć M, Wang Z, Chen J, Wang J, Matyjaszewski K 2016 Bioinspired Polydopamine (PDA) Chemistry Meets Ordered Mesoporous Carbons (OMCs): A Benign Surface Modification Strategy for Versatile Functionalization *Chemistry of Materials* **28** 5013-21.
195. Liu C-Y, Huang C-J 2016 Functionalization of Polydopamine via the Aza-Michael Reaction for Antimicrobial Interfaces *Langmuir* **32** 5019-28.
196. Liu Q, Yu B, Ye W, Zhou F 2011 Highly Selective Uptake and Release of Charged Molecules by pH-Responsive Polydopamine Microcapsules *Macromolecular Bioscience* **11** 1227-34.
197. Dong Z, Gong H, Gao M, Zhu W, Sun X, Feng L, Fu T, li Y, Liu Z 2016 Polydopamine Nanoparticles as a Versatile Molecular Loading Platform to Enable Imaging-guided Cancer Combination Therapy *Theranostics* **6** 1031-42.
198. Banstola A, Pham T T, Jeong J-H, Yook S 2019 Polydopamine-tailored paclitaxel-loaded polymeric microspheres with adhered NIR-controllable gold nanoparticles for chemo-phototherapy of pancreatic cancer *Drug Delivery* **26** 629-40.
199. Poinard B, Neo S Z Y, Yeo E L L, Heng H P S, Neoh K G, Kah J C Y 2018 Polydopamine Nanoparticles Enhance Drug Release for Combined Photodynamic and Photothermal Therapy *ACS Applied Materials & Interfaces* **10** 21125-36.
200. Crippa P R, Cristofoletti V, Romeo N 1978 A band model for melanin deducted from optical absorption and photoconductivity experiments *Biochimica et biophysica acta* **538** 164-70.

201. Riesz J, Gilmore J, Meredith P 2006 Quantitative scattering of melanin solutions *Biophysical journal* **90** 4137-44.
202. Meredith P, Powell B J, Riesz J, Nighswander-Rempel S P, Pederson M R, Moore E G 2006 Towards structure–property–function relationships for eumelanin *Soft Matter* **2** 37-44.
203. Wolbarsht M L, Walsh A W, George G 1981 Melanin, a unique biological absorber *Appl. Opt.* **20** 2184-86.
204. Tran M L, Powell B J, Meredith P 2006 Chemical and structural disorder in eumelanins: a possible explanation for broadband absorbance *Biophys J* **90** 743-52.
205. Pezzella A, Iadonisi A, Valerio S, Panzella L, Napolitano A, Adinolfi M, d'Ischia M 2009 Disentangling Eumelanin "Black Chromophore": Visible Absorption Changes As Signatures of Oxidation State- and Aggregation-Dependent Dynamic Interactions in a Model Water-Soluble 5,6-Dihydroxyindole Polymer *Journal of the American Chemical Society* **131** 15270-75.
206. Ascione L, Pezzella A, Ambrogi V, Carfagna C, d'Ischia M 2013 Intermolecular pi-electron perturbations generate extrinsic visible contributions to eumelanin black chromophore in model polymers with interrupted interring conjugation *Photochemistry and photobiology* **89** 314-8.
207. Chen C T, Chuang C, Cao J, Ball V, Ruch D, Buehler M J 2014 Excitonic effects from geometric order and disorder explain broadband optical absorption in eumelanin *Nature communications* **5** 3859.
208. Micillo R, Panzella L, Iacomino M, Prampolini G, Cacelli I, Ferretti A, Crescenzi O, Koike K, Napolitano A, d'Ischia M 2017 Eumelanin broadband absorption develops from aggregation-modulated chromophore interactions under structural and redox control *Scientific reports* **7** 41532.
209. Spano F C 2010 The Spectral Signatures of Frenkel Polarons in H- and J-Aggregates *Accounts of Chemical Research* **43** 429-39.
210. Meredith P, Riesz J 2004 Radiative relaxation quantum yields for synthetic eumelanin *Photochemistry and photobiology* **79** 211-6.
211. Nofsinger J B, Simon J D 2001 Radiative relaxation of Sepia eumelanin is affected by aggregation *Photochemistry and photobiology* **74** 31-7.
212. Nofsinger J B, Ye T, Simon J D 2001 Ultrafast Nonradiative Relaxation Dynamics of Eumelanin *The Journal of Physical Chemistry B* **105** 2864-66.
213. Chen M, Wen Q, Gu F, Gao J, Zhang C C, Wang Q 2018 Mussel chemistry assembly of a novel biosensing nanoplatform based on polydopamine fluorescent dot and its photophysical features *Chemical Engineering Journal* **342** 331-38.
214. Nighswander-Rempel S P, Riesz J, Gilmore J, Meredith P 2005 A quantum yield map for synthetic eumelanin *The Journal of Chemical Physics* **123** 194901.
215. Perna G, Frassanito M C, Palazzo G, Gallone A, Mallardi A, Biagi P F, Capozzi V 2009 Fluorescence spectroscopy of synthetic melanin in solution *Journal of Luminescence* **129** 44-49.
216. Yang P, Zhang S, Chen X, Liu X, Wang Z, Li Y 2020 Recent developments in polydopamine fluorescent nanomaterials *Materials Horizons* **7** 746-61.
217. Yin H, Zhang K, Wang L, Zhou K, Zeng J, Gao D, Xia Z, Fu Q 2018 Redox modulation of polydopamine surface chemistry: a facile strategy to enhance the intrinsic fluorescence of polydopamine nanoparticles for sensitive and selective detection of Fe3+ *Nanoscale* **10** 18064-73.
218. Lin J-H, Yu C-J, Yang Y-C, Tseng W-L 2015 Formation of fluorescent polydopamine dots from hydroxyl radical-induced degradation of polydopamine nanoparticles *Physical Chemistry Chemical Physics* **17** 15124-30.
219. Eda G, Lin Y Y, Mattevi C, Yamaguchi H, Chen H A, Chen I S, Chen C W, Chhowalla M 2010 Blue photoluminescence from chemically derived graphene oxide *Advanced materials (Deerfield Beach, Fla.)* **22** 505-9.
220. Zhang X, Wang S, Xu L, Feng L, Ji Y, Tao L, Li S, Wei Y 2012 Biocompatible polydopamine fluorescent organic nanoparticles: facile preparation and cell imaging *Nanoscale* **4** 5581-84.
221. Ma B, Liu F, Zhang S, Duan J, Kong Y, Li Z, Tang D, Wang W, Ge S, Tang W, Liu H 2018 Two-photon fluorescent polydopamine nanodots for CAR-T cell function verification and tumor cell/tissue detection *Journal of Materials Chemistry B* **6** 6459-67.

222. Tang L, Mo S, Liu S G, Li N, Ling Y, Li N B, Luo H Q 2018 Preparation of bright fluorescent polydopamine-glutathione nanoparticles and their application for sensing of hydrogen peroxide and glucose *Sensors and Actuators B: Chemical* **259** 467-74.
223. Massiot J, Rosilio V, Makky A 2019 Photo-triggerable liposomal drug delivery systems: from simple porphyrin insertion in the lipid bilayer towards supramolecular assemblies of lipid–porphyrin conjugates *Journal of Materials Chemistry B* **7** 1805-23.
224. Yao J, Feng J, Chen J 2016 External-stimuli responsive systems for cancer theranostic *Asian Journal of Pharmaceutical Sciences* **11** 585-95.
225. Habash R W, Bansal R, Krewski D, Alhafid H T 2006 Thermal therapy, part 1: an introduction to thermal therapy *Critical reviews in biomedical engineering* **34** 459-89.
226. GhavamiNejad A, SamariKhalaj M, Aguilar L E, Park C H, Kim C S 2016 pH/NIR Light-Controlled Multidrug Release via a Mussel-Inspired Nanocomposite Hydrogel for Chemo-Photothermal Cancer Therapy *Scientific reports* **6** 33594.
227. Gao Y, Wu X, Zhou L, Su Y, Dong C M 2015 A sweet polydopamine nanoplatform for synergistic combination of targeted chemo-photothermal therapy *Macromolecular rapid communications* **36** 916-22.
228. Ding Y, Su S, Zhang R, Shao L, Zhang Y, Wang B, Li Y, Chen L, Yu Q, Wu Y, Nie G 2017 Precision combination therapy for triple negative breast cancer via biomimetic polydopamine polymer core-shell nanostructures *Biomaterials* **113** 243-52.
229. Zheng R, Wang S, Tian Y, Jiang X, Fu D, Shen S, Yang W 2015 Polydopamine-Coated Magnetic Composite Particles with an Enhanced Photothermal Effect *ACS Applied Materials & Interfaces* **7** 15876-84.
230. Zhang T, Li Y, Hong W, Chen Z, Peng P, Yuan S, Qu J, Xiao M, Xu L 2019 Glucose oxidase and polydopamine functionalized iron oxide nanoparticles: combination of the photothermal effect and reactive oxygen species generation for dual-modality selective cancer therapy *Journal of Materials Chemistry B* **7** 2190-200.
231. Bai Y, Zhang B, Chen L, Lin Z, Zhang X, Ge D, Shi W, Sun Y 2018 Facile One-Pot Synthesis of Polydopamine Carbon Dots for Photothermal Therapy *Nanoscale Res Lett* **13** 287-87.
232. Zhang L, Yang P, Guo R, Sun J, Xie R, Yang W 2019 Multifunctional Mesoporous Polydopamine With Hydrophobic Paclitaxel For Photoacoustic Imaging-Guided Chemo-Photothermal Synergistic Therapy *Int J Nanomedicine* **14** 8647-63.
233. Ng K K, Zheng G 2015 Molecular Interactions in Organic Nanoparticles for Phototheranostic Applications *Chemical reviews* **115** 11012-42.
234. Li Y, Jiang C, Zhang D, Wang Y, Ren X, Ai K, Chen X, Lu L 2017 Targeted polydopamine nanoparticles enable photoacoustic imaging guided chemo-photothermal synergistic therapy of tumor *Acta biomaterialia* **47** 124-34.
235. Hu D, Zhang J, Gao G, Sheng Z, Cui H, Cai L 2016 Indocyanine Green-Loaded Polydopamine-Reduced Graphene Oxide Nanocomposites with Amplifying Photoacoustic and Photothermal Effects for Cancer Theranostics *Theranostics* **6** 1043-52.
236. Liu Y, Li Z, Yin Z, Zhang H, Gao Y, Huo G, Wu A, Zeng L 2020 Amplified Photoacoustic Signal and Enhanced Photothermal Conversion of Polydopamine-Coated Gold Nanobipyramids for Phototheranostics and Synergistic Chemotherapy *ACS Applied Materials & Interfaces* **12** 14866-75.
237. Shukla T, Upmanyu N, Pandey S P, Sudheesh M S, Chapter 14 - Site-specific drug delivery, targeting, and gene therapy. In *Nanoarchitectonics in Biomedicine*, Grumezescu, A. M., Ed. William Andrew Publishing: 2019; pp 473-505.
238. Ding L, Zhu X, Wang Y, Shi B, Ling X, Chen H, Nan W, Barrett A, Guo Z, Tao W, Wu J, Shi X 2017 Intracellular Fate of Nanoparticles with Polydopamine Surface Engineering and a Novel Strategy for Exocytosis-Inhibiting, Lysosome Impairment-Based Cancer Therapy *Nano Letters* **17** 6790-801.
239. Wang X, Zhang J, Wang Y, Wang C, Xiao J, Zhang Q, Cheng Y 2016 Multi-responsive photothermal-chemotherapy with drug-loaded melanin-like nanoparticles for synergetic tumor ablation *Biomaterials* **81** 114-24.

240. Mandriota G, Di Corato R, Benedetti M, De Castro F, Fanizzi F P, Rinaldi R 2019 Design and Application of Cisplatin-Loaded Magnetic Nanoparticle Clusters for Smart Chemotherapy *ACS Applied Materials & Interfaces* **11** 1864-75.
241. Tang X-l, Jing F, Lin B-l, Cui S, Yu R-t, Shen X-d, Wang T-w 2018 pH-Responsive Magnetic Mesoporous Silica-Based Nanoplatform for Synergistic Photodynamic Therapy/Chemotherapy *ACS Applied Materials & Interfaces* **10** 15001-11.
242. Liu R, Guo Y, Odusote G, Qu F, Priestley R D 2013 Core–Shell Fe3O4 Polydopamine Nanoparticles Serve Multipurpose as Drug Carrier, Catalyst Support and Carbon Adsorbent *ACS Applied Materials & Interfaces* **5** 9167-71.
243. Zhao J, Yang Y, Han X, Liang C, Liu J, Song X, Ge Z, Liu Z 2017 Redox-Sensitive Nanoscale Coordination Polymers for Drug Delivery and Cancer Theranostics *ACS Appl Mater Interfaces* **9** 23555-63.
244. Li W Q, Wang Z, Hao S, He H, Wan Y, Zhu C, Sun L P, Cheng G, Zheng S Y 2017 Mitochondria-Targeting Polydopamine Nanoparticles To Deliver Doxorubicin for Overcoming Drug Resistance *ACS Appl Mater Interfaces* **9** 16793-802.
245. Zhan H, Jagtiani T, Liang J F 2017 A new targeted delivery approach by functionalizing drug nanocrystals through polydopamine coating *European Journal of Pharmaceutics and Biopharmaceutics* **114** 221-29.
246. Wilson B C, Weersink R A 2020 The Yin and Yang of PDT and PTT *Photochemistry and Photobiology* **96** 219-31.
247. Hu D, Liu C, Song L, Cui H, Gao G, Liu P, Sheng Z, Cai L 2016 Indocyanine green–loaded polydopamine–iron ions coordination nanoparticles for photoacoustic/magnetic resonance dual-modal imaging-guided cancer photothermal therapy *Nanoscale* **8** 17150-58.
248. Ge R, Lin M, Li X, Liu S, Wang W, Li S, Zhang X, Liu Y, Liu L, Shi F, Sun H, Zhang H, Yang B 2017 Cu2+-Loaded Polydopamine Nanoparticles for Magnetic Resonance Imaging-Guided pH- and Near-Infrared-Light-Stimulated Thermochemotherapy *ACS Applied Materials & Interfaces* **9** 19706-16.
249. Wu Y, Wang H, Gao F, Xu Z, Dai F, Liu W 2018 An Injectable Supramolecular Polymer Nanocomposite Hydrogel for Prevention of Breast Cancer Recurrence with Theranostic and Mammoplastic Functions *Advanced Functional Materials* **28** 1801000.
250. Hu Z, Zhao F, Wang Y, Huang Y, Chen L, Li N, Li J, Li Z, Yi G 2014 Facile fabrication of a C60–polydopamine–graphene nanohybrid for single light induced photothermal and photodynamic therapy *Chemical Communications* **50** 10815-18.
251. Hopper C 2001 Photodynamic therapy: A clinical reality in the treatment of cancer *The lancet oncology* **1** 212-9.
252. Yan S, Song X, Liu Y, Dai T, Huang M, Chen X, Chen Z 2018 An efficient synergistic cancer therapy by integrating cell cycle inhibitor and photosensitizer into polydopamine nanoparticles *Journal of Materials Chemistry B* **6** 2620-29.
253. Liu W-L, Liu T, Zou M-Z, Yu W-Y, Li C-X, He Z-Y, Zhang M-K, Liu M-D, Li Z-H, Feng J, Zhang X-Z 2018 Aggressive Man-Made Red Blood Cells for Hypoxia-Resistant Photodynamic Therapy *Advanced Materials* **30** 1802006.
254. Wang X, Ouyang X, Chen J, Hu Y, Sun X, Yu Z 2019 Nanoparticulate photosensitizer decorated with hyaluronic acid for photodynamic/photothermal cancer targeting therapy *Nanomedicine* **14** 151-67.
255. Wang J, Guo Y, Hu J, Li W, Kang Y, Cao Y, Liu H 2018 Development of Multifunctional Polydopamine Nanoparticles As a Theranostic Nanoplatform against Cancer Cells *Langmuir* **34** 9516-24.
256. Han J, Park W, Park S-j, Na K 2016 Photosensitizer-Conjugated Hyaluronic Acid-Shielded Polydopamine Nanoparticles for Targeted Photomediated Tumor Therapy *ACS Applied Materials & Interfaces* **8** 7739-47.

257. Chen Y, Ai W, Guo X, Li Y, Ma Y, Chen L, Zhang H, Wang T, Zhang X, Wang Z 2019 Mitochondria-Targeted Polydopamine Nanocomposite with AIE Photosensitizer for Image-Guided Photodynamic and Photothermal Tumor Ablation *Small* **15** 1902352.
258. Yang X, Wang D, Zhu J, Xue L, Ou C, Wang W, Lu M, Song X, Dong X 2019 Functional black phosphorus nanosheets for mitochondria-targeting photothermal/photodynamic synergistic cancer therapy *Chemical Science* **10** 3779-85.
259. Zhan Q, Shi X, Zhou J, Zhou L, Wei S 2019 Drug-Controlled Release Based on Complementary Base Pairing Rules for Photodynamic–Photothermal Synergistic Tumor Treatment *Small* **15** 1803926.
260. Wu F, Liu Y, Wu Y, Song D, Qian J, Zhu B 2020 Chlorin e6 and polydopamine modified gold nanoflowers for combined photothermal and photodynamic therapy *Journal of Materials Chemistry B* **8** 2128-38.
261. Wu R, Wang H, Hai L, Wang T, Hou M, He D, He X, Wang K 2020 A photosensitizer-loaded zinc oxide-polydopamine core-shell nanotherapeutic agent for photodynamic and photothermal synergistic therapy of cancer cells *Chinese Chemical Letters* **31** 189-92.
262. Ou C, Zhang Y, Pan D, Ding K, Zhang S, Xu W, Wang W, Si W, Yang Z, Dong X 2019 Zinc porphyrin–polydopamine core–shell nanostructures for enhanced photodynamic/photothermal cancer therapy *Materials Chemistry Frontiers* **3** 1786-92.
263. Xu F, Liu M, Li X, Xiong Z, Cao X, Shi X, Guo R 2018 Loading of Indocyanine Green within Polydopamine-Coated Laponite Nanodisks for Targeted Cancer Photothermal and Photodynamic Therapy *Nanomaterials* **8** 347.
264. Xing Y, Ding T, Wang Z, Wang L, Guan H, Tang J, Mo D, Zhang J 2019 Temporally Controlled Photothermal/Photodynamic and Combined Therapy for Overcoming Multidrug Resistance of Cancer by Polydopamine Nanoclustered Micelles *ACS Applied Materials & Interfaces* **11** 13945-53.
265. Wang C, Bai J, Liu Y, Jia X, Jiang X 2016 Polydopamine Coated Selenide Molybdenum: A New Photothermal Nanocarrier for Highly Effective Chemo-Photothermal Synergistic Therapy *ACS Biomaterials Science & Engineering* **2** 2011-17.
266. Zeng X, Luo M, Liu G, Wang X, Tao W, Lin Y, Ji X, Nie L, Mei L 2018 Polydopamine-Modified Black Phosphorous Nanocapsule with Enhanced Stability and Photothermal Performance for Tumor Multimodal Treatments *Advanced Science* **5** 1800510.
267. Yu X, Tang X, He J, Yi X, Xu G, Tian L, Zhou R, Zhang C, Yang K 2017 Polydopamine Nanoparticle as a Multifunctional Nanocarrier for Combined Radiophotodynamic Therapy of Cancer *Particle & Particle Systems Characterization* **34** 1600296.
268. Ambekar R S, Kandasubramanian B 2019 A polydopamine-based platform for anti-cancer drug delivery *Biomaterials Science* **7** 1776-93.
269. Jiang Q, Luo Z, Men Y, Yang P, Peng H, Guo R, Tian Y, Pang Z, Yang W 2017 Red blood cell membrane-camouflaged melanin nanoparticles for enhanced photothermal therapy *Biomaterials* **143** 29-45.
270. Kim M, Kim H S, Kim M A, Ryu H, Jeong H J, Lee C M 2017 Thermohydrogel Containing Melanin for Photothermal Cancer Therapy *Macromolecular bioscience* **17**
271. Longo D L, Stefania R, Callari C, De Rose F, Rolle R, Conti L, Consolino L, Arena F, Aime S 2017 Water Soluble Melanin Derivatives for Dynamic Contrast Enhanced Photoacoustic Imaging of Tumor Vasculature and Response to Antiangiogenic Therapy *Advanced Healthcare Materials* **6** 1600550.
272. Solano F 2017 Melanin and Melanin-Related Polymers as Materials with Biomedical and Biotechnological Applications-Cuttlefish Ink and Mussel Foot Proteins as Inspired Biomolecules *Int J Mol Sci* **18** 1561.
273. Wang X, Yang L, Yang P, Guo W, Zhang Q-P, Liu X, Li Y 2020 Metal ion-promoted fabrication of melanin-like poly(L-DOPA) nanoparticles for photothermal actuation *Science China Chemistry* **63** 1295 - 305.

274. Dai M, Huang T, Chao L, Xie Q, Tan Y, Chen C, Meng W 2016 Horseradish peroxidase-catalyzed polymerization of L-DOPA for mono-/bi-enzyme immobilization and amperometric biosensing of H2O2 and uric acid *Talanta* **149** 117-23.
275. Dai M, Huang T, Chao L, Tan Y, Chen C, Meng W, Xie Q 2016 Tyrosinase-catalyzed polymerization of l-DOPA (versus l-tyrosine and dopamine) to generate melanin-like biomaterials for immobilization of enzymes and amperometric biosensing *RSC Advances* **6** 17016-22.
276. Kim B J, Cheong H, Hwang B H, Cha H J 2015 Mussel-Inspired Protein Nanoparticles Containing Iron(III)–DOPA Complexes for pH-Responsive Drug Delivery *Angewandte Chemie International Edition* **54** 7318-22.
277. Kuang J, Guo J L, Messersmith P B 2014 High ionic strength formation of DOPA-melanin coating for loading and release of cationic antimicrobial compounds *Advanced materials interfaces* **1** 1400145.
278. Barclay T G, Hegab H M, Clarke S R, Ginic-Markovic M 2017 Versatile Surface Modification Using Polydopamine and Related Polycatecholamines: Chemistry, Structure, and Applications *Advanced Materials Interfaces* **4** 1601192.
279. Petran A, Mrówczyński R, Filip C, Turcu R, Liebscher J 2015 Melanin-like polydopa amides – synthesis and application in functionalization of magnetic nanoparticles *Polymer Chemistry* **6** 2139-49.
280. Hong D, Lee H, Kim B J, Park T, Choi J Y, Park M, Lee J, Cho H, Hong S-P, Yang S H, Jung S H, Ko S-B, Choi I S 2015 A degradable polydopamine coating based on disulfide-exchange reaction *Nanoscale* **7** 20149-54.
281. Hashemi-Moghaddam H, Zavareh S, Gazi E M, Jamili M 2018 Assessment of novel core–shell Fe3O4@poly l- DOPA nanoparticles for targeted Taxol® delivery to breast tumor in a mouse model *Materials Science and Engineering: C* **93** 1036-43.
282. Kang S M, Rho J, Choi I S, Messersmith P B, Lee H 2009 Norepinephrine: material-independent, multifunctional surface modification reagent *Journal of the American Chemical Society* **131** 13224-25.
283. Chen J, Liang R-P, Wang X-N, Qiu J-D 2015 A norepinephrine coated magnetic molecularly imprinted polymer for simultaneous multiple chiral recognition *Journal of Chromatography A* **1409** 268-76.
284. Yang D, Wang X, Ai Q, Shi J, Jiang Z 2015 Performance comparison of immobilized enzyme on the titanate nanotube surfaces modified by poly(dopamine) and poly(norepinephrine) *RSC Advances* **5** 42461-67.
285. Taskin M B, Xu R, Zhao H, Wang X, Dong M, Besenbacher F, Chen M 2015 Poly(norepinephrine) as a functional bio-interface for neuronal differentiation on electrospun fibers *Physical chemistry chemical physics : PCCP* **17** 9446-53.
286. Baldoneschi V, Palladino P, Scarano S, Minunni M 2020 Polynorepinephrine: state-of-the-art and perspective applications in biosensing and molecular recognition *Analytical and bioanalytical chemistry*
287. Kang S M, Park S, Kim D, Park S Y, Ruoff R S, Lee H 2011 Simultaneous Reduction and Surface Functionalization of Graphene Oxide by Mussel-Inspired Chemistry *Advanced Functional Materials* **21** 108-12.
288. Liu X, Xie Z, Shi W, He Z, Liu Y, Su H, Sun Y, Ge D 2019 Polynorepinephrine Nanoparticles: A Novel Photothermal Nanoagent for Chemo-Photothermal Cancer Therapy *ACS Applied Materials & Interfaces* **11** 19763-73.
289. Lu Z, Douek A M, Rozario A M, Tabor R F, Kaslin J, Follink B, Teo B M 2020 Bioinspired polynorepinephrine nanoparticles as an efficient vehicle for enhanced drug delivery *Journal of Materials Chemistry B* **8** 961-68.
290. Jiang Y, Wang Y, Wang H, Zhou L, Gao J, Zhang Y, Zhang X, Wang X, Li J 2015 Facile immobilization of enzyme on three dimensionally ordered macroporous silica via a biomimetic coating *New Journal of Chemistry* **39** 978-84.

291. Liu Y, Nan X, Shi W, Liu X, He Z, Sun Y, Ge D 2019 A glucose biosensor based on the immobilization of glucose oxidase and Au nanocomposites with polynorepinephrine *RSC Advances* **9** 16439-46.
292. Khetani S, Kollath V O, Eastick E, Debert C, Sen A, Karan K, Sanati-Nezhad A 2019 Single-step functionalization of poly-catecholamine nanofilms for ultra-sensitive immunosensing of ubiquitin carboxyl terminal hydrolase-L1 (UCHL-1) in spinal cord injury *Biosensors and Bioelectronics* **145** 111715.
293. Hong S, Kim J, Na Y S, Park J, Kim S, Singha K, Im G I, Han D K, Kim W J, Lee H 2013 Poly(norepinephrine): Ultrasmooth Material Independent Surface Chemistry and Nanodepot for Nitric Oxide *Angew. Chem., Int. Ed.* **52** 9187.
294. Qiu J, Chen G, Zhu F, Ouyang G 2016 Sulfonated nanoparticles doped electrospun fibers with bioinspired polynorepinephrine sheath for in vivo solid-phase microextraction of pharmaceuticals in fish and vegetable *Journal of Chromatography A* **1455** 20-27.
295. Liu Y, Zhou G, Liu Z, Guo M, Jiang X, Taskin M B, Zhang Z, Liu J, Tang J, Bai R, Besenbacher F, Chen M, Chen C 2017 Mussel Inspired Polynorepinephrine Functionalized Electrospun Polycaprolactone Microfibers for Muscle Regeneration *Scientific Reports* **7** 8197.
296. Park M, Shin M, Kim E, Lee S, Park K I, Lee H, Jang J-H 2014 The Promotion of Human Neural Stem Cells Adhesion Using Bioinspired Poly(norepinephrine) Nanoscale Coating *Journal of Nanomaterials* **2014** 793052.
297. Kim E, Lee S, Hong S, Jin G, Kim M, Park K I, Lee H, Jang J-H 2014 Sticky "Delivering-From" Strategies Using Viral Vectors for Efficient Human Neural Stem Cell Infection by Bioinspired Catecholamines *ACS Applied Materials & Interfaces* **6** 8288-94.
298. He Z, Su H, Shen Y, Shi W, Liu X, Liu Y, Zhang F, Zhang Y, Sun Y, Ge D 2019 Poly(norepinephrine)-coated FeOOH nanoparticles as carriers of artemisinin for cancer photothermal-chemical combination therapy *RSC Advances* **9** 9968-82.
299. Nakatsuka N, Hasani-Sadrabadi M M, Cheung K M, Young T D, Bahlakeh G, Moshaverinia A, Weiss P S, Andrews A M 2018 Polyserotonin Nanoparticles as Multifunctional Materials for Biomedical Applications *ACS nano* **12** 4761-74.